NTNU – Trondheim
Norwegian University of
Science and Technology

Optimalised Carbodiimide Chemistry for RGD-coupled Alginate

Birgitte Hjelmeland McDonagh

Biotechnology (5 year)

Supervisor: Gudmund Skjåk-Bræk, IBT
Co-supervisor: Berit L. Strand, IBT

Norwegian University of Science and Technology
Department of Biotechnology

Acknowledgements

The work described in this study was carried out at the Department of Biotechnology at the Norwegian University of Science and Technology. Encapsulation with RGD-coupled alginate was performed by co-student Marthe Fredheim Fjelldal at the Department of Cancer Research and Molecular Medicine.

First of all I would like to thank my supervisors, Berit L. Strand, Finn L. Aacmann and Gudmund Skjåk-Bræk for supporting my ideas and letting me participate in planning this study. This has been really important to me, and has inspired me to further pursue my academic career.

Secondly, I would like to thank Wenche I. Strand for invaluable help in the laboratory, and for always being positive and solution oriented.

Third, I would like to thank my mother, my father, Kirsten, Magnus, Hans, and my extended family in Drammen, for supporting me. A special thank you to Atle, who is always there to encourage and inspire me. I love you all.

I dedicate this work to my grandmother, Aase, who thought me to believe in myself and in hard work. I love you, and miss you.

Summary

Alginate is a naturally ocurring polyanion of (1→4)linked β-d-mannuronic acid (M) and its C-5 epimer α-l guluronic acid (G). The polyanion, and particularly long stretches of guluronic acids, chelates and form hydrogels in the presence of divalent cations such as Ca^{2+}. Chelation occur at physiological conditions and the formed hydrogels are biocompatible and stable. These properties nominates alginate hydrogels as promising biomaterials in tissue engineering applications. Encapsulation of cells in alginate beads is easily prepared by mixing cells with high molecular weight alginate, and dripping the solution into a $CaCl_2$ solution. When alginate comes into contact with Ca^{2+} ions, alginate beads are immediately formed and the cells are captured in a three dimensional alginate matrix. Once inside the alginate capsule, the cells can be transplanted into a host deficient in the particular cells. The alginate protects the cells against the immune system of the host, opening for allograf transplantation without immunosuppressiva. The pores in the alginate network are big enough to enable diffusion of waste and nutrition through the membrane, which is important for cell survival.

Alginate is in itself not cell adhesive. However, alginate can be tailored into a cell adhesive biomaterial by attachement of cell adhesive peptides, such as the RGD motif found in extracellular matrix molecules such as fibronectin. Coupling of cell adhesive peptides increase cell survival in three dimensional alginate matrices. In this study, RGD-alginate is tailored with a chemoenzymatic approach that ensures RGD-coupling to non-gelling residues. This procedure starts with non-gelling mannuronan that is chemically modified by attachement of the cell adhesive peptide GRGDYP by carbodiimide chemistry. Gelling residues are introduced to peptide coupled mannuronan by a two step epimerisation catalyzed by the epimerases AlgE4 and AlgE6.

In this study, the carbodiimide chemsitry used for coupling GRGDYP to mannuronan is optimalised to create alginate with more than 0.2% bound peptide. The model molecules fluoresceinamine, 4-aminophenol and L-tyrosine-methyl ester are used for optimalisation, and the latter model molecule was found to give the best representation of peptide coupling to mannuronan. The carbodiimide mediated coupling to mannuronan is investigated by varying the pH, temperature and reactant concentrations. The degrees of coupling for each intervention is assessed by ^{1}H NMR and UV/vis spectroscopy. The presence of covalently bound by-products, named N-acylurea adducts, to mannuronan is assessed by ^{1}H NMR spectroscopy and a controlled reduction of these unwanted compounds is attempted. The results from

the optimalisation indicates that coupling of Me-O-Tyr and GRGDYP to mannuronan is concentration-dependent, as an increase in coupling was observed when the GRGDYP and Me-O-Tyr concentrations was increased. The highest peptide incorporation described in this study was 3.4% GRGDYP coupled to mannuronan, which is higher compared to similar studies.

The optimalised carbodiimide chemistry is applied to a large scale batch of RGD-coupled alginate that is to be used for cell encapsulation of olfactory ensheating cells from neonatal rat brain.

High molecular weight alginate was coupled with 0.45% GRGDYP and filtrated with active coal before cell encapsulation. The coal filtration removed a substantial amount of the unwanted N-acylurea adducts but also removed peptides, resulting in a GRGDYP coupling of 0.1% calculated from UV/vis spectroscopy, and 0.4% calculated from ^{1}H NMR spectroscopy. This indicates that peptides are associated with N-acylurea adducts and that active coal filtration is necessary to remove them.

Encapsulation of olfactory ensheating cells to RGD-coupled alginate gave no morphology changes or enhanced cell viability compared to non-peptide coupled alginate. It is believed that the low enzymatic action of the AlgE6 epimerase, a low concentration of peptides or a combination of both, have influenced the cell viability and lack of morphology changes. Enhanced peptide incorporation can be achieved by increasing the reactant concentrations of the peptides, but this would lead to a more expensive procedure. Increased efficacy, meaning a higher peptide coupling with lower adduct formation, at lower peptide concentrations was not achieved. However, the use of sodium borohydride in combination with periodate oxidised alginates for peptide coupling should be assessed as a novel approach for increased peptide yields at lower peptide concentrations.

Sammendrag

Alginat er en naturlig forekommende negativt ladet biopolymer som er bygd opp av (1→4) koblede β-d-mannuronsyre (M) og dens C-5 epimer α-l guluronsyre (G). Denne biopolymeren, og da spesielt repeterende enheter av guluronsyre, kan danne hydrogeler med divalente ioner som Ca^{2+}. Geldannelsen skjer ved fysiologiske betingelser og gelene er biokompatible og stabile. Celler av terapeutisk verdi, som for eksempel insulinproduserende celler, kan innkapsles i alginat ved å blande dem med høymolekulær alginat for deretter å dryppe blandingen i en væske med $CaCl_2$. I det øyeblikket alginat-celle-blandingen kommer i kontakt med kalsiumioner, innkapsles cellene i et tredimensjonalt alginatnettverk. Denne egenskapen ved alginat gjør at den kan benyttes som biomateriale innenfor regenerativ og terapeutisk medisin, fordi celler innkapslet i alginat kan transplanteres inn i menneskekroppen og samtidig beskyttes mot kroppens immunforsvar. Sammensetningen av alginatet bestemmer porestørrelsen på kapslene, og denne kan justeres på en slik måte at avfallsstoffer og næringsstoffer som cellene kvitter seg med og trenger, kan diffundere fritt over membranen. Kapselen muliggjør derfor for allograf transplantasjon uten bruk av immunosuppressiva.

En forutsetning for at cellene skal kunne overleve inne i alginatkapselen er at de kan binde seg til kapselen. Alginat er i utgangspunktet ikke celleadhesiv, men kan modifiseres ved å kjemisk koble på celleadhesive peptider ved hjelp av karbodiimidkjemi. Et velkjent peptid brukt i dette formålet er tripeptidsekvensen RGD som fins i ekstracellulære molekyler, som for eksempel fibronektin. Ved å koble på slike celleadhesive peptider til alginat øker overlevelsesraten av cellene inne i alginatkapselen.

Denne masteroppgaven beskriver hvordan GRGDYP-koblet alginat lages ved bruk av en kjemoenzymatisk prosedyre. Utgangspunktet for denne prosedyren er å koble peptidet til mannuronan ved hjelp av karbodiimidkjemi, for videre å epimerisere ikke-peptidkoblede mannuronan monomere til guluronan på polymernivå, ved hjelp av epimerasene AlgE4 og AlgE6. Denne metoden sørger for at peptidet ikke forstyrrer gelingsegenskapene til alginatet, slik at celler kan innkapsles i en stabil alginathydrogel.

Karbodiimidkjemien som benyttes til å koble på peptidet GRGDYP på alginat, optimaliseres i denne oppgaven ved hjelp av modellmolekylene fluoreseinamin, 4-aminofenol og L-tyrosin-metylester. Sistnevnte modellmolekyl ble vist til å representerte peptidkoblingen bedre enn de andre modellmolekylene. Koblingen til mannuronan foregår under ulike pH-verider, reaktantkonsentrasjoner og temperaturer for å kunne bestemme hvilke faktorer som gir høyest kobling av peptid. De faktorene som

gir ønsket kobling i optimaliseringsdelen overføres til en storskalaprøve med RGD-koblet alginat som skal benyttes til celleinnkapsling av olfactory ensheating celler fra neonatal rottehjerne. Mengden modellmolekyl og peptid koblet på mannuronan bestemmes ved hjelp av UV/vis og ^{1}H NMR spektroskopi. Bruk av karbodiimidkjemi muliggjør kovalent bindig mellom peptid og mannuronan, men uønskede biprodukter er ofte tilstede i større konsentrasjoner. Mengden biprodukter kan detekteres ved hjelp av ^{1}H NMR og mengdene forsøkes redusert.

Den optimaliserte karbodiimidkjemien som beskrives her ble applisert på en større prøve mannuronan, og 0.45% peptid ble koblet på før filtrering med aktivt kull og celleinnkapsling. Kullfiltreringen viste seg å fjerne store deler av de uønskede biproduktene, men også store deler av peptidet ble fjernet. Dette indikerer at peptidet kan være assosiert med biprodukter, i det som i denne oppgaven kalles addukter.

Innkapsling av olfactory ensheating celler i RGD-koblet alginat ga ingen morfologiendringer eller økte celleoverlevelser sammenlignet med alginat uten RGD. Dette kan ha sammenheng med den lave AlgE6 enzymaktiviteten, den lave peptidinkorporeringen, eller en kombinasjon av disse. Økt peptidkobling kan oppnås ved å øke reaktantkonsentrasjonene av peptidet, men dette vil igjen føre til forhøyde kostnader. Økt effektivitet av karbodiimidkjemien, det vil si økte mengder peptidkoblinger ved lavere peptidkonsentrasjoner, er ønskelig men ble ikke oppnådd i denne oppgaven. Bruk av natriumborhydrid i kombinasjon med periodatoksiderte alginater burde undersøkes for økte utbytter ved lavere peptidkonsentrasjoner, da andre har vist lovende resultater for peptidkobling med denne metoden.

Contents

List of abbreviations

4AP: 4-aminophenol

CAM: Cell adhesion molecule

DMAP: *N,N*-dimethylaminopyridine

ECM: Extracellular matrix

EDC: N-(3-dimetylaminopropyl)-N'-ethylcarbodiimide hydrochloride

EDTA: Ethylenediaminetetraacetic acid

EtOH: Ethanol

FA: Fluoresceinamine

G: α-L guluronic acid

G-block: Homopolymeric domain of guluronic acids

GRGDYP: Peptide sequence consisting of glycine-arginine-glycine-aspartate-tyrosine-proline

HOBt: hydroxybenzotriazole

M: β-D-mannuronic acid

M-block: Homopolymeric domain of mannuronic acids

Me-O-Tyr: L-Tyrosine methyl ester

MES-buffer: 2-[N-morpholio]ethanesulfonic acid

MOPS: 3-N[morpholino]propanesulfonic acid

MQ: Milli-Q

NMR: Nuclear Magnetic Resonance

PBS: Phosphate buffered saline

RGD: arginine-glycine-aspartate

sulfo-NHS: N- hydroxysulfosuccinimide sodium salt

TTHA: Triethylenetetraminehexacetic acid

w/v: weight/volume

1 Introduction

1.1 Background

Alginate is a naturally occuring polyanion typically obtained from brown algae (*Phaeophyta*). A similar structure is produced as an exocellular material by *Azotobacter vinelandii* and *Pseudomonas* species[1]. It is a structural biopolymer consisting of two monomers: guluronic acid (G) and mannuronic acid (M)[2]. Alginate, particularly G-blocks and MG-blocks, chelates with divalent cations and form hydrogels under mild conditions. Alginate hydrogels of high guluronic content (higher than 60 %) offer strength, low shrinkage and high stability[3],are also biocompatible and are relatively cheap[4] [5] [6]. These properties makes alginate an interesting material for tissue engineering applications. The cells in human tissues have cellular interactions in three dimensions, which are difficult to represent in a two-dimensional culture of cells. Therefore, alginate is introduced as a three dimensional matrix for tissue engineering. Cells encapsulated by alginate gels are easily prepared by dripping high molecular weight sodium alginate mixed with cells into a $CaCl_2$-solution.

Hydrogels of alginate are biologically inert, and does not adsorb proteins or other positively charged macromolecules. To enhance the interaction of alginate hydrogels with encapsulated cells, cell adhesive peptides can be chemically attached. Peptide coupled alginates can interact with the encapsulated cell surface, offering a three dimensional matrix for living cells[4] [7] [8]. Functional biomaterials with peptides may control the cellular growth, differentiation and behaviour of cells in a culture[9]. Thus, the interaction of biomaterials with the encapsulated cells is governed by the amount and distribution of coupled peptide[10] [11]. This is the motivation for controlling the amounts of peptides coupled to alginate, as various combinations can serve as immobilisation matrices for a range of different cell types.

Peptides are commonly coupled to alginate by carbodiimide chemistry. The N-terminal of the peptide is connected to carboxylic acids in alginates via a peptide bond[12] [13]. Peptide coupled alginate is in this study prepared in a two-step procedure named chemoenzymatical modification of mannuronan[14]. In the first step, mannuronan is grafted with the peptide glycine-arginine-glycine-aspartate-tyrosine-proline (GRGDYP) by carbodiimide chemistry. The second step is catalyzed by recombinant epimerases AlgE4 and AlgE6 from the bacterium *A. vinelandii* that enzymatically introduce geling residues to the polymer. Only the residues that are not coupled to peptides are epimerised, as it is believed that the coupled peptide hinder the enzymatic action. Introducing geling residues after peptide coupling, ensures

that the peptide is coupled to non-geling residues.

Litterature regarding control of the carbodiimide coupling reaction is scarce, and presenting a predicitive relationship between added peptide and peptide coupled to mannuronan is the aim of this study. The carbodiimide chemistry for coupling the peptide sequence GRGDYP to mannuronan is optimalised and applied to a large scale batch that are being used for encapsulation of olfactory ensheating cells from neonatal rat brain.

1.2 Alginate Composition

Alginate is a block copolymer consisting of (1→4)linked β-d-mannuronic acid (M) and its C-5 epimer α-l guluronic acid (G)[2] [15]. As shown in figure 1, mannuronic acid exists predominantly in $^4C_1$ and l-guluronic acid in $^1C_4$ conformation[16]. The regions can be either homopolymeric ($\cdots$MMM$\cdots$ or $\cdots$GGG$\cdots$) or heteropolymeric ($\cdots$MGM$\cdots$). A homopolymeric domain of M-monomers is referred to as an *M-block*, while a homopolymeric domain of G-monomers is referred to as a *G-block*[17].

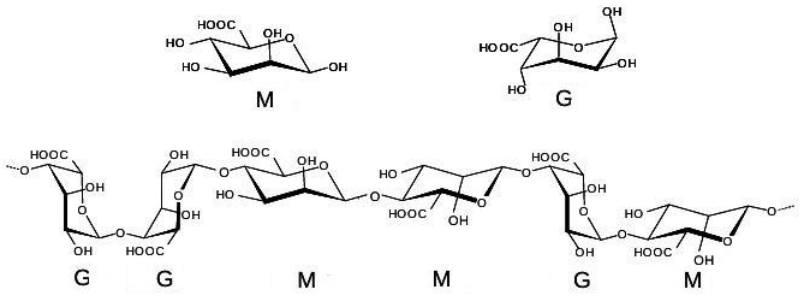

Figure 1: Guluronic acid and mannuronic acid. The figure show the chair conformations of the two monomers of alginate; G and M, and their binding geometry when linked together. The linkage between two G-monomers is diaxial and the linkage between MM and GM is diequatorial and axial-equatorial, respectively[18]. The diaxial linkage prevents free rotation around the glycosidic linkage, and a GG-sequence will form a cavity-like structure as depicted[17] [6] [1].

The monomer sequence of naturally derived alginates is a result of a complex biochemical pathway, and a complete sequencing is not possible. However, the composition of alginates can be determined by high-resonance proton and carbon nuclear

magnetic resonance (^{1}H NMR and ^{13}C NMR, respectively. A complete description of how the alginate composition can be determined, is included in appendix R).

1.3 Alginates chelate with divalent cations

Alginates chelate by selectively binding divalent cations, such as Ca^{2+} [6]. The gel formation is mainly driven by G-blocks which associate to tightly held junctions when divalent cations are present [9].

The Eggbox Model describes how G-blocks merge together forming chelates with divalent ions. The name of the model refers to calsium ions that are situated in guluronic cavities like eggs in a carton, as illustrated in figure 2 [18].

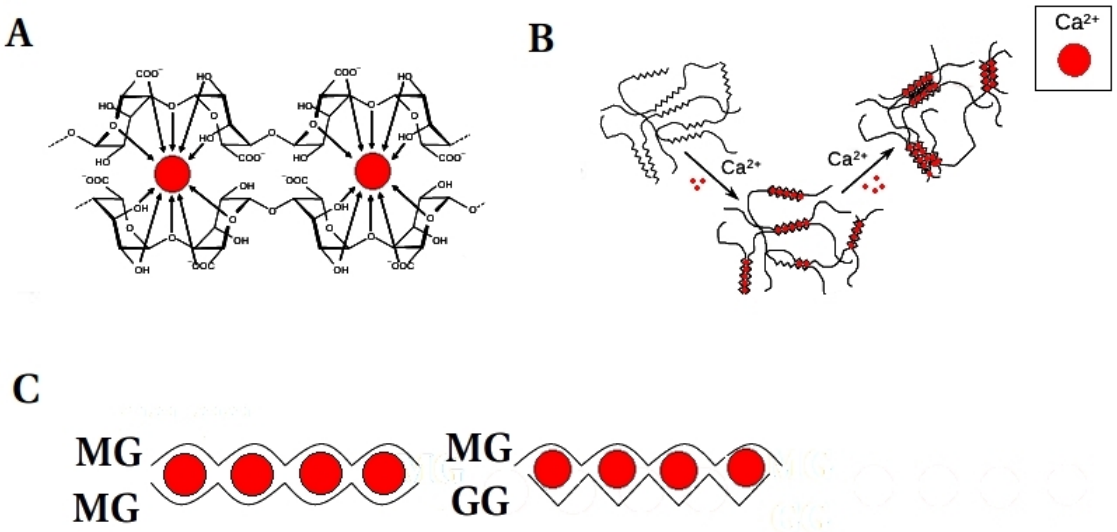

Figure 2: The Eggbox model. **A**: One calsium ion requires four G-units for ionotropic gel formation and cross-linking. **B**: Merging of alginate chains around calsium ions [1] is required for gel formation. The second step show a lateral association of chains which increases with increasing Ca^{2+} concentration and G-content [1]. The enthalpic gain for crosslinking has to be larger than the entropy for free calsium ions and alginate chains in order for crosslinking to occur [15] [2]. **C:** *The Eggbox Model* does not give a full description of gel formation as it fails to account for other interchain interactions, as MG-blocks can cross-bind with other MG or G-blocks and contribute to the chelation with divalent ions [19] as shown. The figure has been modified from Mørch, *et.al* [1]

The ring oxygen and axial oxygen in position 1 of guluronic acids form a favorable geometry for binding of divalent ions, compared to the equatorial oxygen at position 1 in mannuronic acid[20]. The rigid structure of a G-block show higher affinity towards divalent cations than M-, or MG-blocks[15] as the cavity created between G-monomers functions as an ion binding site. Thus, *alginates with high G contents yield stronger gels*[9]. Therefore, the gel strength and porosity can be adjusted by adjusting the composition of alginate.

1.3.1 Biological origin of alginates

Alginates are found in brown algae (*Phaeophyceae*) and bacteria such as *P. aeruginosa*, *P. mendocina*, *P. putida*, *P. fluorescens* and *A. vinelandii*[6] [1]. The main difference between alginate from algae and bacteria is the presence of O-acetyl groups on the second and/or third carbon(s) in mannuronic acid residues in bacterial alginates[21].

In algae, the alginates are thought to be a structural component, giving the plant both mechanical strength and flexibility. It has been compared to cellulose which is the main structural component of terrestial plants[6]. The bacterias, such as *P.aeruginosa*, can produce alginate as an extracellular material[21].

1.3.2 Alginate epimerases

Seven mannuronan C-5-epimerases are identified from the genome of the bacterium *A. vinelandii*. They are named *AlgE1* to *AlgE7*. AlgE4 catalyze the Ca^{2+}-dependent epimerization of mannuronan to guluronic acid in an alternating fashion(MGM)[22], while the epimerase AlgE6 introduces long stretches of guluronic acids(GGG)[23] [22] [24]. The enzymes can be utilized to introduce G-blocks in mannuronan to increase the gelling properties of the polymer.

1.4 Tissue Engineering

Tissue engineering can be defined as:

The creation of synthetic or semisynthetic tissue that can be used instead of human tissue in surgery[25].

The aim of tissue engineering is to repair or replace diseased or damaged tissue[25].

Alginate can undergo chemical modifications for cellular interactions and has properties which is considered highly important in tissue engineering, such as biocompatibility and non-immunogenicity[16][14]. Gelling occur under physiological conditions[6], which is beneficial for cell encapsulation. Cells are easily encapsulated by mixing with high molecular weight sodium-alginate that is dripped into a solution of calsium chloride. The cells are immediately encapsulated in the three dimensional network as alginate and calsium ions chelate. Since this process can take place at physiological conditions, the viability of the cells is not affected[4].

For many commercial alginates, the molecular weight is higher than the renal clearance threshold of the kidneys, and degradation of alginate chains are necessary for removal[26]. Mammals lack the enzyme *alginate lyase* which cleaves the polymer chains. However, hydrolysis of alginate backbone will occur over time causing removal through the kidneys. Ions in biological fluids, such as Na^+, contribute to degradation as they exchange the chelated calsium ions situated in the alginate network. This results in a porous, and over time, dissolved gel[14][4][5].

1.5 The Extracellular Matrix

A major constituent of animal tissue is the extracellular space that surrounds cells. This space consists of a variety of macromolecules, such as sugar molecules and proteins. These are secreted locally by the cells and organized and anchored to the cell that produce them[27]. The interactions between the cell and extracellular matrix (ECM) molecules are crucial for the development of tissue.

The ECM defines the physical microenvironment for the cell and serves as a substrate for cell anchorage and as a tissue scaffold. Further, it determines cell migration in the embryogenesis and is responsible for transmitting environmental signals to vicinal cells. These interactions ultimately determine most aspects of a cells life, including

its proliferation, differentiation and death [28] [29] [10] [30] [31]. The composition and properties of the ECM are tissue specific and changes during the developmental stages. These tissue specific differences have profound implications on tissue function [31], and choosing an appropriate matrix for tissue engineering experiments is crucial to attain the wanted cellular response [28].

Alginates are hydrophilic and lack cell adhesivity, but this can be modified by attachement of adhesion ligands by water-soluble carbodiimide chemistry [13] [32]. A variety of short amino acid sequences that are found in ECM molecules can introduce cell adhesion to otherwise non-adhesive surfaces [16]. The tripeptide RGD has been widely used as an adhesion ligand [5] because the corresponding receptor integrin is present in virtually every type of cell membrane [33]. Alginate grafted with RGD will have increased cell adhesiveness, as it can bind to membrane bound integrin receptors of the cells.

1.5.1 Fibronectin is an adhesion molecule in the ECM

Fibronectin was the first cell adhesion molecule (CAM) found to be involved in adhesion of cells to extracellular substrates [34]. Analysis of amino acid fragments in fibronectin show that some sequences bind stronger to adhesion receptors than others. The specific fragment, named the cell attachment region, has been localized to a tripeptide of arginine-glycine-aspartate (RGD) [31] [34]. This sequence is depicted in figure 3.

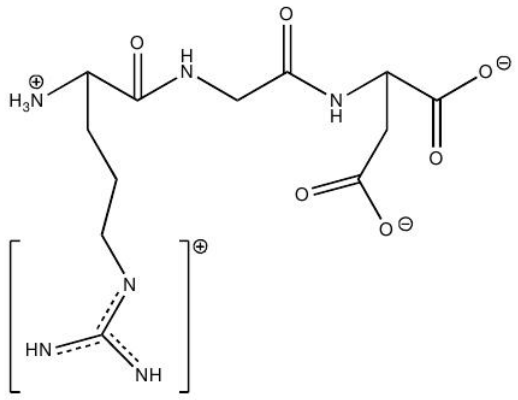

Figure 3: Tripeptide Arginine(R)-Glycine(G)-Aspartate(D) [25]. The figure show the structural formula of the peptide at physiological pH. The side group of R is depicted with resonance bonds.

The RGD-sequence is not confined to fibronectin, a large number of CAMs contains this sequence [10]. The RGD-sequence is often surrounded by other amino acids that specify the receptor binding sequence, which indicate that specific binding is not confined to RGD alone, but depends on surrounding amino acids as well [27]. For example, the sequence found in fibronectin is RGDS, collagen 1 has RGDT and laminin A has the amino acid sequence LRGDN [31].

1.5.2 Integrin receptors bind RGD

The integrins are adhesion receptors of dimeric proteins consisting of an α- and a β-subunit. They are involved in both cell-matrix and cell-cell interactions, and is present in almost every cell type [33] [31] [34] [35] [36]. Families of these receptors consists of members with the same or very similar β-subunit, whereas the α-subunits are distinct and restrict the receptors affinity to one or a few CAMs [28] [27]. More than 20 different $\alpha\beta$ combinations has been described [35]. Each integrin regonizes its own set of matrix molecules, and *the classical fibronectin receptor* $\alpha_5\beta_1$ binds specifically to fibronectin [28] [27]. The interactions between integrin and RGD is illustrated in figure 4.

The RGD sequence is recognized by the extracellular α-, and β- subunits of integrin. The binding induces conformational changes that affect intracellular association to talin, a cytoskeletal protein that connects integrin to actin filaments in the cytoskeleton [37].

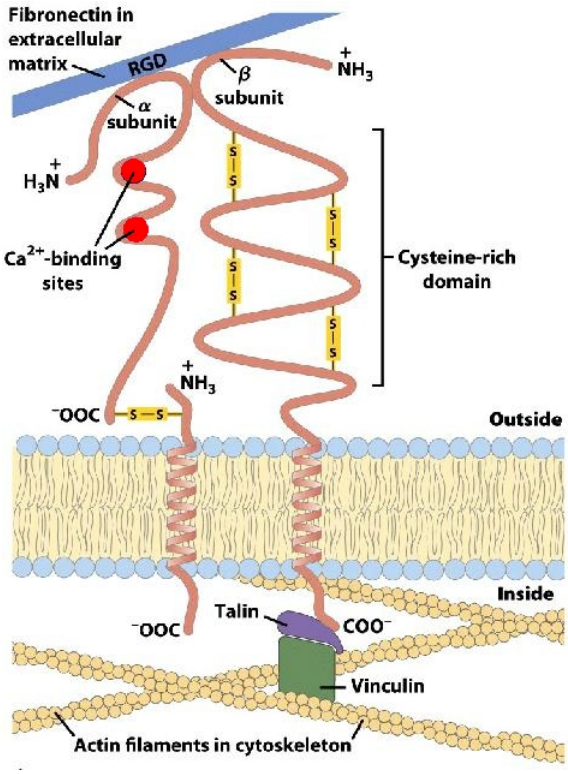

Figure 4: Transmembranal signaling by integrin receptors. The integrins have one α-, and one β- subunit, which spans the cell membrane with a transmembrane helix. The intracellular domains interacts with cytoskeletal proteins, such as vinculin and talin, connecting the receptor to the cytoskeleton of the cell. Each subunit has a large extracellular domain with a ligand binding site. The β- subunit is particularly cysteine rich with extensive interchain disulfide bonding. The α-subunit has several binding sites for divalent cations, such as Ca^{2+}, which is important for ligand-binding activity. Modified from Lehninger[37].

The interactions between integrins and its ligands provides an anchor for the cells which is crucial to avoid apoptosis[35] [36]. Not only the type of ligand, but also its distribution and concentration seem to influence the cell binding properties of a material[30]. Thus, a minimum concentration of RGD is necessary for cell adhesion and growth, and this concentration is probably cell type specific[5] [10].

Peptide coupled alginates can interact with the encapsulated cell surface, offering a three dimensional matrix for living cells[4] [7] [8]. Functional materials with peptides may control the cellular growth, differentiation and behaviour of cells in a culture[9]. Thus, interactions of the biomaterial with the encapsulated cells are governed by the amount and distribution of coupled peptides[10].

Coupling short peptides is beneficial compared to coupling native ECM molecules, as the latter tends to adsorp on the surface, causing a denaturation of the structure and hiding the receptor binding domains[38]. Alginate grafted with small peptides has been shown to be a promising model for a synthetic extracellular matrix[8], and specifically the RGD-sequence as grafted peptide mimic the cell binding properties of the ECM[39] [8] [7] [16]. Other peptides that can be used for adhesion receptor binding is REDV, which is derived from fibronectin, and YGYYGDALR, derived from laminin 1[40] [38].

The flexibility of an RGD-sequence also seems to be of importance, as spacers have shown to increase cell adhesivity[41]. Using an inert spacer of glycine between the RGD sequence and mannuronan has two advantages: first, it increases the flexibility of the peptide and enables a greater interaction between the biomaterial and the ligands[39]. Secondly, glycine has a small side group which will not hinder the backbone amine in peptide coupling[42]. A spacer with more than four and less than twelve glycines has been shown to be favourable for fibroblast cell adhesion and growth[41].

1.5.3 Chemoenzymatically modified alginate

The chemoenzymatic approach utilize carbodiimide chemistry for peptide attachment and enzymes for epimerisation. Figure 5 illustrates the approach for modifying mannuronan into a matrix for tissue engineering. The first step involves grafting of RGD by carbodiimide chemistry, while step two and three utilise enzymes to alter the monomer composition to obtain wanted geling properties.

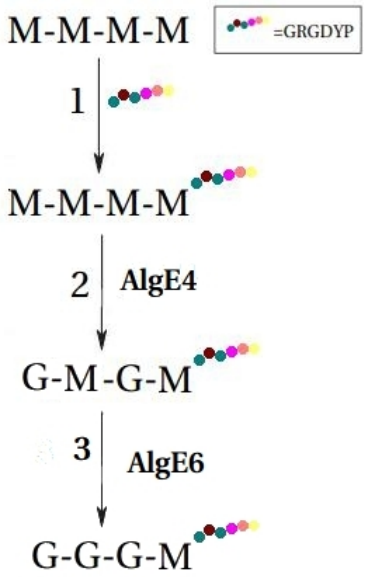

Figure 5: Chemoenzymatical approach for alginate-peptide coupling. **1**: The peptide GRGDYP, illustrated as dots, is coupled to mannuronan by carbodiimide chemistry. **2**:AlgE4 introduce alternating sequences to RGD-coupled mannuronan. **3**: AlgE6 epimerise mannuronic acids to G-blocks, increasing the gel binding properties of the polymer[14].

The chemoenzymatic approach protects the mannuronic units from the catalytic action of the enzymes. This ensures epimerization of non-modified mannuronic acids into guluronic acids that have higher Ca^{2+} affinity[14] [4]. How the peptides can be grafted to mannuronan is described in the next subsection.

1.6 Grafting peptides to alginate

A peptide bond is formed when a carboxylic acid group of one molecule reacts with an amine group of another molecule with the release of water. In the cytosol of the cell, the formation of peptide bonds is catalyzed by enzymes. Alginate is built up of monomers that posess a carboxy group which can form peptide bonds with the amine terminus of peptides. To manage this *in vitro*, carbodiimide chemistry can be used. The anchoring of RGD onto a material needs to be strong in order to induce proper cell adhesion[11]. In theory, coupling alginates with RGD-peptides via an amide bond is a logic approach, as the peptide bond offer a strong linkage between the peptide and the biomaterial.

Carbodiimides are a collective term for unsaturated compounds with an allene structure, such as RN=C=NR′[12]. The nitrogen atoms pull the bonding electrons, resulting in a partial negative charge on the nitrogen atoms, and a corresponding positive charge on the central carbon. This creates an electrophilic carbon atom that is readily attacked by nucleophiles such as mannuronic carboxylate ions (see figure 6).

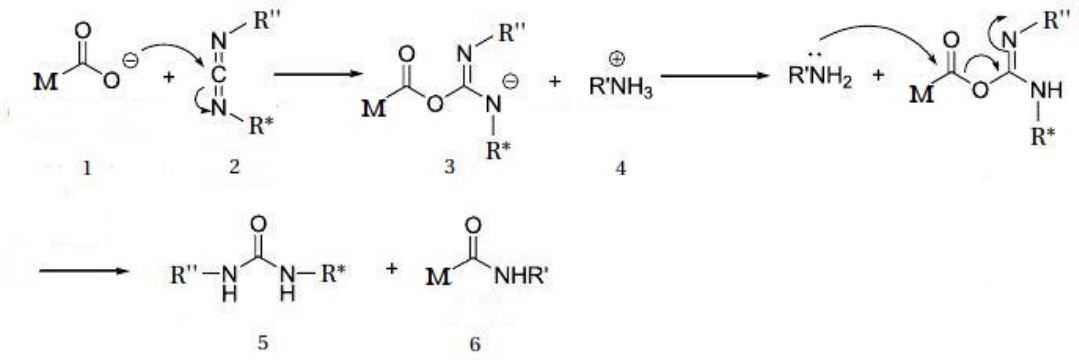

Figure 6: Reaction scheme for carbodiimides The carboxylic acid (1) on mannuronan, assigned with M, attack the carbon situated between the two nitrogen atoms of the carbodiimide(2). This leads to the formation of O-acylisourea (3). This compound attacks a primary amine(4), creating an amide (6) and a urea derivate(5), the latter being the thermodynamic driving force for this reaction[13].

N-(3-dimetylaminopropyl)-N'-ethylcarbodiimide hydrochloride (EDC) is frequently being used as a carbodiimide for amide bond formation and its structure is depicted in figure 7.

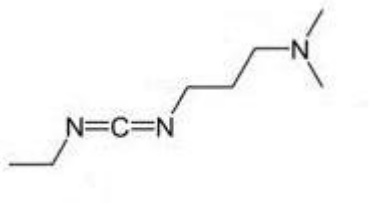

Figure 7: 1-ethyl-3-(3'-dimethylamino)carbodiimide

EDC reacts with mannuronic acids, as shown in figure 8. Protons are substrates in the carbodiimide reaction and the pH will thus influence the reaction. EDC is water soluble and very reactive, particularly in the pH-interval 3.5-4.5[12]. At this pH, the formation of the second carbocation is faster due to higher proton concentrations (figure 8). Mannuronic acids have a pK_a of 3.38[6], and above this pK_a, the acid groups of mannuronan are deprotonated and can act as nucleophiles as shown in figure 8. Below pH = 3.5, the carboxylic acids of mannuronan are protonated, leading to a reduced formation of O-acylisourea[12] [17].

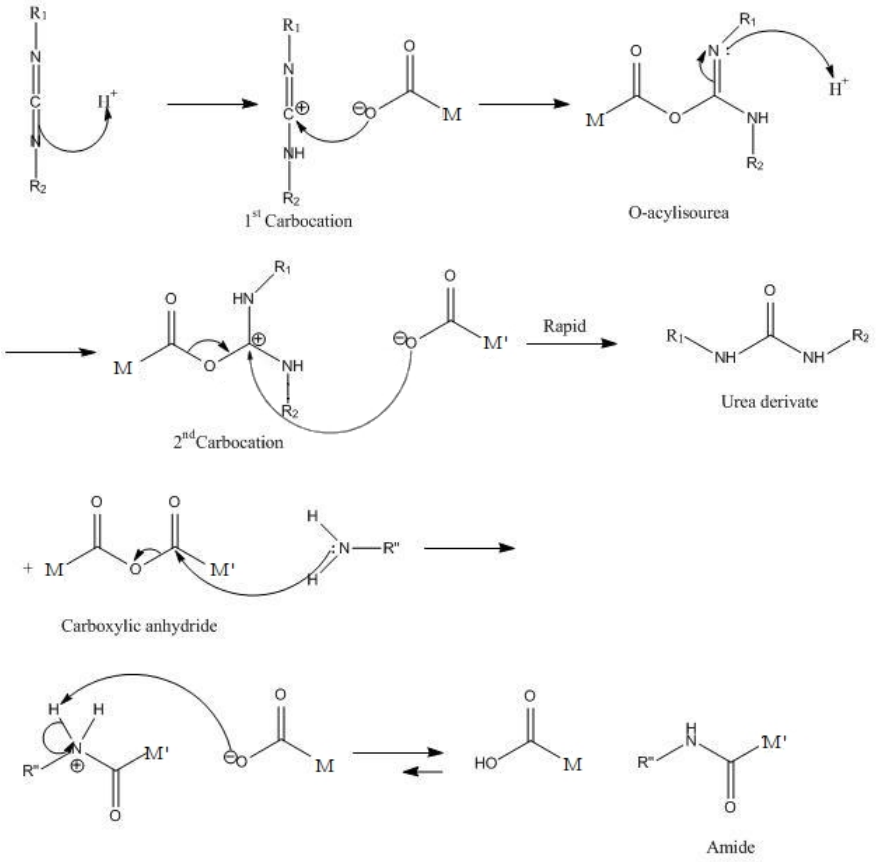

Figure 8: Reaction mechanism for amide formation between carboxylic acids in alginate and amines from *e.g* RGD in the presence of carbodiimide EDC in aqueous media. For EDC: R_1 = CH_3-CH_2, and R_2 = $(CH_2)_3N$-$(CH_3)_2$ [12] [13].

The first carbocation is formed by nucleophilic attack of protons. The carbocation is further attacked by nucleophiic mannuronic acids, and the compound O-acylisourea is formed. The stochiometry show that one proton is consumed for each O-acylisourea formed. A proton is attacked by the lone electron pair of the nitrogen atom of O-acylisourea, creating a second carbocation. The second carbocation is attacked by another nucleophilic mannuronic acid, creating a carboxylic anhydride and a urea derivate. The carboxylic anhydride will form an amide when amines ($R''-NH_2$) are present [12] [13].

Consumption of protons requires a buffer to maintain the acidity of the solution. The buffer can not have any carboxylic acids, as these will react with O-acylisourea. The compound 2-[N-morpholio]ethanesulfonic acid (MES-buffer) is frequently used

as a buffer in carbodiimide chemistry because it contains no carboxylic acids, and has a pK_a of 6.15 at 20°C[43]. Its structure is depicted in figure 9.

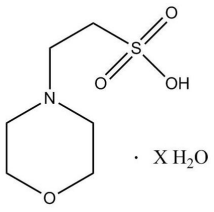

Figure 9: 2-[N-morpholio]ethanesulfonic acid. A buffer frequently used for carbodiimide chemistry.

The benefits of using carbodiimide chemistry is the use of an aqueous environment and non-hazardous reagents. Excess reagents and water soluble urea derivates are readily removed by dialysis. Unfortunately, the carbodiimide reaction has several by-products depending on the concentrations of reactants and temperature[12], leading to lowered amounts of coupled peptides. Particularly the formation of one by-product, named N-acylurea, is problematic as it is not removed with dialysis, and can associate with the molecule that is to be coupled to mannuronan.

1.6.1 Side reactions

As shown in figure 8, the first carbocation that is formed reacts with a carboxylate ion and O-acyliosurea is formed. If no mannuronic carboxylate ions are present, the carbocation is hydrolysed, as shown in figure 10.

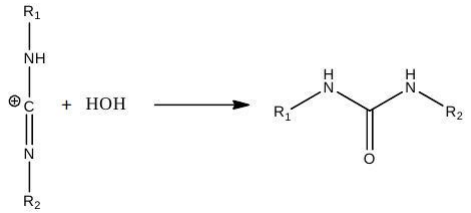

Figure 10: Hydrolysis of carbocation. If the amounts of carboxylate ions is not sufficient in the solution, the carbocation is hydrolyzed and a urea derivate is formed. The compound is very stable and it is not likely to react further in the carbodiimide reaction[12].

If O-acylisourea is succesfully formed, hydrolysis will occur if the concentration of carboxylate ions is low. The reaction mechanism is illustrated in figure 11.

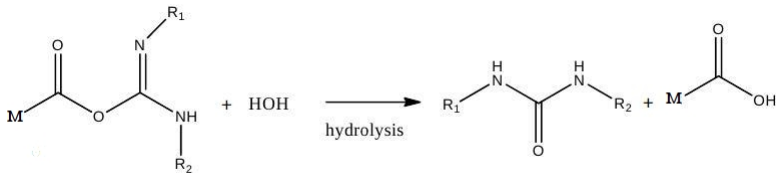

Figure 11: Hydrolysis of O-acylisourea. If there are no carboxylate ions in the solution, O-acylisourea is hydrolyzed to a carboxylic acid and a urea derivate.[12]

Another side reaction is also possible between O-acylisourea and amines, but this ultimately leads to the wanted product as shown in figure 12.

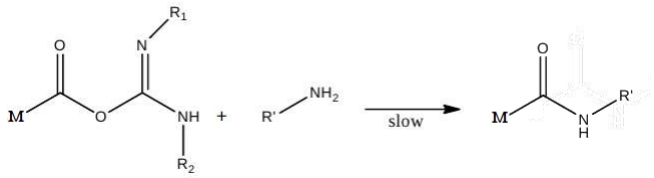

Figure 12: Formation of amide. This reaction is slow compared to the reaction illustrated in figure 8, but leads to the formation of the wanted amide[12].

There is a chance for unspecific binding between the carboxylic anhydride and the amine groups in the peptide GRGDYP. Arginine has several amine groups in its side chain that are available for binding (see figure 3). If this occurs, the conformation of the RGD-sequence will be distorted, which will probably affect integrin binding. A consequence of this may be that the viability of the cells is lowered. However, the side chain of arginine is on average slightly protonated at physiological pH, as illustrated in figure 3, which makes the amines in the side chain less reactive.

The mentioned by-products which is urea derivates, are not associated to mannuronan (see figure 8) and are small water-soluble molecules that are removed by dialysis.

The most frequent and most unwanted side reaction is the rapid formation of the energetically more favoured N-acylurea from N→O displacement of O-acylisourea, as shown in figure 13.

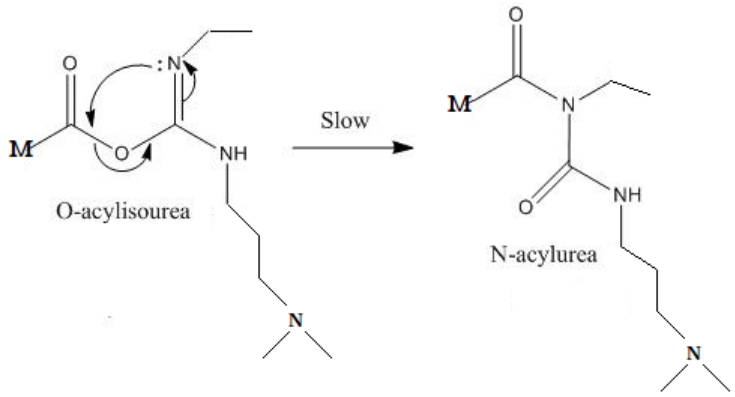

Figure 13: Reaction mechanism for formation of N-acylurea from molecular rearrangement of O-acylisourea [13].

N-acylurea can undergo conjugation of double bonds which results in more resonance structures and higher stability compared to O-acylisourea.

The formation of N-acylurea is problematic because it is associated with mannuronic acids and can not be removed by dialysis. The association of N-acylurea to mannuronan is in this study referred to as an adduct, which is a complex formed between N-acylurea covalently bound to mannuronan [44].

Although the carbodiimide has a strong preference for deprotonated carboxylgroups, it may also react with hydroxyl groups to form stable adducts. The MES-buffer (figure 9), the model molecules L-tyrosine methyl ester (Me-O-Tyr) and 4-aminophenol (4AP) has a hydroxyl group in its side chain which may in fact react with the carbodiimide [45](see subsection 1.6.2). GRGDYP has several hydroxy groups that can associate with N-acylurea. These are situated at the tyrosine residue, at the C-terminus and at the aspartic acid side chain [11] [46]. Figure 14 show how N-acylurea are associated in adducts with mannuronan and mannuronan that is coupled with the model molecule Me-O-Tyr.

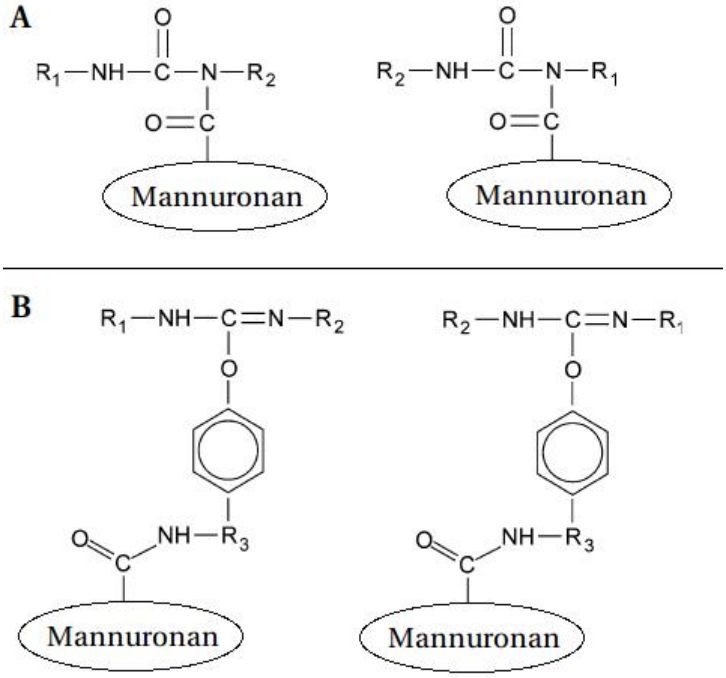

Figure 14: Formation of adducts between A: N-acylurea and mannuronan and B: mannuronan, Me-O-Tyr and N-acylurea. A: The top part of the figure show the adduct between mannuoronan and N-acylurea. **B:** The lower part of the figure show N-acylurea coupled to Me-O-Tyr-mannuronan. The figure has been modified from Darr *et.al*[44]. R_1: CH_2CH_3, R_2: $CHC(O)OCH_3$, R_3: $(CH_2)_3NH^+(CH_3)_2Cl^-$.

It is believed that the peptide GRGDYP is also coupled in adducts as shown in figure 14, as it contains a tyrosine residue and several other hydroxyl groups.

Since the adducts shown in the figure above are not removed by dialysis, they are present in the sample analysed by ^{1}H NMR. Adducts can be detected in ^{1}H NMR as described below.

EDC and N-acylurea both have an amide group with two branched methyl groups in the approximately same chemical environment. A sample of pure EDC was prepared for ^{1}H NMR and its specter is shown in figure 15.

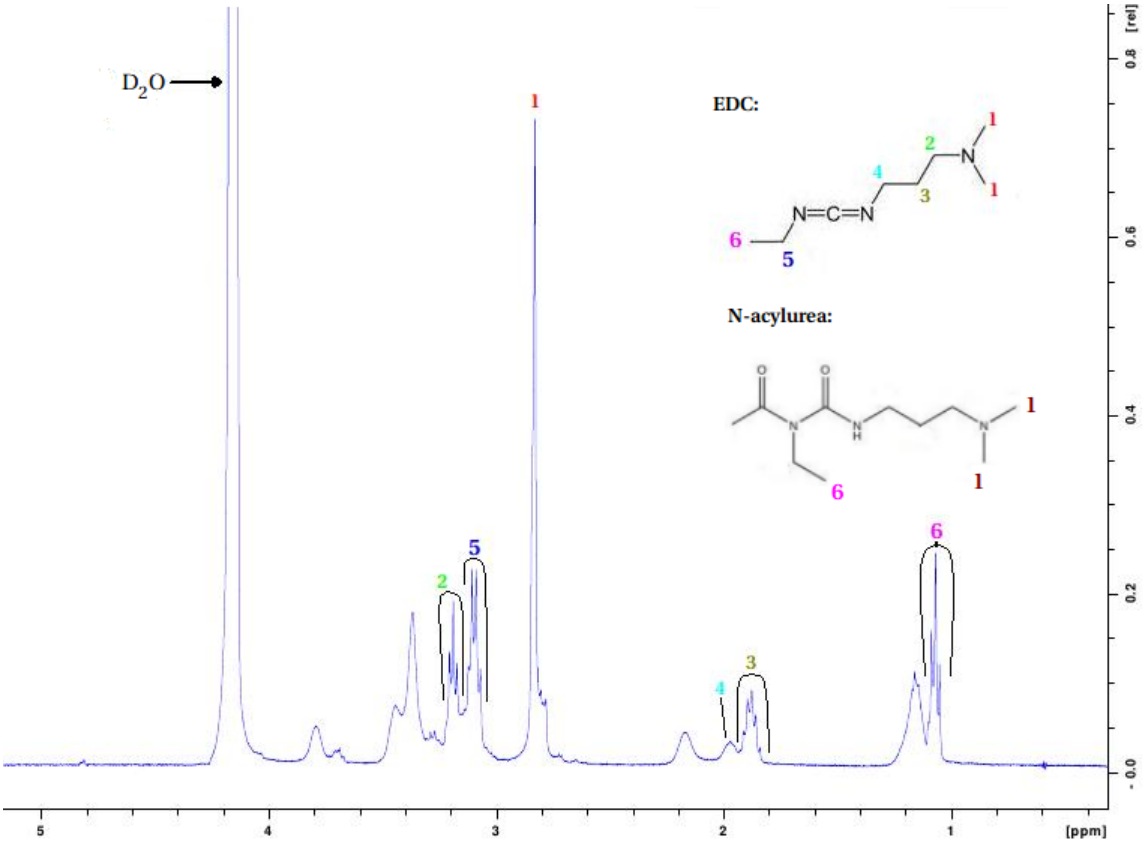

Figure 15: ^{1}**H NMR of EDC**.The sample with EDC was prepared in D_2O with chemical shift reference TSP. The chemical shifts for N-acylurea has been assigned, assuming that the chemical shift of the methyl protons one and six are similar to EDC.

The chemical shift for proton number one (in figure 15) in EDC, are observed as a singlet at 2.90 ppm. It is expected that the equivalent protons in N-acylurea will peak at this chemical shift. EDC and N-acylurea both have an ethyl group bound to a nitrogen atom. The methyl protons of this side chain, number six in figure 15, is identified as a triplet at 1.15 ppm for EDC, and the same peak is expected for N-acylurea. Thus, proton peak number six and one in figure 15, can deduce the amount of adducts present.

Problems arise if N-acylurea associates with mannuronan shown as structure B in figure 14, as the aromatic protons of the benzene ring are used to calculate the amount of product coupled to mannuronan. However, N-acylurea coupled to mannuronan in this way will probably give aromatic proton peaks that are somewhat higher compared to the wanted product of mannuronan coupled with Me-O-Tyr. This is

due to the eter bond connecting the benzene ring and N-acylurea [44] shown in figure 14.

Since by-products from the carbodiimide reaction are removed by dialysis, the main focus will be to diminish the formation of adducts.

Increasing the carbodiimide concentration increase the probability of forming adducts, because of higher formation of O-acylisourea [12] [13]. The hydrolysis rate of O-acylisourea has been estimated to 2-3 s^{-1} at pH=4.75. This fast hydrolysis rate leads to lower coupling of amines (figure 8). However, adding N- hydroxysulfosuccinimide sodium salt (sulfo-NHS) can prolong the deactivation time. This compound stabilize O-acylisourea and lower the probability of rearrangement to N-acylurea. The reaction involves creation of a succinimidyl ester that hydrolyze slowly in aqueous media and can enhance the coupling efficiency for carbodiimides because of hindered N→O displacement. The proposed reaction mechanism is shown in figure 16 [43].

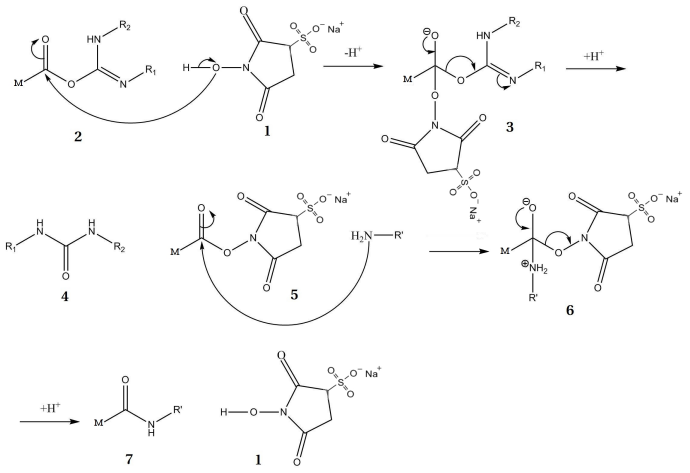

Figure 16: Hindered N→O displacement by sulfo-NHS. Sulfo-NHS (1) reacts with O-acylisourea(2), via an intermediate(3) creating a succinimidyl ester(5) and an urea derivate (4). The stable and active ester hydrolyze slowly in aqueous media and reacts with amines creating an amide (7) and recreating sulfo-NHS (1).

Incubating sulfo-NHS with EDC and mannuronic acids before adding amines ensures formation of the succinimidyl ester. The reaction between sulfo-NHS activated EDC-molecules and primary amines is most efficient at pH 7-8. Grabarek *et. al* suggest activation of EDC with sulfo-NHS in MES-buffer at pH= 5.0-6.0, and then raising the pH to 7.2-7.5 with phosphate buffer before adding the amine[46] [47].

The formation rate of N-acylurea from O-acylisourea (figure 13) is temperature dependent. The displacement can thus be diminished by letting the reaction between mannuronan and EDC take place at 0°C before adding the amine.

Some nucleophiles, such as *N,N*-dimethylaminopyridine (DMAP), Oxyma or hydroxybenzotriazole (HOBt), reacts faster with O-acylisourea. This prevents acyl transfer in O-acylisourea to N-acylurea[13]. However, HOBt has been reported to have explosive properties, making it a less attractive approach for diminishing adduct formation[48].

1.6.2 Model molecules for GRGDYP

Peptides are expensive and this is the main reason for using model molecules for optimalisation the reaction conditions for the carbodiimide mediated coupling of peptides to mannuronan. Model molecules have to be detected by the same analytical methods as the peptide, have the same solubility and have the same reactivity in the carbodiimide reaction.

Three molecules are suggested and tested as model molecules for GRGDYP in this study: fluoresceinamine(FA), 4-aminophenol(4AP) and L-tyrosine methyl ester (Me-O-Tyr). Their structure is shown in figure 17.

These model molecules are detectable at chemical shifts that does not interfere with the alginate peaks in ^{1}H NMR. They are also visible with UV/vis spectroscopy due to their benzene ring(s). Fluoresceinamine and Me-O-Tyr is even fluorescent and can be detected by fluorescent methods. The tyrosine structure in Me-O-Tyr is present in the peptide GRGDYP that is coupled to mannuronan, and they can both be detected at 280nm.

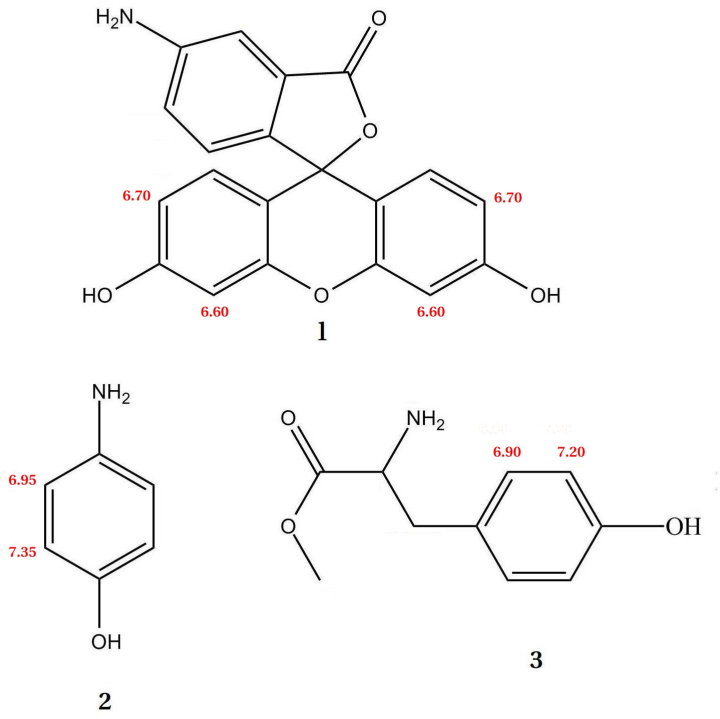

Figure 17: Model molecules used for coupling RGD to mannuronan. The numbers indicate the expected chemical shifts in ^{1}H NMR spectroscopy. **1:** Fluoresceinamine is detected by a multiplet at ∼6.60 ppm which represents the four protons indicated in the figure[49]. **2**: 4-aminophenol is detected by its four aromatic protons at 7.35 and 6.95 ppm. **3**: L-tyrosine methyl ester has four aromatic protons that peak at 6.90 and 7.20 ppm.

A ^{1}H NMR sample of GRGDYP was prepared in order to identify the protons in GRGDYP, and the sample was prepared as described in section 2.1. The resulting ^{1}H NMR specter is shown in figure 18.

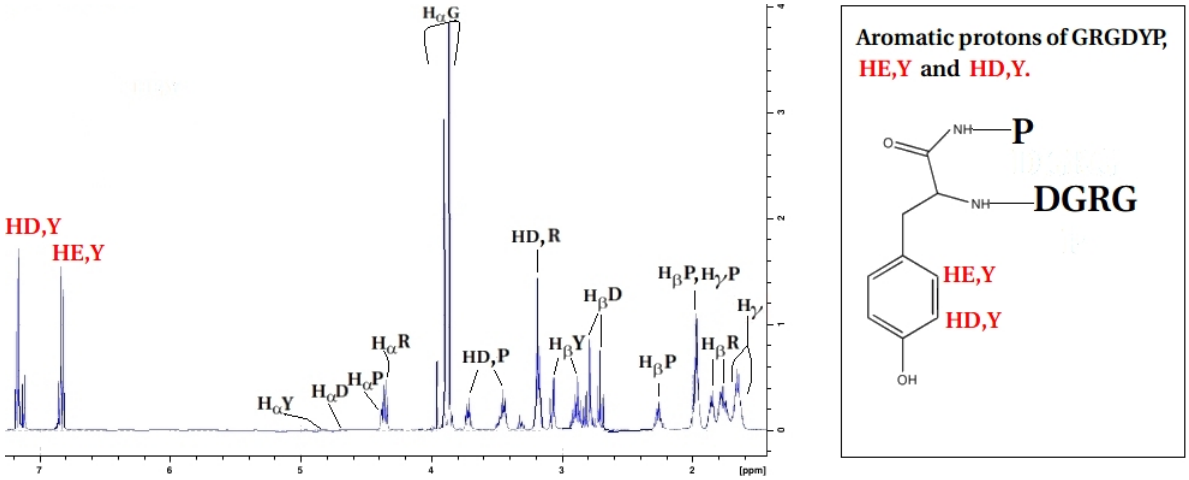

Figure 18: ^{1}H NMR spectrum for GRGDYP. The aromatic protons assigned *HD,Y* and *HE,Y* assigned at 6.90 and 7.20 ppm can be used for calculating the amount of GRGDYP coupled to mannuronan. The double peak adjacent to proton number *HD, Y* may be caused by isomerism. The spectra were recorded at 600MHz and 363K and the shifts were assigned by Finn L. Aachmann.

A ^{1}H NMR sample of Me-O-Tyr was prepared in order to compare the aromatic proton peaks with GRGDYP. The sample was prepared as described in section 2.1, and the ^{1}H NMR specter is shown in figure 19.

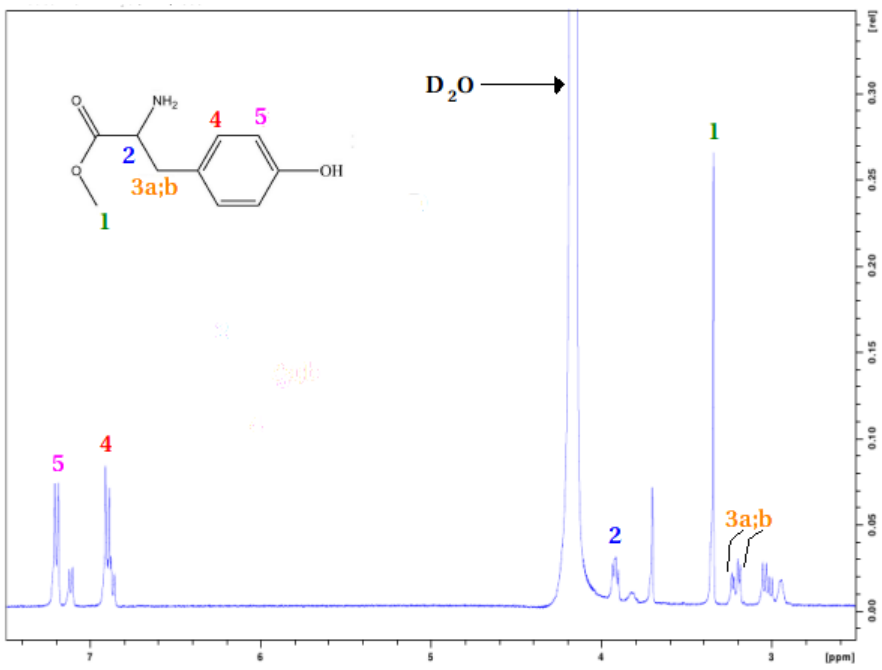

Figure 19: ^{1}H NMR spectrum for Me-O-Tyr. The aromatic protons assigned 5 and 4 can be used for deducing the amount of Me-O-Tyr coupled to mannuronan. Their chemical shift is not affected by coupling to mannuronan. As can be observed from the figure, there may be some isomerism in the sample, represented by the doublet situated between proton peak 5 and 4. The spectra were recorded at 400MHz.

The structural similarities between GRGDYP and Me-O-Tyr nominates Me-O-Tyr as an attractive model molecule.

2 Methods and materials

This section has been divided into four main parts. The first part lists the materials used in this study. The second part, named *Methods for optimalisation*, describes the protocols for how the carbodiimide chemistry was optimalised for maximum coupling, by varying reaction conditions such as pH, temperature and reactant concentrations. The reaction conditions that gave the wanted coupling degrees were implemented in the third part of this section, named *Large scale RGD-alginate*. Here, two batches of mannuronan were prepared for encapsulation. One batch was chemoenzymatically modified to RGD-alginate, while the other batch was prepared as a reference and is referred to as the non-peptide coupled sample. The fourth and final part describes the protocol for coupling chitosan dimers and insulin to mannuronan by utilising the optimalised carbodiimide chemistry described in the first part of this section.

2.1 Materials

Three sources of alginate were used in this study. High molecular mass mannuronan from epimerase-negative mutant ($AlgG^-$) of *P. fluorescens* purchased from SINTEF(batch: 206-011-01-TP, F_M=1, $[\eta]$=872 ml/g) was used for optimalising the carbodiimide reaction and served as a non-peptide coupled reference for large scale production of alginate. Ultrapure mannuronan from NovaMatrix (Ref. H3:512-216-01TP, F_M=1) was used for large scale peptide coupling, and alginate from Protanal (batch: S12727, LF 10/60, F_G=0.66, *L. hyperborea*, stipe) was used for coupling Me-O-Tyr onto alginate beads.

2-[N-morpholio]ethanesulfonic acid (MES-buffer), the coreactant [7] N- hydroxysulfosuccinimide sodium salt (sulfo-NHS), N-(3-dimetylaminopropyl)-N'-ethylcarbodiimide hydrochloride (EDC), hydroxylamine hydrochoride, 3-N[morpholino]propanesulfonic acid (MOPS), 4-aminophenol(4AP), L-Tyrosine methyl ester (Me-O-Tyr), bovine (5733.49Da) and porcine insulin (5777.54Da) were purchased from Sigma-Aldrich.

The peptide GRGDYP was purchased from AlBioTech and Caslo Laboratory. GRGDYP from AlBioTech was used for optimalising peptide coupling, while GRGDYP from Caslo Laboratory was used for large-scale peptide coupling.

$Cacl_2$ and NaCl was purchased from Merck. Phosphate buffered saline (PBS) was purchased from Calbiochem. Ethylenediaminetetraacetic acid(EDTA) was purchased from VWR International. Fluoresceinamine (FA) was purchased from Fluka analytical.

2.2 Methods for optimalisation

The following general coupling protocol describes how 4AP, Me-O-Tyr and GRGDYP are coupled to mannuronan and is followed unless otherwise stated. Coupling of FA to mannuronan is described in subsection 2.4.

General coupling protocol for optimalisation of carbodiimide reaction

High molecular weight polymannuronan (SINTEF) was degraded as described in subsection 2.3. One parallel corresponds to 10mg mannuronan dissolved in 1mL 0.1M MES-buffer with 0.3M NaCl. This equals a mannuronan concentration of 1% (w/v).

Sulfo-NHS and EDC were solvated in separate eppendorf tubes in MES-buffer with the same pH and saline concentration as in the reaction tube. Solutions of 5.05mM EDC and sulfo-NHS were freshly made for each experiment. The amount of sulfo-NHS and EDC added is shown as a relative percentage to the carboxylic units in mannuronic acids (-*COOH in M*). Sulfo-NHS was added prior to EDC. After addition of EDC, the reaction was incubated for 20 minutes at room temperature by rotation.

The coupling molecule was solvated in the same MES-buffer system as the reaction tube in a separate eppendorf tube. The amount of coupling molecule added is also shown as a relative percentage to the mannuronic acids.

Upon addition of the coupling molecule, the reaction tube was incubated at room temperature by rotation.

The samples were dialysed as described below.

Dialysis and purification protocol

This protocol describes how the dialysis and purification was performed. The protocol is valid for the optimalisation reactions.

Dialysis was performed with membranes from Spectrum Laboratories (Spectra/Por Dialysis Membrane, MWCO: 12-14000) at room temperature unless otherwise stated, with three shifts of MQ-water, three shifts of 50mM NaCl and finally shifts of MQ-water until the conductivity was below 2μSiemens.

The samples were filtrated with non-sterile Acrodisc 25mm Syringe Filter, with 5μm Versapor Membrane, before lyophilization and analysis. Filters from the same producer with filter size 0.2μm was used for filtration of FA.

Analysis of product

Experiments describing coupling of FA, 4AP, insulin and chitosan were analysed by ^{1}H NMR. Experiments describing coupling of Me-O-Tyr and GRGDYP were analysed by UV/vis spectroscopy at 280nm in addition to ^{1}H NMR. The analysis with ^{1}H NMR was recorded with 400MHz at 363K unless otherwise stated.

For UV/vis detection, NanoDrop Spectrophotometer(abs.scan λ=210-530nm), ND-1000, from Saveen Werner, was used. Absorbance of Me-O-Tyr and GRGDYP was measured at 280nm.

1D proton NMR spectra were recorded by Wenche I. Strand (NTNU, Department of Biotechnology) or Finn L. Aachmann (NTNU, Department of Biotechnology) on a Bruker Avance 300 MHz equipped with QNP probe or Bruker Avance 400 MHz equiped with DUL probe. The temperatures were set to 363K. NMR Diffusion experiments were carried out on a Bruker Avance 600 MHz spectrometer equipped with a 5mm z-grad CP-TCI probe capable of generating a field gradient of 0.6 T$\cdot$m^{-1}. The temperatures for 600MHz were set to 363K. ^{1}H diffusion spectroscopy was performed by Finn L. Aachmann. The experimental setup for diffusion spectroscopy was based on stimulated echo pulsed gradient spin echo (SE-PGSE) pulse sequence. Gradient pulses of 2 ms duration and 32 different strengths varying from 0.03 T$\cdot$m^{-1} to 0.57 T$\cdot$m^{-1} were employed for dephasing and refocusing. The diffusion delay was set to 120 ms.

Spectra processing and analysis were performed with XWinNMR 2.6, 3.5 or Topspin 3.0 (Bruker Biospin). Samples were prepared by adding 600 μL 99.9% deuterium oxide (D_2O) and 5μL of a chemical shift reference compound (trimethylsilylpropionic acid, 1%) to substituted mannuronan ($\sim$10mg). For determining alginate composition, 20μL TTHA(Triethylenetetraminehexacetic acid) was added for Ca^{2+} chelation.

2.3 Degradation of mannuronan

Mannuronan was dissolved in Milli-Q-water (MQ, 800mL) by stirring with magnet. The pH was adjusted to 5.60 and incubated at 95°C (water bath) for 1 hour. The samples were cooled and adjusted to pH=3.80 before incubation at 95°C (water bath) for 30 minutes. The samples were cooled again and the pH adjusted to 6.90 before lyophilization.

The average degree of polymerisation was calculated by ^{1}H NMR and was approximated to 40-50. The ^{1}H NMR spectra and calculations are included in appendix A.

2.4 Coupling of FA

Fluoresceinamine was used as a model molecule because it can be detected at ∼6.65 ppm in ^{1}H NMR. It is also fluorescent and has an absorption maximum of 496nm. Work performed by master student Marita Westhrin on coupling FA to mannuronan, gave no clear correlation between added FA and coupled FA [49]. It was hypothesized that the solubility of FA probably affected the coupling reaction and this was investigated as described below. The coupling protocol of FA described here was based on Westhrins work.

2.4.1 Coupling of solvated and dry FA

The amount of FA added in this protocol corresponds to 5% relative to the carboxylic units of mannuronic acids.

Two samples were prepared for this experiment. Sample 1 was prepared by adding 4.9mg dry FA to each parallel. Sample 2 was prepared by adding 300μL of a 19.6mM suspension of FA, solvated in 0.1M MES-buffer with 0.3M NaCl to each parallel. The procedure was performed under protection from light to avoid photodecay of FA.

Table 1 show the amount of FA, sulfo-NHS and EDC added to the different samples.

Table 1: Added reactants for coupling of FA

Sample	Parallel	Added FA	Added EDC and sulfo-NHS(Rel.% to -COOH in M)
1	1 2 3 4 5	4.9mg	10
2	1 2 3 4 5	300μL of 19.6mM FA	10

One parallel was prepared as described in the following paragraph:

50 mg mannuronan ($\overline{DP_n}$=40-50, see subsection 2.3) was dissolved in 5mL 0.1M MES-buffer with 0.3M NaCl (pH=5.5) giving a mannuronan concentration of 1% (w/v). Dry weight sulfo-NHS was added and left to dissolve before adding dry weight of EDC. After solvation of EDC, the beaker was incubated at room temperature under stirring with magnet for 10 minutes. FA was added as described in table 1 and the reaction was left to incubate at room temperature under stirring with magnet for two hours.

The samples were filtrated, dialysed and lyophilased as described under the **Dialysis and purification protocol** with the following changes:

Dialysis was performed at 4°C and protected from light. Lyophilization was performed under protection from light.

2.4.2 Solubility of FA in Ethanol-MES-buffer

The solubility of FA in 0.1M MES-buffer was examined by increasing the polarity of the solvent with ethanol (EtOH).

Solvents (1.5mL) of 0, 20, 50, 70 and 96% EtOH were prepared in 0.1M MES-buffer with 0.3M NaCl (pH=5.5). A parallel of each solvent was added to a micro plate to serve as a reference.

0.042mM solutions of FA were prepared in the solvents described above, and stirred with magnet for 2.5 hours at room temperature under protection from light. The samples were filtrated as described in the **Dialysis and purification protocol**. Five parallels (200μL) of each filtrate was pipetted on to a micro plate for qualitative comparison.

2.5 Coupling of 4AP

The solubility of FA in 0.1M MES-buffer was not considered adequate for coupling to mannuronan, and 4AP was tested as a novel model molecule for coupling GRGDYP to mannuronan. The solubility in MES and PBS, pH-dependance and kinetics of coupling 4AP were investigated to determine if these reaction conditions changed the degree of coupling to mannuronan.

For the coupling of 4AP, the **General coupling protocol** was followed with the following changes: 4AP was added to a theoretical coupling of 5% to the carboxylic units of mannuronan. The amount of EDC and sulfo-NHS added corresponds to 10% for all samples described below.

2.5.1 Coupling 4AP in MES-buffer or PBS

Phosphate buffered saline is a buffer commonly used in biological research and is an alternative standard buffer to MES. Comparing coupling of 4AP to mannuronan in both buffers can indicate which buffer system gives the highest coupling percentages.

The **General coupling protocol** was followed with the following changes:

Three parallels of mannuronan were dissolved in MES-buffer (pH=5.5) and three parallels were dissolved in PBS (140mM NaCl, 3mM KCl, pH=5.5). Mannuronan was incubated with 4AP for two hours.

2.5.2 Kinetics of coupling 4AP

The reaction time between 4AP and activated mannuronic acids may be longer than the 2 hours suggested by Westhrin[49]. To determine the reaction curve of coupling 4AP to mannuronan, a time series was set up.

The **General coupling protocol** was followed with the following changes:

Seven samples were prepared and coupled with 4AP in MES-buffer (pH=5.5). 130μL 10mM of the quencher hydroxylamine hydrochloride[46] was added after 15 minutes, 30 minutes, 1 hour, 2, 4, 8 and 24 hours reaction time. The amount of quencher added corresponds to 10 000 times the amount of sulfo-NHS and EDC added.

Two parallels were made for each sample, except for the 2 hour sample. As a reference, the quencher was not added to one of the 2 hour parallels.

2.5.3 Varying pH for coupling 4AP

The **General coupling protocol** was followed with the following changes:

Three samples were prepared in MES-buffers with different pH-values (pH= 5.5, 6.0 and 6.5) and two parallels were made for each sample. The parallels were rotated for 10 hours before dialysis. Mannuronan was incubated with 4AP for two hours.

An absorbance experiment was conducted in order to determine the percentage coupling of 4AP to mannuronan. Standards of 4AP in MQ-water were prepared (1mM, 0.5mM and 0.25mM) and compared to the 4AP-mannuronan parallels.

2.6 Coupling of Me-O-Tyr

4AP showed some drawbacks as a model molecule for GRGDYP as it changed its absorbance spectrum once coupled to mannuronan. This means that UV/vis spectroscopy can not be used as a detection method for 4AP coupled to mannuronan. Also, 4AP demand careful handling as it is a possible mutagen[50].

Me-O-Tyr was tested as a model molecule for GRGDYP as it has a closer resemblance to an amino acid, is detectable by UV/vis spectroscopy and peaks at approximately the same chemical shift as tyrosine protons of GRGDYP in ^{1}H NMR.

Variations in coupling degrees when changing temperature, pH, and amounts of reactants added were investigated to deduce the optimal coupling of GRGDYP.

Results from the kinetics of coupling 4AP to mannuronan indicated that the reaction time should be increased from the initial two hours[49] to above eight.

2.6.1 Varying temperature for Me-O-Tyr coupling

The amount of adducts can be lowered by reducing the temperature, as the conversion of O-acylisourea to N-acylurea is slowed down[13]. The influence on the incubation temperature was investigated in this experiment.

Me-O-Tyr was added to a theoretical coupling of 5%. The **General coupling protocol** was followed with the following changes:

Two mannuronan samples were dissolved in MES-buffer(pH=6.0) as shown in table 2.

Table 2: Added reactants and temperature for coupling Me-O-Tyr

Sample	Parallel	Temperature (°C)	Added EDC and sulfo-NHS (Rel.% to -COOH in M)
1	1 2	20	10
2	1 2	0	10

The samples were incubated by rotation over night at room temperature.

2.6.2 Optimal reaction time at 0°C

The incubation time at 0°C may influence the amount of Me-O-Tyr coupled[13] and the degree of coupling was investigated as a function of incubation time at 0°C.

Me-O-Tyr was added to a theoretical coupling of 5%. The **General coupling protocol** was followed with the following changes:

Three mannuronan samples were prepared and dissolved in MES-buffer (pH=6.0). Mannuronan in MES-buffer was cooled (ice bath) before sulfo-NHS and EDC were added. Sulfo-NHS, EDC and mannuronan were incubated at different incubation times as shown in table 3.

Table 3: Added reactants and incubation time at 0°C for coupling Me-O-Tyr

Sample	Parallel	Time at 0°C (min)	Added EDC and sulfo-NHS (Rel.% to -COOH in M)
1	1 2	20	10
2	1 2	40	10
3	1 2	60	10

Me-O-Tyr was added and the samples were incubated by rotation over night at room temperature.

A standard series (1mM, 0.75mM, 0.50mM and 0.25mM) of Me-O-Tyr was prepared in MQ-water for UV/Vis- detection of tyrosine[51].

2.6.3 Varying pH at 0°C for coupling Me-O-Tyr

Me-O-Tyr was added to a theoretical coupling of 5%. The **General coupling protocol** was followed with the following changes:

Three mannuronan samples were prepared as shown in table 4

Table 4: Added reactants and pH for coupling Me-O-Tyr

Sample	Parallel	pH in MES-buffer	Added EDC and sulfo-NHS (Rel.% to -COOH in M)
1	1 2	5.5	10
2	1 2	6.0	10
3	1 2	6.5	10

Mannuronan in MES-buffer was cooled (ice bath) before sulfo-NHS and EDC were added. Sulfo-NHS, EDC and mannuronan were incubated at 0°C for 60 minutes before Me-O-Tyr was added. The coupling of Me-O-Tyr to mannuronan was incubated by rotation over night at room temperature.

2.6.4 Coupling Me-O-Tyr to alginate beads

Coupling Me-O-Tyr to mannuronic acids that are immobilized in an alginate network offer a novel approach to carbodiimide coupling. The hypothesis is that EDC can activate mannuronic acids inside the network and facilitate coupling as the mannuronic acids are not as tightly linked in junctions as G-blocks.

0.45 g alginate from Protanal (LF 10/60) was solvated in 25mL distilled water corresponding to an alginate concentrations of 1.8% (w/v). Alginate was dripped into an aqueous solution containing Ca^{2+} ions (50mM $CaCl_2$)[52] utilising an electrostatic bead generator with the following settings:

- Voltage: 700kV
- Flow: 40mL/hour
- Distance between needle and geling bath: 2.5 cm
- Four needles with needle size 0.35mm

The beads were left in the geling bath for ten minutes to ensure proper geling. The beads were collected from the gelling solution and washed three times with an aquoeus solution containing 0.9M NaCl and 2mM $CaCl_2$. The average bead size was estimated from 30 beads to be 494.8±21.17μm by light microscopy (Nikon Eclipse TS100, 40x magnification).

The water phase was exchanged with 15mL EtOH in a stepwise manner (25%, 30%, 40%, 50%, 60%, 70%, 80%, 90%, 96%). The beads were left in each solvent for 20 minutes before increasing the EtOH concentration[53]. The average bead size was estimated from 30 beads to be 359.8±16.20μm.

The solvent was further exhanged to formamide in two steps (50%, 100%) and the bead size from 30 beads was estimated to 463.4±9.56μm. The beads swelled with 28% from 96% EtOH to 100% formamide.

Beads corresponding to ∼32mg alginate (∼3 mL) were transferred to a beaker and stirred gently with a magnet. Sulfo-NHS corresponding to 10% of the carboxy units in alginic acids was added before adding 10% EDC. The reaction was incubated for 20 minutes at room temperature by gentle stirring with magnet. Me-O-Tyr corresponding to 20% of the alginic acids was added. The beads were incubated over night at room temperature by gentle stirring by magnet.

The beads were removed from the reaction beaker and washed with 5mL 100% formamide three times and 5mL MQ-water three times. 5mL of 50mM EDTA(pH=7.01) was added to dissolve the beads before dialysis.

The sample was degraded by acid hydrolysis (see paragraph 2.3) before filtration and lyophilization as described in the **Dialysis and purification protocol**.

2.6.5 Varying amount of EDC and Me-O-Tyr added

Differences in reactant concentrations was previously shown by Westhrin to influence the coupling of FA to mannuronan[49]. Westhrin found that if the concentration of sulfo-NHS exceeded EDC, the coupling was effected in a negative manner. Therefore, the concentrations of EDC and sulfo-NHS were kept equal in this protocol, while the added Me-O-Tyr was increased.

The **General coupling protocol** was followed with the following changes:

Mannuronan samples were prepared in MES-buffer (pH=6.0) as described in table 5.

Table 5: Added reactants in relative percentage to carboxy units in mannuronan

Added EDC and sulfo-NHS	Added Me-O-Tyr
10	5 10 15 20
20	5 10 15 20

The parallels were incubated over night by rotation at room temperature.

2.6.6 Coupling with excess of Me-O-Tyr

The results from coupling with increasing amounts of Me-O-Tyr indicated that there might be a correlation between the amount Me-O-Tyr added and the amount Me-O-Tyr coupled. The degree of coupling Me-O-Tyr to mannuronan, when Me-O-Tyr>> EDC and sulfo-NHS, was tested by keeping sulfo-NHS and EDC concentrations constant while the Me-O-Tyr concentrations were increased up to 100% of the carboxylic groups of mannuronan.

The **General coupling protocol** was followed with the following changes:

Samples were prepared in MES-buffer (pH=6.0) as described in table 6.

Table 6: Added amount of reactants relative to the carboxylic acids of mannuronan

Sample	Parallel	Added Me-O-Tyr (%)	Added EDC and sulfo-NHS (%)
1	1 2	20	10
2	1 2	40	10
3	1 2	60	10
4	1 2	80	10
5	1 2	100	10

The parallels were incubated over night by rotation at room temperature.

2.7 Coupling of GRGDYP

Determining which model molecule that mimics the coupling of GRGDYP to mannuronan best, can be determined by comparing the coupling of GRGDYP under the same reaction conditions as the model molecules. Here, the pH for coupling GRGDYP was varied as was done for 4AP and Me-O-Tyr. Increasing the GRGDYP concentrations with constant sulfo-NHS and EDC concentrations was performed in a similar fashion to Me-O-Tyr (see subsection 2.6.5). If the results show similarities, this would indicate that Me-O-Tyr is a suitable model molecule for GRGDYP.

2.7.1 Activating mannuronan at pH=4.2

The formation of O-acylisourea is faster at pH-values 3.5-4.5[13]. Incubating mannuoronan with EDC and sulfo-NHS at lower pH-values than 6.0, can deduce if the coupling is enhanced at lower pH-levels.

The **General coupling protocol** was followed with the following changes:

Mannuronan (200 mg) was dissolved in MES-buffer (pH=4.2). Sulfo-NHS and EDC corresponding to 10% of the carboxylic acids of mannuronan was added to the beaker. The solution was stirred for 20 minutes by magnet at room temperature. The pH was adjusted to 5.8 before adding 5% GRGDYP. The pH was further adjusted to 6.0 before incubation by magnetic stirring over night at room temperature.

2.7.2 Varying pH for coupling GRGDYP

GRGDYP was added to a theoretical coupling of 5%. The **General coupling protocol** was followed with the following changes:

Two mannuronan samples were prepared as shown in table 7.

Table 7: Added reactants and pH for coupling Me-O-Tyr

Sample	Parallel	pH in MES-buffer	Added EDC and sulfo-NHS (Rel.% to -COOH in M)
1	1 2	5.5	10
3	1 2	6.5	10

The parallels were left to incubate with GRGDYP by rotation over night at room temperature.

2.7.3 Varying amount of GRGDYP added and pH

Comparing coupling at low pH with higher pH-values with constant EDC and sulfo-NHs concentrations, and at the same time increasing the amount of peptide added, can indicate whether these factors increase the coupling degree.

The **General coupling protocol** was followed with the following changes:

Table 8 show the pH and added amounts of GRGDYP, sulfo-NHS and EDC in relative concentration to the carboxylic acids of mannuronan.

Table 8: Added GRGDYP when varying the pH and added GRGDYP

pH	Parallel	Added GRGDYP (%)	Added sulfo-NHS and EDC (%)
4	1	5	10
	2	10	
	3	15	
	4	20	
6	1	5	10
	2	10	
	3	15	
	4	20	

The samples were incubated over night by rotation at room temperature.

2.8 Large scale RGD-alginate

This subsection describes how two samples of mannuronan were epimerised by two different enzymes: AlgE4 and AlgE6. One of the samples was coupled with peptides while the other was not. The protocol is based on previous work by master student Kristin Karstensen[54] and involves three steps:

First, an epimerisation test was performed in order to determine which incubation time with AlgE6 gave the wanted F_G on a polyalternating backbone. Second, one of the samples was coupled with GRGDYP, implementing the results from the optimalisation section such as pH and relative reactant concentrations. Third, both mannuronan samples were epimerised before the final step of purification with active coal filtration.

In order to follow the reaction steps described above, samples of ∼10mg were taken out for ^{1}H NMR analysis.

2.8.1 Epimerisation test

The epimerase AlgE4 from *A. vinelandii* produced in *Hansenula polymorpha* was used to introduce alternating MG-blocks to mannuronan[22] to an expected F_G value of 0.40-0.47[55], while the epimerase AlgE6 from *E. coli* was used to insert G-blocks[23]. A time series was set up for epimerisation to find the incubation time for AlgE6 which gave approximately F_G value of 0.50-0.60 on a polyalternating backbone[55].

The mannuronan sample (0.25% (w/v)) was prepared as described in the following paragraph:

50mg of mannuronan was dissolved in 13mL MQ-water by magnetic stirring over night at room temperature. 50mL stock solution of 200mM MOPS-buffer with 40mM NaCl and 10mM $CaCl_2$ was prepared and pH-adjusted to 6.9. 5mL of the stock solution was added to the dissolved mannuronan, giving a MOPS concentration of 50mM, a $CaCl_2$ concentration of 2.5mM and a NaCl concentration of 10mM.

The sample was left to incubate at 37 °C for one hour before adding AlgE4 (dissolved in 1mL MQ-water) to an enzyme:mannuronan-ratio of 2:50. The sample was left to incubate by magnetic stirring over night at the same temperature. A sample was taken out for ^{1}H NMR analysis. 200mM NaCl was added to the reaction beaker to a total concentration of 75mM before adding AlgE6 (dissolved in 1mL MQ-water) in an enzyme:alginate-ratio of 1:200.

Samples of 50mL were taken from the incubation beaker after 1,2,4 and 6 hours. The enzymatic reaction was stopped by adding 50mM EDTA (pH=7.0) to a total concentration of 4mM. The sample was heated immediatly in water bath (95°C) for ten minutes to inactivate the enzyme.

The samples were cooled in room temperature before dialysis (Spectra/Por Dialysis Membrane, MWCO: 12-14000) against three shifts of 50mM NaCl to remove the Ca-EDTA complex, and shifts of MQ-water until the conductivity was below 2μSiemens.

The degree of epimerisation was calculated by ^{1}H NMR spectroscopy.

2.8.2 Chemoenzymatically modified RGD-alginate

Two samples of mannuronan were prepared. One sample was collected from ultrapure mannuronan and was used for peptide coupling. This sample is referred to as *the peptide coupled sample*. The other sample, referred to as *the non-coupled sample*, was collected from epimerase-negative mutant *P. fluorescens* and served as a reference to the peptide coupled sample.

Peptide coupled sample

Ultrapure mannuronan (500mg) was dissolved in 0.1M MES-buffer with 0.3M NaCl (pH=6.0) with magnetic stirring, to a mannuronan concentration of 0.25%(w/v).

Sulfo-NHS and EDC, corresponding to 10% of the carboxylic acids of mannuronan, were added and left to stir in 20 minutes before adding GRGDYP corresponding to 5%. The sample was incubated by magnetic stirring in room temperature over night, before dialysis (Spectra/Por Dialysis Membrane, MWCO: 12-14000) with three shifts of MQ-water, three shifts of 50mM NaCl and one shift of 20mM NaCl.

One sample, corresponding to ∼10mg mannuronan, was taken out in order to deduce the peptide coupling by ^{1}H NMR. This sample was further dialysed with shifts of MQ-water until the conductivity was below 2μSiemens. The sample was degraded as described in subsection 2.3, before analysis with ^{1}H NMR.

Epimerisation

The peptide coupled, and the non-peptide coupled samples were epimerised as described below.

500mg of mannuronan was dissolved in 130mL MQ-water by magnetic stirring over night at room temperature, corresponding to a 0.25% (w/v) mannuronan solution. 50mL stock solution of 200mM MOPS-buffer with 40mM NaCl and 10mM $CaCl_2$ was prepared and pH-adjusted to 6.9. The stock solution was added to the dissolved mannuronan, giving a MOPS concentration of 50mM, a $CaCl_2$ concentration of 2.5mM and a NaCl concentration of 10mM.

The sample was left to incubate at 37 °C for one hour before adding AlgE4 (dissolved in 10mL MQ-water) to an enzyme:mannuronan-ratio of 2:50. The sample was left to incubate by magnetic stirring over night at the same temperature. A 10mg sample was taken out for ^{1}H NMR analysis. 200mM NaCl was added to the reaction beaker to a total concentration of 75mM before adding AlgE6 (dissolved in 10mL MQ-water) in an enzyme:alginate-ratio of 1:20. AlgE6 was incubated at 37°C with gentle stirring for 2.5 hours, before stopping the reaction with 50mM EDTA (pH=7.0) to a total concentration of 4mM. The sample was heated immediatly in water bath (95°C) for ten minutes, in order to inactivate the enzyme.

The samples were cooled in room temperature before dialysis (Spectra/Por Dialysis Membrane, MWCO: 12-14000) against three shifts of 50mM NaCl to remove the Ca-EDTA complex.

Samples (∼10mg) were taken out after AlgE4 and AlgE6 epimerisation. These were further dialysed with MQ-water until the conductivity was below 2μSiemens. The samples were degraded as described in subsection 2.3, before analysis with ^{1}H NMR.

Purification by active coal filtration

Alginates contain biological compounds such as endotoxins (LPS), proteins, complex polysaccharides and polyphenols. AlgE6 contributes to contaminants as it is produced in *E.coli*. These contaminants are potentially harmful to sensitive cells and must be removed before encapsulation[56]. Removal of these compounds can be achieved by active coal filtration as the filter retain hydrophobic molecules in the pore walls due to van der Waals interactions[57].

The following procedure was performed in a water bath at 50°C. The concentration of NaCl in the alginate samples was adjusted to 0.171M (1%), assuming that the initial concentration of NaCl was the same as the dialysis water of 50mM NaCl.

Tubes connected to the filters were filled with 0.1M NaOH and left for 20 minutes before rinsing with 900mL MQ water. Filters from Millipore (Millistak+® media in μPod(TM) format CR40 26sq.cm) were attached to the tubes and saturated with MQ-water. The system was rinsed with 900mL of 0.1M HCl and MQ-water until the pH was approximately 4-5. The exterior of the tubes were rinsed with 70% EtOH before the sample was applied.

The samples were run through the filter once, before recirculation over night. The non-coupled sample was filtrated twice due to its bacterial origin.

After filtration, 200mL of sterile water was rinsed through the tubes to collect any remaining alginate. The samples were transferred to dialysis membranes (Spectra/-Por Dialysis Membrane, MWCO: 12-14000) that had been washed with sterile water. The dialysis was performed in sterile containers with MQ-water at room temperature until the conductivity was below 2μSiemens.

The pH was adjusted to 7 before lyophilization and use for encapsulation of olfactory ensheating cells from neonatal rat brain, performed by co-student Marthe Fredheim Fjelldal at the Department of Cancer Research and Molecular Medicine.

2.9 Coupling of chitosan and insulin

This final and fourth part of the *Methods*-section demonstrates how carbodiimide chemistry can be utilised to couple other molecules than peptides to mannuronan.

Theoretically, any molecule that contains an amine residue and that is soluble in aqueous solvents can be coupled to mannuronan with carbodiimide chemistry. Here, two insulin types and a chitosan dimer are coupled to mannuronan. Bovine and porcine insulin both have tyrosine residues that are visible in ^{1}H NMR (as shown in subsection *1.6.2 Model molecules*), and contain amine-residues that can be coupled to mannuronan with EDC[58]. Chitosan dimers consisting of N-acetylglucosamine(A) and D-glucosamine (D) was tested as a possible coupling agent to mannuronan as D has a vacant amine group. The presence of acetyl protons in A can be calculated by ^{1}H NMR. The AD-structure is enclosed in appendix U.

For coupling of insuline, the **General coupling protocol** was followed with the following changes:

Two mannuronan samples were prepared in MES-buffer (pH=6.0) before adding 10% sulfo-NHS and EDC. Bovine and porcine insulin were added in a relative percentage of $\sim$10% to the carboxylic acids of mannuronan.

For coupling of chitosan, the **General coupling protocol** was followed with the following changes:

Four mannuronan samples were prepared in MES-buffer (pH=6.0) with 10% sulfo-NHS and EDC. Samples with 5, 10, 15 and 20% of chitosan were prepared.

3 Results

The *Results* section is divided into three main parts: The first part describes the results from optimalising the coupling to mannuronan with FA, 4AP, Me-O-Tyr and GRGDYP, respectively. The second part show the results from the large scale production of RGD-coupled alginate, while the third part show the results from coupling insulin and chitosan to mannuronan.

^{1}H NMR spectra, tables and UV/vis spectra are included in the appendicies.

3.1 Coupling of FA

FA was initially used as a model molecule for peptide coupling as described previously by student Marita Westhrin[49]. FA contain three aromatic rings which have low water solubility compared to GRGDYP.

3.1.1 Coupling of solvated and dry FA

Mannuronan was activated with 10% EDC and sulfo-NHS, while 5% FA was added. Two samples with five parallels (n=5) were made. The sample named *dry FA* was prepared by adding dry weight FA corresponding to 5% of the mannuronic acids. The sample named *solvated FA* was prepared by adding 300μL of a 19.6mM suspension of FA in 0.1M MES-buffer with 0.3M NaCl, also corresponding to 5% FA.

The degree of coupling dry FA (black) and solvated FA (purple) are shown graphically in figure 20. The figure shows that the highest degrees of coupling were achieved when adding dry FA.

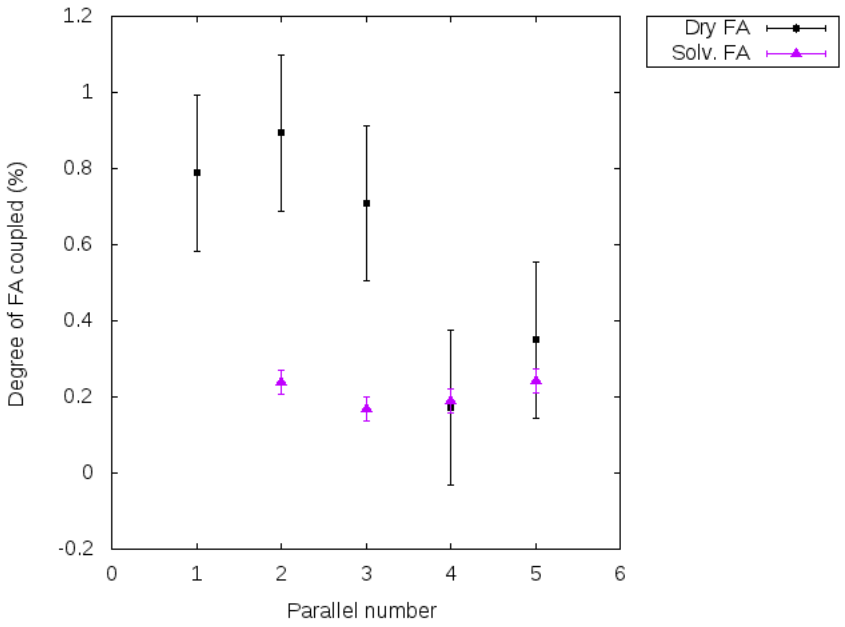

Figure 20: Coupling dry weight and suspended FA (%) to mannuronan in MES-buffer(pH=5.5). The degree of coupling FA to mannuronan was calculated from ^{1}H NMR spectra. By setting the aromatic proton peak for fluoresceinamine (6.65 ppm) equal to one, and integrating the mannuronan peak at 4.70 ppm, the relative amounts of FA can be calculated (see appendix B for a detailed description of calculations). Four parallels are shown for the solvated FA. Parallel 1 for this sample gave no signal when analysed by ^{1}H NMR. This was probably due to large precipitates of FA observed under dialysis. Errorbars show calculated standard deviations from parallels (Dry: n=5 and Solv.: n=4) for each sample. Integrals and calculations are included in appendix C.

3.1.2 Solubility of FA in Ethanol-MES-buffer

FA is hydrophobic (figure 17) and is less soluble in aqueous solvents such as 0.1M MES-buffer. Lowering the polarity of the MES-buffer with EtOH can indicate which solution is beneficial for increased FA solubility.

Five different solvents were prepared with increasingly amounts of EtOH, and stock solutions of FA was prepared to a total concentration of 0.042mM. 200μL of each solvent was pipetted to a microplate for qualitative comparison of FA solubility.

Figure 21 show the micro plate with FA in different ratios of EtOH-MES solvents. It can be seen from the figure that the solubility of FA increases with increasing

concentration of EtOH, and that the most prominent change takes place from 20% EtOH to 50% EtOH.

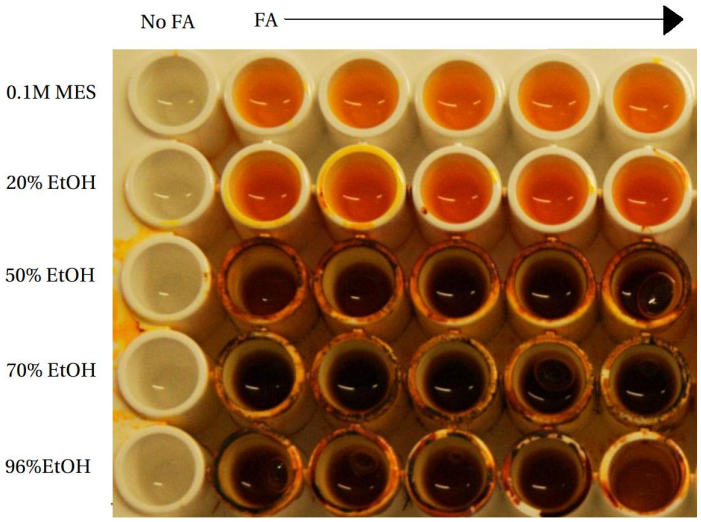

Figure 21: Micro plate with FA in different ratios of EtOH-MES solvents. The wells, starting from the top left row, contains 0.1M MES, 20% EtOH, 50% EtOH, 70%EtOH and 96% EtOH, respectively. The leftmost coulumn in each row contains pure solvent, followed by five parallels of the solvent with fluoresceinamine.

3.2 Coupling of 4AP

The solubility of FA in 0.1M MES-buffer was considered too low, and performing carbodiimide mediated coupling in 50% EtOH-MES-buffer would cause precipitation of mannuronan. Based on these conclusions, 4AP was tested as a novel model molecule for peptide coupling to mannuronan.

3.2.1 Coupling 4AP in MES-buffer or PBS

An alternative buffer to MES is PBS, and the coupling of 4AP to mannuronan was tested in both buffers to detect any changes in the degree of coupling.

Figure 22 show coupling 4AP to mannuronan when the theoretical coupling is 5%. Three parallels (n=3) were prepared for each sample.

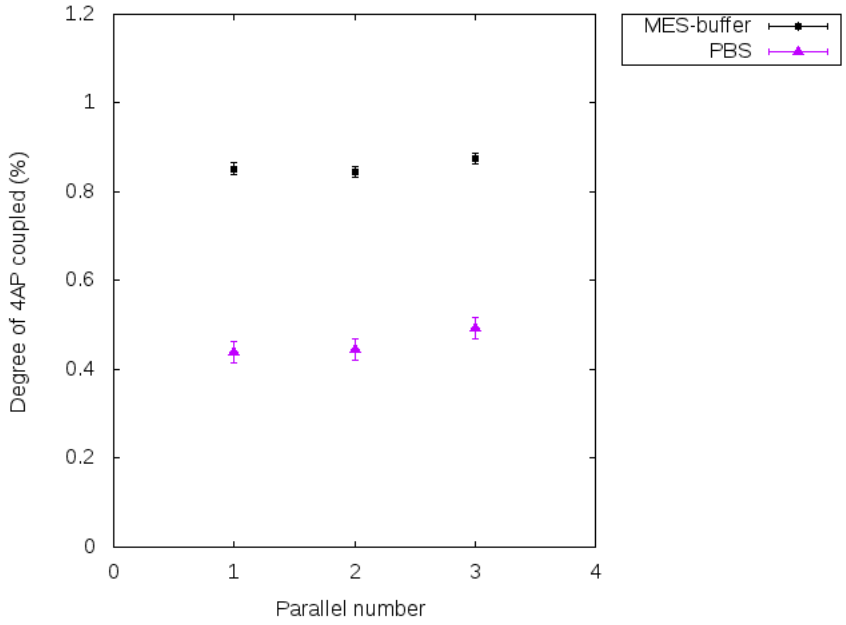

Figure 22: Degreee of coupling of 4AP in 0.1M MES-buffer (pH=5.5) and PBS (pH=5.5). 5% 4AP was added to mannuronan activated with 10% EDC and sulfo-NHS. The degree of coupling 4AP to mannuronan was calculated from integration of aromatic protons of 4AP at 6.95 ppm and 7.35 ppm in ^{1}H NMR spectra (see appendix B for detailed description of calculations). Standard deviations were calculated (n=3) for both samples and are indicated as error bars in the figure. Integrals, ^{1}H NMR spectra and calculations are included in appendix D

3.2.2 Kinetics of coupling 4AP

The coupling efficiancy of 4AP was tested as a function of time. The reaction was quenched with hydroxylamine hydrochloride after 15 min, 30 min, 1 hour, 2, 4, 8 and 24 hours. Seven samples were prepared, with two parallels (n=2) for each sample except the two hour sample where only one parallel (n=1) was prepared.

Figure 23 show that the percentage bound 4AP continued to increase after two hours, levelling off between four to eight hours and dropping between eight and 24 hours.

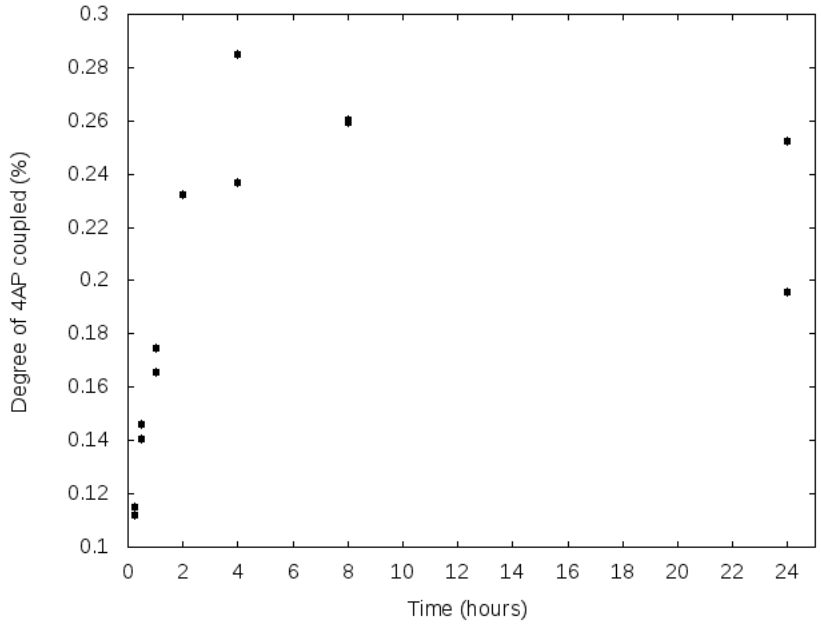

Figure 23: Percentage bound 4AP as a function of time. 5% 4AP was coupled to mannuronan in 0.1M MES-buffer (pH=5.5) activated with 10% EDC and sulfo-NHS. The percentage bound 4AP to mannuronan was calculated from integration of aromatic proton peaks of 4AP at 6.95 ppm and 7.35 ppm from ^{1}H NMR spectra (see appendix B for detailed description of calculating percentage bound 4AP to mannuronan). The reaction was quenched after 15 min, 30 min, 1 hour, 2, 4, 8 and 24 hours. ^{1}H NMR spectra and tables are included in appendix E.

Figure 24 show the proton peaks of 4AP at 7.28 ppm and 6.88 ppm for coupling of 4AP to mannuronan in MES-buffer (pH=5.5) at different reaction times, recorded with ^{1}H NMR spectroscopy. The adducts are observed at 2.90 ppm.

Based on the results, the reaction time was increased from eight hours or more.

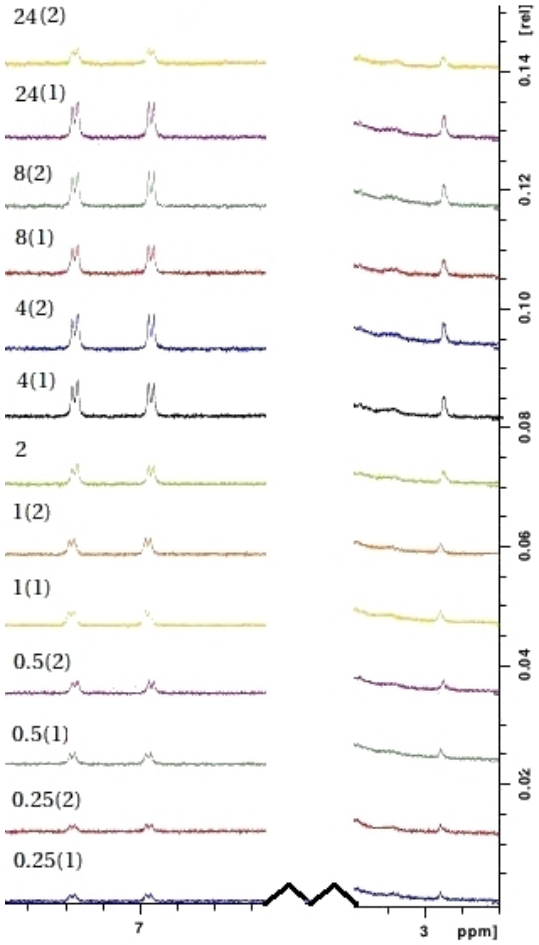

Figure 24: ^{1}H NMR spectra for coupling 4AP to mannuronan in 0.1M MES-buffer (pH=5.5) at different reaction times (hours). The samples are identified as *hours of incubation time(parallel number)*, meaning that the sample named *0.25(2)* has been incubated for 0.25 hours and is parallel number 2 for the 0.25 hour sample. The proton peaks at 7.28 and 6.88 ppm represents aromatic proton peaks of 4AP. The singlet at 2.90 ppm is methyl protons of N-acylurea and indicate the amount of adducts present. The spectra were recorded at 300MHz at 363K. The entire ^{1}H NMR spectra are included in appendix E.

3.2.3 Varying pH for coupling 4AP

4AP was coupled to mannuronan in MES-buffers at different pH-values to determine if the pH affects the degree of coupling.

Three samples were prepared for pH-values of 5.5, 6.0 and 6.5. Two parallels (n=2) were made for each sample. The percentage degree of coupling 4AP to mannuronan is shown graphically in figure 25.

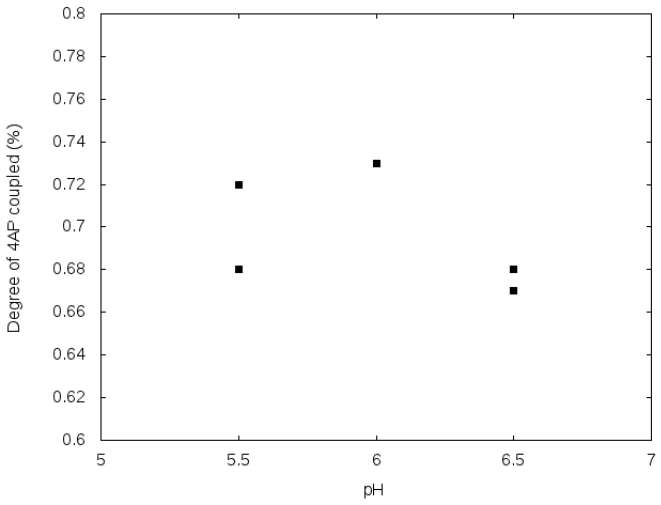

Figure 25: Degree of 4AP coupled to mannuronan when the pH is varied. 5% 4AP was coupled to mannuronan activated with 10% EDC and sulfo-NHS in 0.1M MES-buffers with varying pH (5.5, 6.0 and 6.5) . The percentage bound 4AP to mannuronan was calculated from integration of aromatic proton peaks of 4AP at 7.90 ppm and 7.45 ppm (see appendix B for detailed description of calculations). Calculations and ^{1}H NMR spectra are included in appendix F.

Coupling of 4AP to mannuronan was 0.7% for all samples. The lowest coupling at 0.67% (pH=6.5) and the highest coupling of 0.73% (pH=6.0).

The degree of coupling 4AP to mannuronan can be analysed by UV/vis methods as 4AP absorbs energy in the ultraviolet region of the electromagnetic spectrum. An absorbance screen of 4AP coupled to mannuronan was performed and compared to standard series of 4AP in MQ-water. It was found that the absorbance spectra for 4AP (figure 26) changes upon binding to M, and shifts towards lower wavelengths as 4AP is coupled to alginate.

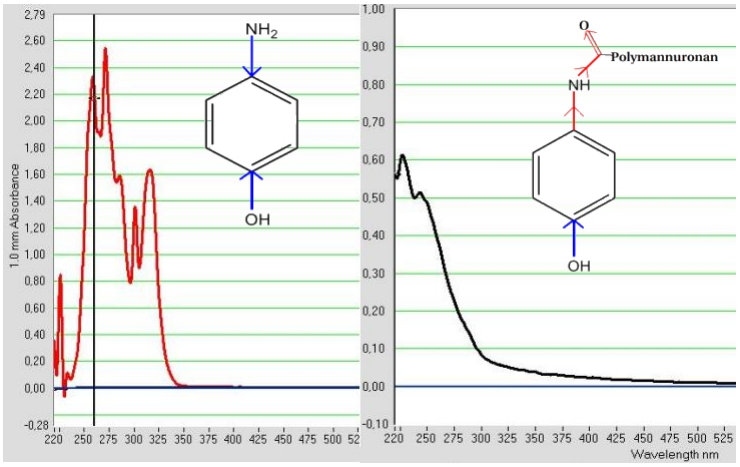

Figure 26: Absorbance as a function of wavelength. The graph to the left show the absorbance spectrum of 4AP in MQ-water, the graph to the right show the absorbance spectrum of 4AP coupled to alginate in MES-buffer (pH=6.5)

This change in absorbance energy happens because electrons are withdrawn from the benzene ring towards the more electronegative oxygen groups of mannuronan, as indicated by red arrows in figure 26. In particular, the keton group adjacent to the peptide bond cause the large shift in the dipole moment of 4AP because of its proximity to the benzene ring. When the dipole moment changes, the energy of the benzene ring increase and thereby absorbs energy at lower wavelengths as shown in the figure above.

From these results (figure 26), it was demonstrated that 4AP cannot be used as a model molecule for calculating the coupling of 4AP to alginate. Instead, a standard series of 4AP-alginate-samples has to be prepared as they will absorbe energy at the same wavelengths. Preparation of such standards is impossible at this point.

A new requirement for the model molecule was based on these results. The model molecule can not change its absorbance specter in such a degree as 4AP, once coupled to mannuronan. Me-O-Tyr (figure 17) was suggested as a model molecule, as it has an amine group that is positioned further from its benzene ring via an alkyl chain. Coupling to mannuronan will not affect the absorbance in such an extent as 4AP because the electron withdrawing peptide bond in Me-O-Tyr is situated further away from the benzene ring.

Me-O-Tyr contains a tyrosine residue that is also present in GRGDYP. This enables a better comparison between the model molecule and GRGDYP in ^{1}H NMR and

UV/vis spectroscopy.

3.3 Coupling of Me-O-Tyr

Me-O-Tyr was chosen as a model molecule for peptide coupling to mannuronan to allow detection of grafted product with both ^{1}H NMR and UV/vis spectroscopy. The coupling of Me-O-Tyr to mannuronan is performed by varying the pH, temperature, and amounts of reactants added. In addition, coupling Me-O-Tyr to alginate is performed.

3.3.1 Varying temperature for Me-O-Tyr coupling

Unwanted adducts can be reduced by using acidic pH and by letting mannuronan and EDC react at 0°C before adding the amine[13]. Detection of adducts can be determined by ^{1}H NMR. Adducts of N-acylurea have a secondary amine group with two methyl groups attached to it. These protons give rise to a singlet at 2.90 ppm which can be seen in figure 27.

Two samples were prepared in this experiment with 2 parallels (n=2) each. One sample was incubated at 0°C and the other sample was incubated at 20°C. The ^{1}H NMR spectra are shown in figure 27.

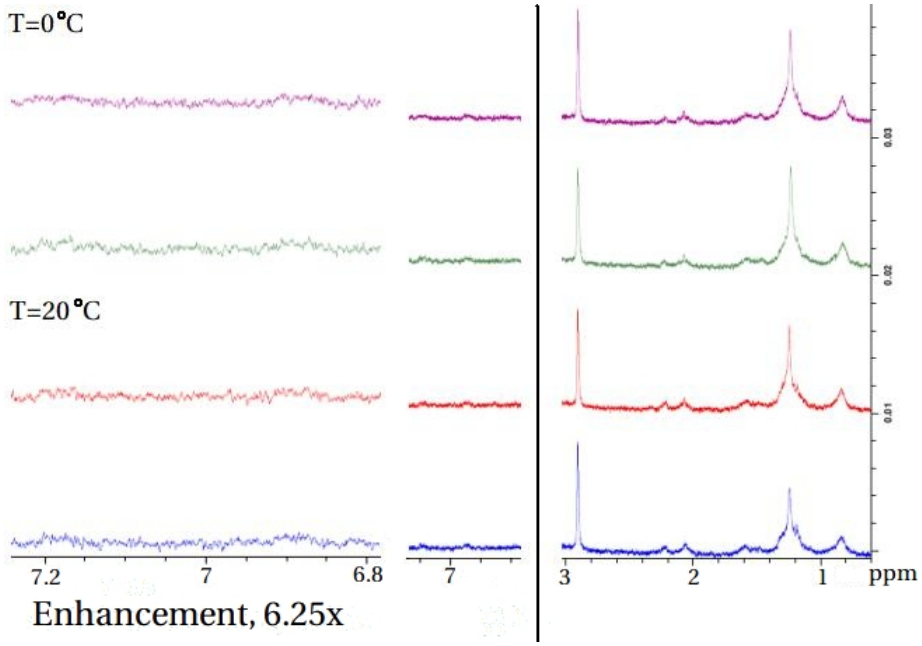

Figure 27: Presence of adducts and Me-O-Tyr coupled to mannuronan, ^{1}H NMR. 5% Me-O-Tyr was coupled to mannuronan activated with 10% EDC and sulfo-NHS in 0.1M MES-buffer (pH=6.0) at 0°C and 20°C. The right part of the figure show prescence of adducts indicated by a singlet at 2.90 ppm. This proton peak represents methyl protons of N-acylurea. The right part of the figure show the chemical shifts of Me-O-Tyr protons expected to peak at 6.90 ppm and 7.20 ppm. The left most part show a 6.25 times enhancement of this area. Integrals and ^{1}H NMR spectra are included in appendix H.

Comparing ^{1}H NMR spectra at 2.90 ppm for the 20°C sample to the sample prepared at 0°C did not indicate any changes in adduct formation when the temperature was lowered. The amount of Me-O-Tyr bound to mannuronan at 0°C was calculated to 0.21% and 0.20%, and the parallels prepared at 20°C was calculated to 0.18 and 0.23% (see appendix G for integrals). However, the signal to noise ratio for the aromatic proton peaks of Me-O-Tyr at 6.90 and 7.20 ppm were so small that integration was considered highly erroneous, as can be seen in figure 27.

Absorbance measurements were performed on the samples and the absorbance detected at 280nm was used to calculate the percentage coupling of Me-O-Tyr to mannuronan (for calculations and spectra, see appendix G). The percentage coupling to mannuronan was calculated to 0.30% and 0.43% for the parallels prepared at 20°C, while the coupling for the parallels prepared at 0°C were calculated to 0.51 and

0.42%, respectively.

3.3.2 Optimal reaction time at 0°C

The reaction rate between mannuronan and EDC slows down when lowering the temperature[13]. Thus, the incubation time at 0°C will probably reduce the coupling to mannuronan but also reduce the formation of adducts.

Three different samples were prepared. Mannuronan was cooled to 0°C and incubated with 10% EDC and sulfo-NHS. 5% Me-O-Tyr was added and the different samples were incubated at 20, 40, and 60 minutes at 0°C. The coupling of Me-O-Tyr was calculated based on integrating aromatic proton peaks of tyrosine at 6.90 and 7.20 ppm.

Figure 28 show the amount of Me-O-Tyr bound to mannuronan calculated by ^{1}H NMR spectroscopy and UV/vis spectroscopy.

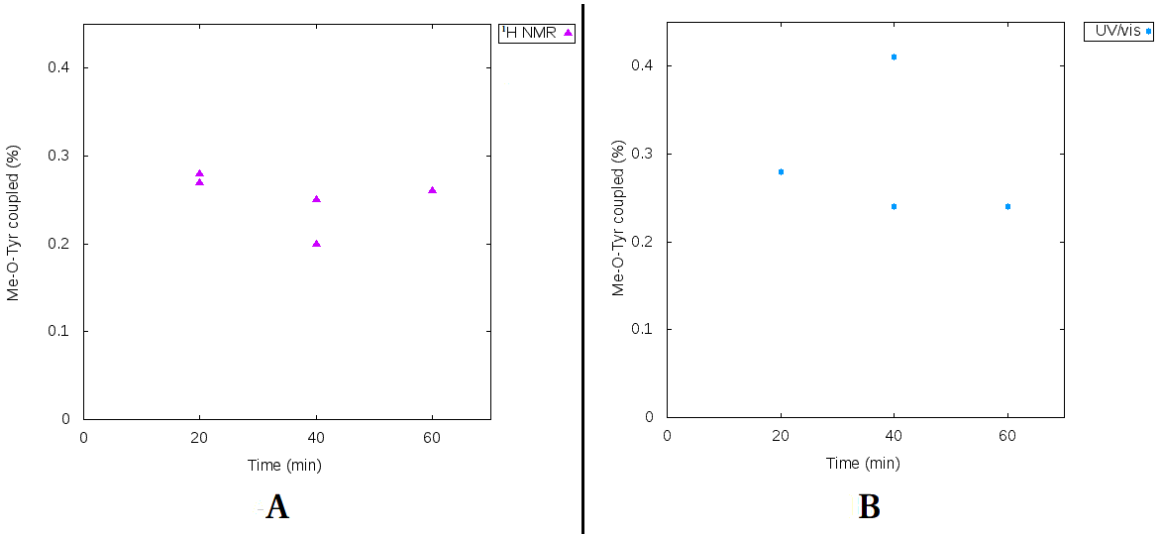

Figure 28: Coupled Me-O-Tyr to mannuronan at 0°C with incubation times of 20, 40 and 60 minutes, A: calculated form ^{1}H NMR spectroscopy and B: calculated from UV/vis spectroscopy. Three samples with two parallels (n=2) each were prepared. Parallel 1 for the 60 minute sample was lost during the experiment. Mannuronan was cooled with ice in 0.1M MES-buffer (pH=6.0) and activated with 10% EDC and sulfo-NHS. 5% Me-O-Tyr was added and the samples were left to incubate at different incubation times at 0°C. A: The percentage bound Me-O-Tyr was calculated from integrating aromatic protons of Me-O-Tyr peaks at 6.90 and 7.20 ppm (see appendix B for examples of calculations). B: The amount of Me-O-Tyr bound to mannuronan was calculated from absorbance measurements at 280nm (See appendix G example of calculations, for absorbance measurements see appendix I).

From figure 28 it can be seen that the measurements at 20 and 60 minutes incubation time at 0°C is quite similar for ^{1}H NMR spectroscopy and UV/vis spectroscopy. However, at 40 minutes reaction time, a coupling degree of >0.4% is calculated based on UV/vis spectroscopy.

The ^{1}H NMR spectra for the samples are depicted in figure 29.

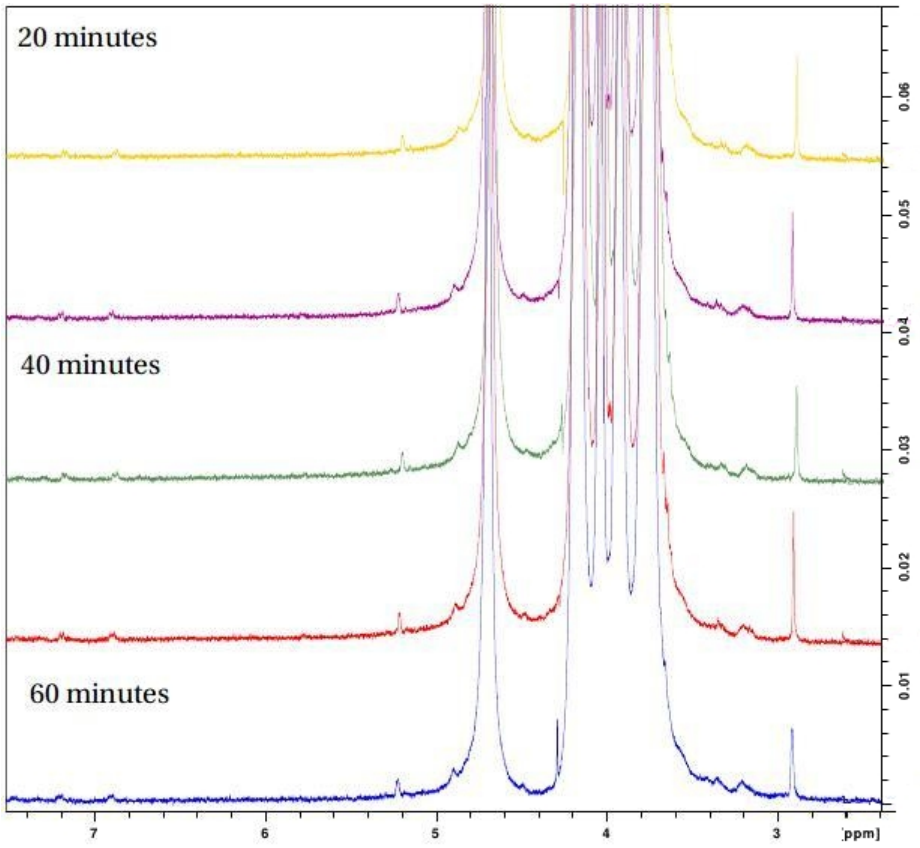

Figure 29: Coupling Me-O-Tyr to mannuronan at 0°C with incubation times of 20,40 and 60 minutes. Mannuronan was cooled with ice in 0.1M MES-buffer (pH=6.0) and activated with 10% EDC and sulfo-NHS. 5% Me-O-Tyr was added and the samples were left to incubate at different incubation times at 0°C. Three samples with two parallels (n=2) each were prepared. Parallel 1 for the 60 minute sample was lost during the experiment. Aromatic protons of Me-O-Tyr peaks at 6.90 and 7.20 ppm and integration of these peaks would determine the amount coupled to mannuronan. The singlet observed at 2.90 ppm is methyl protons of N-acylurea adducts. The differences between peak intensity at 2.90 ppm between the sample incubated for 20 minutes is small compared to the 40 minute sample. However, the differences between the 60 minute sample and the 40 and 20 minute sample is more prominent. The peak at 4.60-4.70 ppm represents proton number one of mannuronan and is set as reference integral when calculating the amount of Me-O-Tyr present (for examples of calculations, see appendix B).

3.3.3 Varying pH at 0°C for coupling Me-O-Tyr

Lowering the temperature to 0°C and incubating the coupling of Me-O-Tyr to mannuronan for 60 minutes decreased the formation of N-acylurea (figure 29). Varying the pH at these incubation conditions would indicate whether the adduct formation is affected. Coupling of Me-O-Tyr to mannuronan was performed in 0.1M MES-buffers with different pH-values at 0°C.

Figure 30 show the aromatic proton peaks of Me-O-Tyr at 6.90 ppm and 7.20 ppm, N-acylurea adducts are detected at 2.90 ppm.

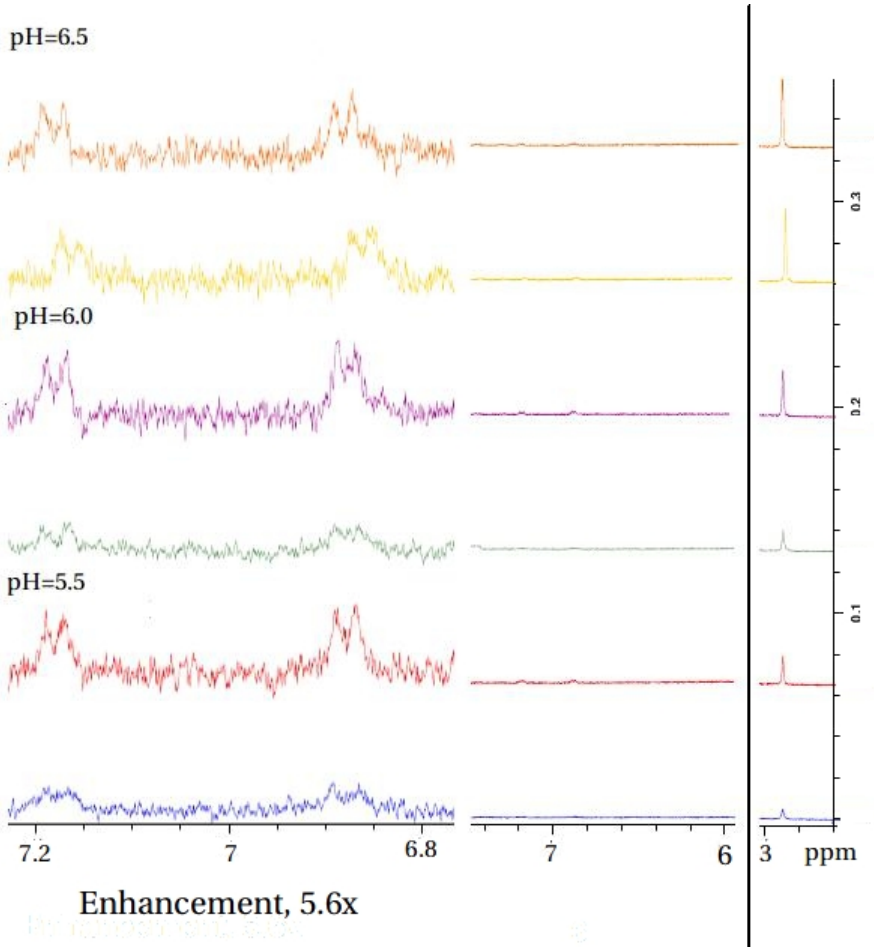

Figure 30: Coupling Me-O-Tyr to mannuronan at different pH-values. 5% Me-O-Tyr was coupled to mannuronan activated with 10% EDC and sulfo-NHS in 0.1M MES-buffer (pH=6.0 and pH=5.5). Three samples were prepared, with two parallels each (n=2). The right part of the figure show prescence of adducts indicated by a singlet at 2.90 ppm. This proton peak represents methyl protons of N-acylurea. The right part of the figure show the chemical shifts of Me-O-Tyr protons expected to peak at 6.90 ppm and 7.20 ppm. The left most part show a 5.6 times enhancement of this area. Integrals and ^{1}H NMR spectra are included in appendix J.The spectra were recorded at 300MHz at 363K.

It can be seen from figure 30 that the intensity of the proton peaks of Me-O-Tyr varies in the same manner as the intensity of the N-acylurea peaks, *i.e* a large intensity at 2.90 ppm is followed by accordingly intense peaks at 6.90 and 7.20 ppm. This may indicate that the N-acylurea adducts are coupled to Me-O-Tyr.

As can be seen in the rightmost part of figure 30, the adduct formation increase with increased pH. The coupling of Me-O-Tyr to mannuronan, as shown in the enhanced part of figure 30, is highest for one of the samples at 6.0 (purple) with 0.22% Me-O-Tyr coupled to mannuronan. This parallel also had the largest absorbance at 280nm in UV/vis spectroscopy (see appendix J).

3.3.4 Coupling Me-O-Tyr to alginate beads

Coupling a peptide directly to alginate beads compared to mannuronan simplifies the procedure of making beads for cell encapsulation. This is because enzymes are not used to introduce gelling residues to mannuronan. The coupling is thought to occur at non-gelling residues, since guluronic residues are ionically bound to Ca^{2+}.

One sample of alginate beads were prepared and activated with 10% EDC and sulfo-NHS, before adding 20% Me-O-Tyr. No aromatic proton peaks of Me-O-Tyr were observed at 6.90 ppm and 7.20 ppm. This means that the ^{1}H NMR specter could not be used to calculate the the amount of Me-O-Tyr coupled. By UV/vis detection, the amount of Me-O-Tyr present was calculated to 0.09% by measuring the absorbance at 280nm. The ^{1}H NMR specter and absorbance specter is included in appendix K.

3.3.5 Varying amount of EDC and Me-O-Tyr added

The idea was that increasing the amount of activated mannuronic acids and added Me-O-Tyr would lead to a higher degree of coupling.

Figure 31, part A, show the coupling of Me-O-Tyr as a function of Me-O-Tyr added. When activating mannuronan with 20% EDC, the relationship between added and coupled Me-O-Tyr is almost linear. The percentage coupling of Me-O-Tyr is largest when 20% EDC and 20% Me-O-Tyr is added (purple). A coupling of 0.48% is achieved at these concentrations. The lowest coupling is achieved when 20% EDC and 5% Me-O-Tyr is added (purple), when only 0.18% is coupled.

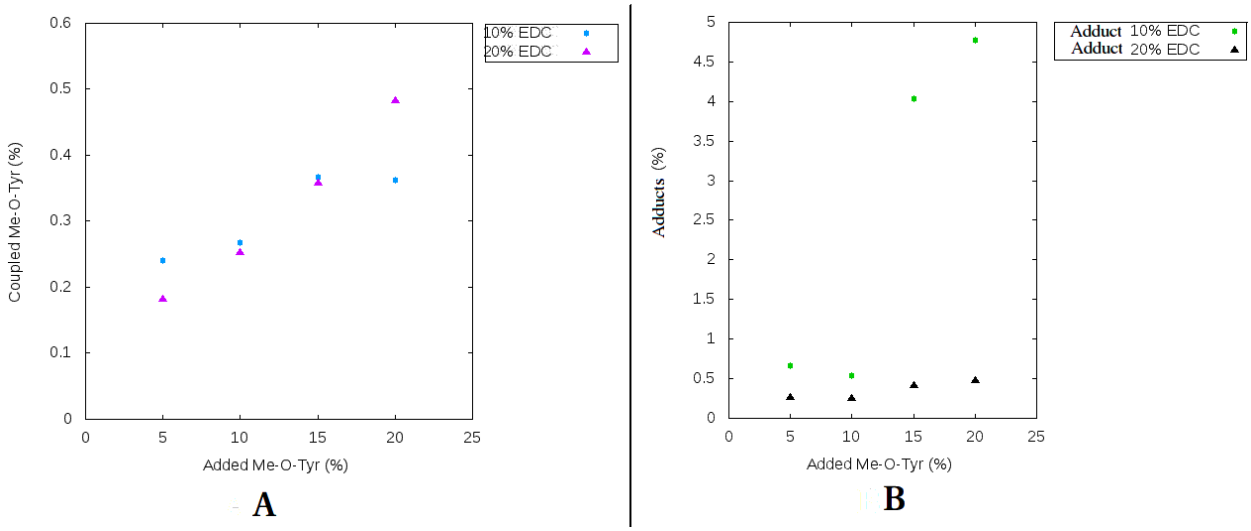

Figure 31: A: Coupled Me-O-Tyr as a function of amount Me-O-Tyr added, B: Adduct-formation as a function of Me-O-Tyr added. The coupling was performed in 0.1M MES-buffer (pH=6.0) at room temperature. One sample was prepared for each variable. A: The blue dots and the pink triangles show the amount of Me-O-Tyr coupled when the EDC concentration is 10% and 20%, respectively. The percentages of coupling Me-O-Tyr was calculated from integration of proton peaks at 6.90 and 7.20 ppm from spectra recorded with ^{1}H NMR spectroscopy. B: The green dots and the black triangles show the formation of adducts when the EDC concentration is 10% and 20%, respectively. The amount of adducts present was calculated from integrating methyl protons of N-acylurea represented as a singlet at 2.90 ppm from spectra recorded with ^{1}H NMR spectroscopy. The calculations were performed as described in appendix B. Tables and ^{1}H NMR spectra are included in appendix L.

Figure 31, part A, demonstrate that increasing the activation of mannuronic acids

and at the same time increasing the amount of Me-O-Tyr present will increase the degree of coupling.

Adduct formation was assessed by integration of the proton peaks at 2.90 ppm. Although protons of N-acylurea adducts also peak at 1.15 ppm, this peak is more difficult to integrate as it has a tendency to shift and also interfere with other peaks in the spectrum.

Table 9 show the calculated amount of Me-O-Tyr calculated by UV/vis spectroscopy and ^{1}H NMR. Measuring the amount of adducts is not possible with UV-methods, but an estimation on the amount of Me-O-Tyr can be calculated.

Table 9: Bound Me-O-Tyr(%) to mannuronan

sulfo-NHS&EDC(%)	Me-O-Tyr(%)	Bound Me-O-Tyr(%), UV	Bound Me-O-Tyr, ^{1}H NMR
10	5	0.32	0.24
	10	0.31	0.27
	15	0.47	0.37
	20	0.32	0.36
20	5	0.36	0.18
	10	0.35	0.25
	15	0.31	0.36
	20	0.31	0.48

The trend of coupling Me-O-Tyr to mannuronan when calculated with ^{1}H NMR spectroscopy, show an increased coupling when the EDC and Me-O-Tyr concentrations are increased. This is not the case for the results calculated from UV/vis spectroscopy.

3.3.6 Coupling with excess of Me-O-Tyr

Increasing the amount of Me-O-Tyr seem to increase the total coupling as shown in the previous results (figure 31). Thus, a larger coupling can be expected with Me-O-Tyr concentrations above 20%. In this experiment, the amounts of added Me-O-Tyr were increased up to 100% in 20%- intervals, while the added amounts of EDC and sulfo-NHS were kept constant at 10%.

Figure 32 show how the coupling of Me-O-Tyr to mannuronan is affected when the amount of Me-O-Tyr is much larger than added EDC and sulfo-NHS.

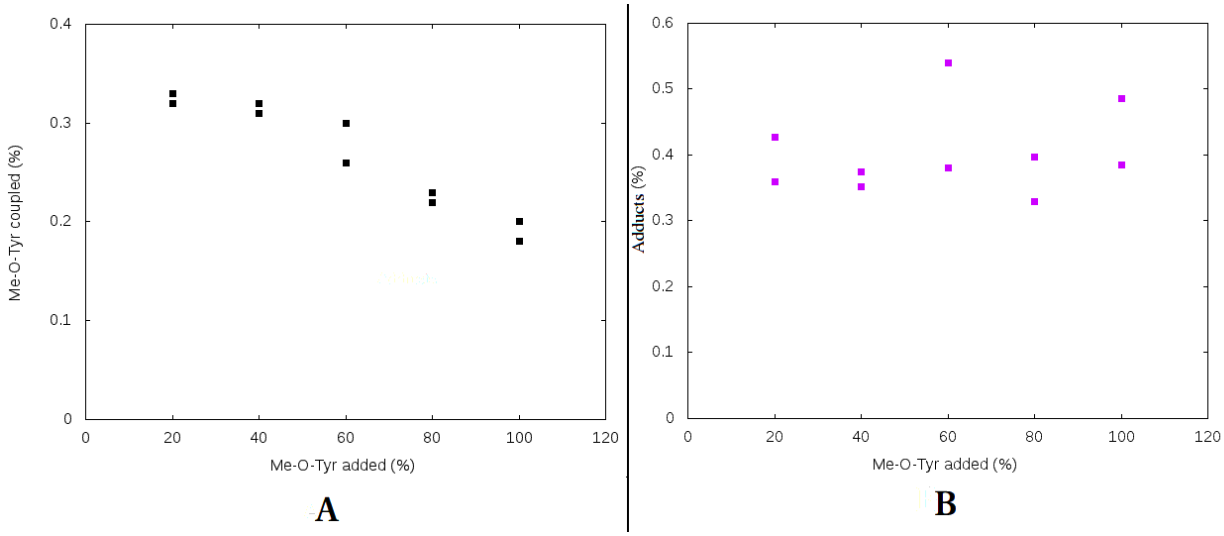

Figure 32: A: Coupled Me-O-Tyr to mannuronan as a function of added Me-O-Tyr, B: formation of adducts as a function of Me-O-Tyr added. The coupling of Me-O-Tyr to mannuronan was performed in 0.1M MES-buffer (pH=6.0) with 10% EDC and sulfo-NHS at room temperature. One sample and two parallels (n=2) were prepared for each 20% increase of Me-O-Tyr. Part A show the percentage bound Me-O-Tyr as a function of amount of Me-O-Tyr added. The percentages were calculated from integration of aromatic proton peaks of Me-O-Tyr at 6.90 and 7.20 ppm from spectra recorded with ^{1}H NMR spectroscopy. Part B show the relative amounts of adducts formed as the amount of Me-O-Tyr is increased. The amount of N-acylurea adducts were calculated from integrating methyl proton peaks of N-acylurea at 2.90 ppm from spectra recorded with ^{1}H NMR spectroscopy. For a detailed description of calculations, see appendix B. For tables and ^{1}H NMR spectra, see appendix M.

As shown in part A of figure 32, the highest coupling was achieved at 20% added Me-O-Tyr with a coupling of 0.33%. The average coupling at 20% has decreased compared to the equivalent parallels in figure 31 (part A, blue dots) where the coupling was calculated to 0.36%. The graph show that adding more than 20% Me-O-Tyr caused a reduction in coupling to mannuronan.

The presence of adducts (part B in figure 32) varied between ∼0.3-0.6% and did not appear to be affected in the same way as bound Me-O-Tyr. The smallest amount of adducts were present at 80% added Me-O-Tyr and the largest at 60%. The average adduct formation was below 0.6% for all samples, which is markedly low compared to the previous experiments, where adducts were shown to exceed 4% (figure 31, part B, green dots).

Figure 33 show the proton peaks of Me-O-Tyr coupled to mannuronan at 6.90 and 7.20 ppm.

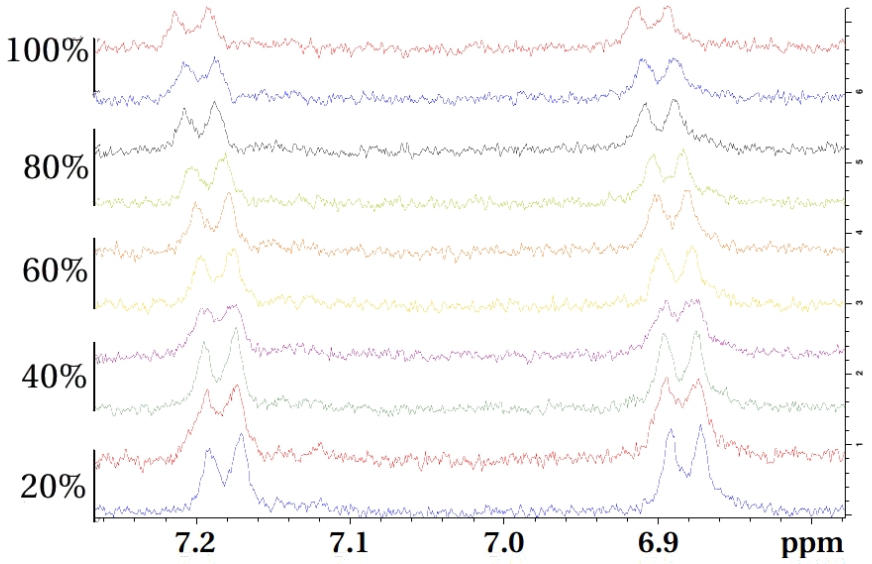

Figure 33: Molecular peaks of benzene protons of Me-O-Tyr coupled to mannuronan at 7.20 and 6.90 ppm, ^{1}H NMR. The coupling of Me-O-Tyr to mannuronan was performed in 0.1M MES-buffer (pH=6.0) with 10% EDC and sulfo-NHS at room temperature. One sample and two parallels (n=2) were prepared for each 20% increase of Me-O-Tyr. The y-axis indicate the amount of Me-O-Tyr added shown in relative percentage to the carboxylic acids of mannuronan. There is a decrease in peak intensities as the amount of Me-O-Tyr increase.

Table 10 show the amounts of Me-O-Tyr calculated by UV/vis spectroscopy.

Table 10: Bound Me-O-Tyr(%) to mannuronan, determined by UV/vis spectroscopy

Me-O-Tyr(%)	Parallel	Bound Me-O-Tyr(%)
20	1	0.34
	2	0.38
40	1	0.31
	2	0.32
60	1	0.37
	2	0.29
80	1	0.30
	2	0.26
100	1	0.28
	2	0.29

Here, the trend for both ^{1}H and NMR and UV/vis spectroscopy showed a decrease of coupling as the amount of Me-O-Tyr increased. However, the calculated bound Me-O-Tyr to mannuronan based on absorbance measurements were higher compared to the coupling calculated from UV/vis spectroscopy.

See appendix M for average absorbance at 280nm and appendix G for caclulations of amount of Me-O-Tyr coupled based on absorbance measurements.

3.4 Coupling of GRGDYP

Determining if Me-O-Tyr is a suitable model molecule for coupling GRGDYP can be assessed by performing GRGDYP coupling under the same reaction conditions as coupling Me-O-Tyr. The reaction conditions that were considered sutiable for coupling GRGDYP to mannuronan were applied to the large scale coupling of GRGDYP to mannuronan.

3.4.1 Activating mannuronan at pH=4.2

O-acylisourea formation is preferred over N-acylurea in the pH-interval 3.5-4.5 [12], meaning that the amount of adducts will be lower in this pH-interval. It was therefore interesting to incubate the carbodiimide reaction in this pH-level. The amount of GRGDYP added corresponds to a theoretical coupling of 5%.

Figure 34 show the ^{1}H NMR spectra of GRGDYP coupled to mannuronan when the pH was kept at 4.2.

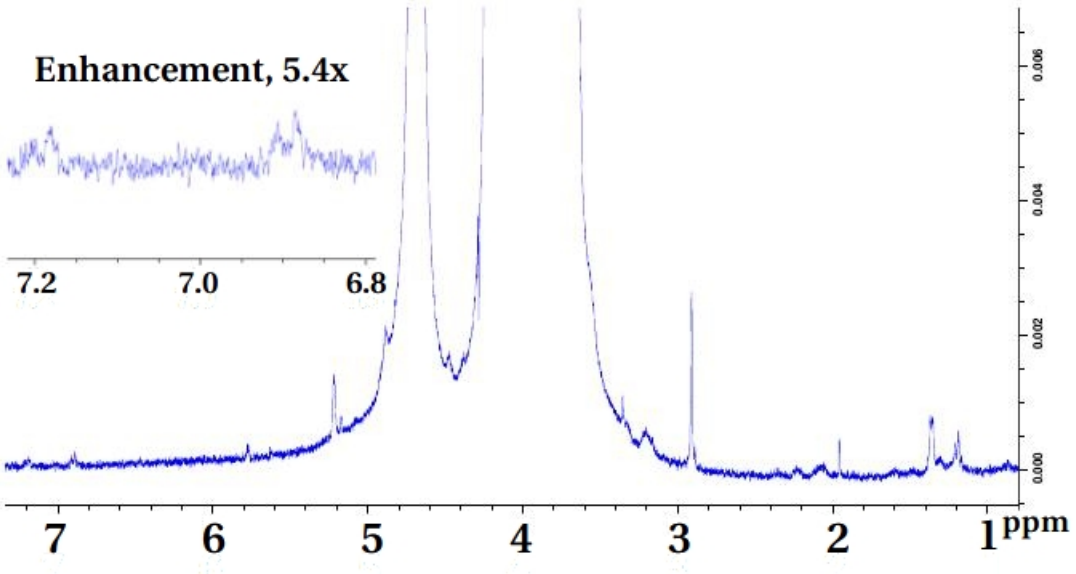

Figure 34: Mannuronan activated with EDC at pH=4.2, ^{1}H NMR. Mannuronan was activated with 10% EDC and sulfo-NHS in 0.1M MES-buffer at room temperature at pH=4.2. The pH was raised to 5.8 before adding 5% GRGDYP. The pH was further increased to 6.0 before incubation over night by stirring with magnet. The enhanced part show the proton peaks of tyrosine protons of GRGDYP expected at 6.90 ppm and 7.20 ppm. The singlet at 2.90 ppm represents proton peaks of N-acylurea and represents unwanted adducts in the sample.

Calculations from integrating the proton peaks of GRGDYP in ^{1}H NMR gave a coupling of 0.08% GRGDYP to mannuronan at pH=4.2. The results from absorbance measurements gave a calculated coupling of 0.24% (see appendix N for examples of calculating and GRGDYP based on absorbance measurements, and appendix O for raw data). The singlet at 2.90 ppm indicate that N-acylurea adducts are present in the sample, to a larger extent than the proton peaks of GRGDYP observed at 6.90 and 7.20 ppm. The low coupling of GRGDYP to mannuronan was probably a direct result of a larger portion of protonated mannuronic acids, causing a reduction of nucleophiles in the solution (see figure 8). This prevents the formation of O-acylisourea and may lower the probability of coupling. The results demonstrate that lowering the pH is not an option when using EDC as a carbodiimide for coupling to alginate.

3.4.2 Varying pH for coupling GRGDYP

The peptide coupling may be affected by the pH of the buffer, as was the case for 4AP and Me-O-Tyr. Comparing coupling of GRGDYP at a higher pH with a lower pH, would indicate how pH differences affect coupling and formation of adducts. MES-buffers with pH-values of 5.5 and 6.5 were chosen to examine the degree of coupling as well as the amount of adducts present.

Figure 35 show the ^{1}H NMR spectra of GRGDYP coupled to mannuronan when the pH was 5.5 and 6.0.

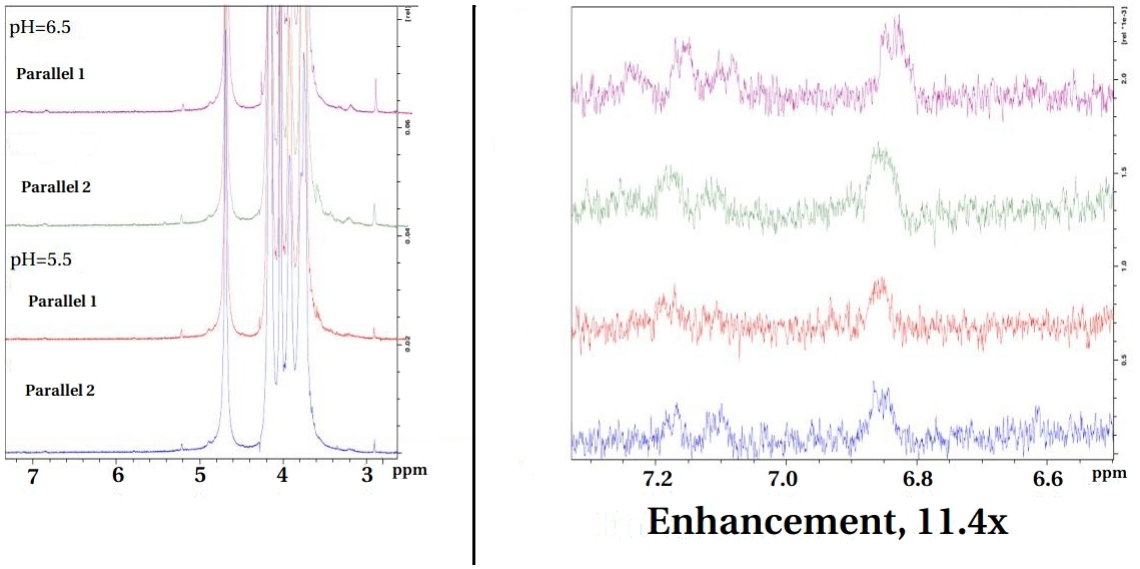

Figure 35: GRGDYP coupled to mannuronan at pH 5.5 and 6.5, ^{1}H NMR spectra. 5% GRGDYP were coupled to mannuronan activated with 10% EDC and sulfo-NHS in 0.1M MES-buffer at room temperature. One sample was made for each pH-value with two parallels (n=2) for each sample. The left part of the figure show the enlarged spectrum, where the adducts, represented by methyl protons of N-acylurea, can be seen at 2.90 ppm. The right part is an enlargement of the aromatic protons in tyrosine in GRGDYP which appear at 6.90 ppm and 7.20 ppm. The peak at 4.70 ppm is proton number one of mannuronan and this peak is set as reference when calculating the amount of GRGDYP coupled to mannuronan. For examples of calculations, see appendix B.

Integration of the peaks at 6.90 ppm and 7.20 ppm, shown in figure 35, gave a coupling of ∼0.1% GRGDYP to mannuronan at pH 5.5 and ∼0.2% at pH 6.5. The calculated bound GRGDYP to mannuronan based on UV/vis spectroscopy was 0.24% (see appendix N for examples of calculating amount GRGDYP coupled to mannuronan based on absorbance measurements and appendix P for raw data). As can bee seen in the right part of figure 35, the signal to noise ratio were lower for the peaks at 7.20 ppm compared to the peaks at 6.90 ppm. As can be seen from the figure, the adducts (singlet at 2.90 ppm), increases as the pH is increased.

3.4.3 Varying amount of GRGDYP added and pH

Coupling of 5, 10, 15 and 20% GRGDYP with constant amounts of EDC and sulfo-NHS (10%) will indicate if the amount of peptide added affects the amount coupled. Varying the pH can determine if the formation of products and adducts is affected. Assessing the amounts of N-acylurea adducts present was calculated with ^{1}H NMR by integrating the peaks at 2.90 ppm. Methyl protons of N-acylurea also peaks at 1.15 ppm, however, the singlet at 2.90 ppm is easier to integrate and identify, as it does not interfer with chemical shifts of protons of the peptide. The triplet at 1.15 ppm overlaps with proton peaks of GRGDYP (see figure 18).

Figure 36, part A, show an increase in peptide coupling when added peptide (purple and black) approach twice the amounts of EDC added. The same trend was observed for Me-O-Tyr (figure 31). The coupling was highest at 20% added peptide when the pH was 6.0 (purple). The adducts (part B, in figure 36) decreased as the peptide concentration increased (green and blue) and the formation of adducts were lower at pH=4.0 (green).

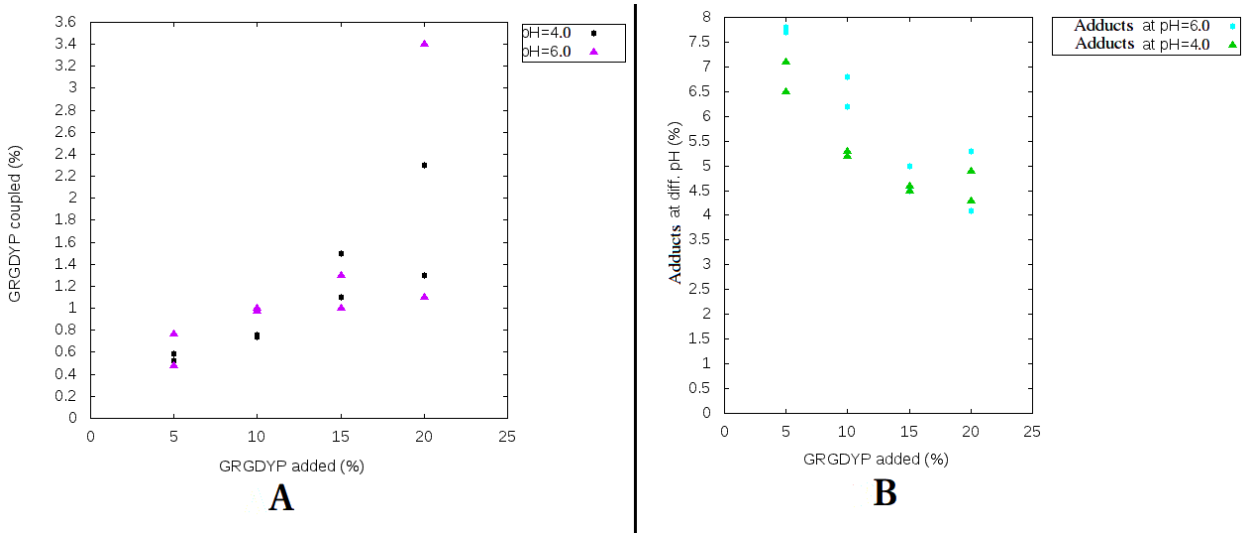

Figure 36: A: Coupled GRGDYP to mannuronan as a function of GRGDYP added and pH, B: formation of adducts as a function of GRGDYP added and pH. GRGDYP was coupled to mannuronan activated with 10% EDC and sulfo-NHS in 0.1M MES-buffer (pH=4.0 and 6.0) at room temperature. One sample and two parallels (n=2) were prepared for each variable. Part A show the increase in GRGDYP coupled to mannuronan as the amount of GRGDYP is added. The percentages were calculated from integration of aromatic peaks of GRGDYP at 6.90 and 7.20 ppm from ^{1}H NMR spectra. Part B show the amounts of adducts formed as the amounts of GRGDYP were increased. The amount of adducts were calculated from integrating proton peak at 2.90 ppm, representing methyl protons of N-acylurea. For a detailed description of calculations, see appendix B. For ^{1}H NMR spectra and tables, see appendix Q.

Figure 37 show an enhanced ^{1}H NMR spectra of the tyrosine peaks at 7.20 and 6.90 ppm of GRGDYP coupled to mannuronan.

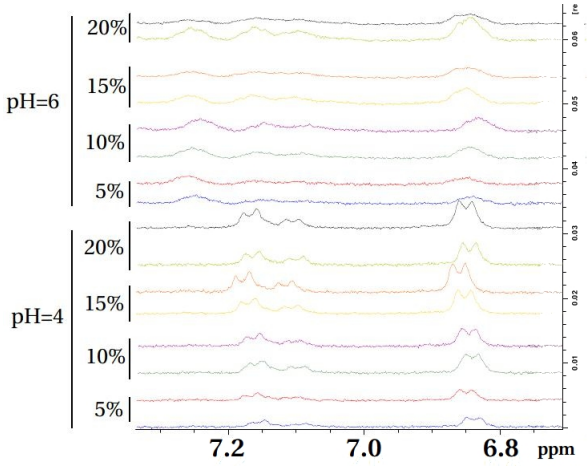

Figure 37: GRGDYP coupled to mannuronan at pH=4.0 and pH=6.0 when the amount of peptide added is varied. The y-axis of the figure show the pH and the amount of GRGDYP added in relative amounts to the carboxylic acids of mannuronan. GRGDYP was coupled to mannuronan activated with 10% EDC and sulfo-NHS in 0.1M MES-buffer (pH=4.0 and 6.0) at room temperature. One sample and two parallels (n=2) were prepared for each variable.

The results from UV/vis spectroscopy (see appendix Q) also indicate an increased absorbance as the amounts of GRGDYP is increased.

3.5 Large scale RGD-alginate

Two samples of 500mg mannuronan was used as starting point for large scale production of a peptide-coupled alginate sample and a non-coupled sample. Both samples were epimerised with AlgE4 that introduced alternating sequences and AlgE6 that introduced G-blocks. Both products were to be used for cell encapsulation of olfactory ensheating cells from neonatal rat brain. The encapsulation was performed at the department of Cancer Research and Molecular Medicine by co-student Marthe Fredheim Fjelldal.

An epimerisation test with AlgE6 was performed by incubating the enzyme with polyalternated alginate for 1, 2, 4 and 6 hours in the enzyme:alginate ratio 1:200. The results for the epimerisation test are shown in appendix S.

The expected F_G value after AlgE4 epimerisation was 0.40-0.47[55], while epimerisation of AlgE6 was expected to further increase F_G to 0.50-0.60 on a polyalternating backbone[55]. For the epimerisation test, F_G was calculated to 0.40 after AlgE4 epimerisation, while after six hours incubation time with AlgE6, the F_G had only increased to 0.42. The low values after AlgE6 epimerisation were probably due to the low enzyme concentration. Based on the results from the epimerisation test, it was decided to adjust the AlgE6:alginate ratio to 1:20 and set the incubation time to 2.5 hours in order to increase the F_G. This incubation time and enzyme:mannuronan ratios were shown to give favorable F_G in previos work performed by student Kristin Karstensen[54]. Table 11 show the calculations of the G and M fractions of the samples prepared for large scale production, before and after active coal filtration (a.c.f).

Table 11: Bound GRGDYP (%) to mannuronan, ^{1}H NMR

Sample	Enzyme	F_G	F_M	F_{GG}	F_{GM}	F_{MM}	F_{GGM}	F_{MGM}	F_{GGG}	$N_{G>1}$
RGD	AlgE4	0.28	0.72	0.0	0.28	0.42	0.0	0.38	0.0	0
	AlgE4+AlgE6	0.34	0.66	0.073	0.27	0.39	0.018	0.27	0.050	2
	AlgE4+AlgE6 a.c.f	0.34	0.66	0.059	0.28	0.39	0.023	0.28	0.032	3
No RGD	AlgE4	0.47	0.53	0.0	0.47	0.056	0.0	0.47	0.0	0
	AlgE4+AlgE6	0.50	0.50	0.11	0.39	0.11	0.038	0.50	0.079	4
	AlgE4+AlgE6 a.c.f.	0.50	0.50	0.11	0.39	0.11	0.038	0.50	0.079	4

The frequencies are calculated as described in appendix R, under the subsection named *Maximum averaging*.

The F_G is higher for the non-coupled sample after AlgE4 epimerisation, and reaches the expected value of 0.5 after AlgE6 epimerisation. This was not seen for the peptide coupled sample, where the F_G was below 0.4 for all samples.

F_{GG} of the peptide coupled sample was lower than the non-coupled sample, which is probably a result of the lower F_G. As can be seen in table 40, epimerisation of the non-coupled sample seem to be higher than the peptide-coupled sample. The average block length ($N_{G>1}$) was also larger for the non-coupled sample.

Figure 38 and figure 39 show the effect on the epimerisation steps performed on the peptide coupled sample and the non-peptide coupled sample, respectively.

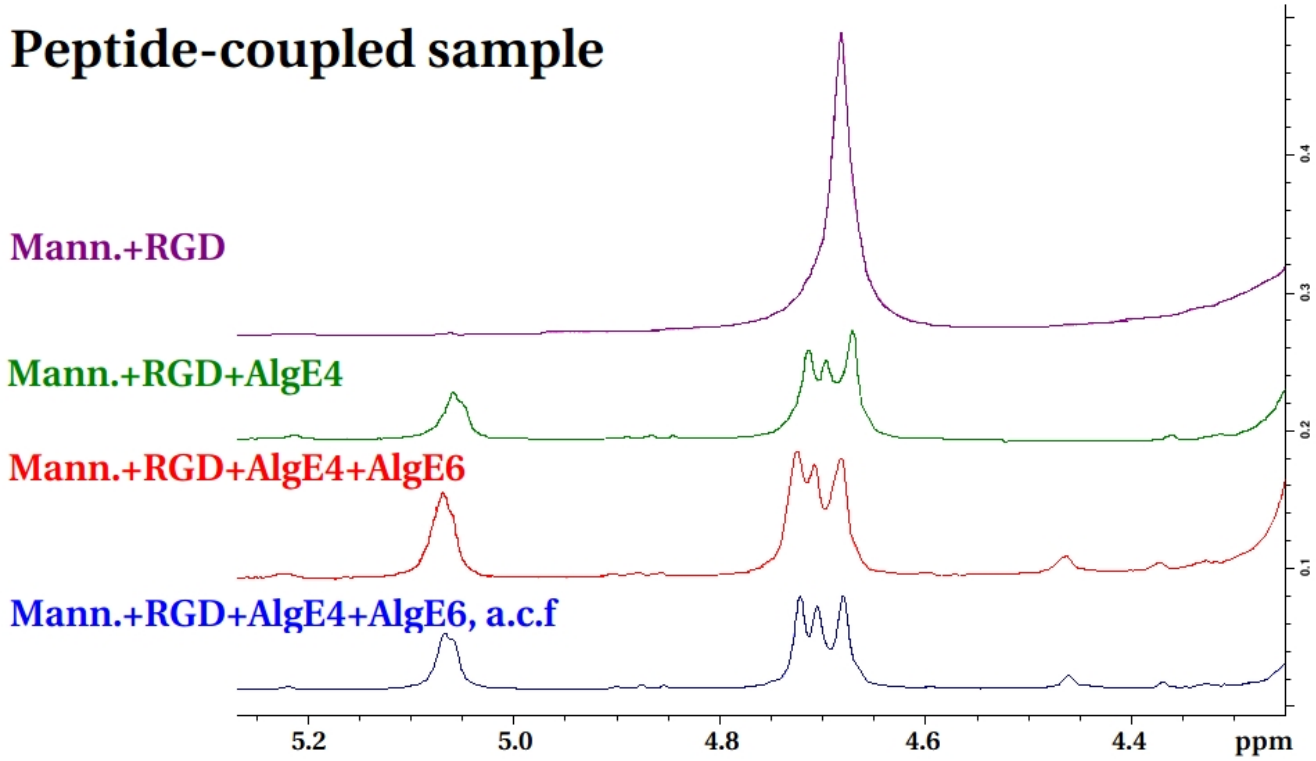

Figure 38: Epimerisation of AlgE4 and AlgE6 for peptide coupled sample, ^{1}H NMR spectra. The peak at 4.70 ppm represents the mannuronan protons in the sample, the peak at 5.06 and 4.46 ppm represents guluronic residues. For a full description of the proton peaks, see appendix R. Epimerisation was performed with AlgE4 from *H. polymorpha* in 50mM MOPS buffer (2.5mM $CaCl_2$, 10mM NaCl). AlgE4 was added in an enzyme-mannuronan ration of 2:50, and left to incubate over night at 37 °C. Polyalternating alginate was further epimerised with AlgE6 from *E. coli* in 50mM MOPS-buffer (2.5mM $CaCl_2$, 75mM NaCl) for 2.5 hours. *Mann.+RGD* is the mannuronan sample before epimerisation. *Mann.+RGD+AlgE4* show the ^{1}H NMR spectrum peptide-coupled sample after epimerisation of AlgE4, and the ^{1}H NMR spectrum named *Mann.+RGD+AlgE4+AlgE6* show the ^{1}H NMR spectrum after AlgE4 and AlgE6 epimerisation. The final ^{1}H NMR spectrum named *Mann.+RGD+AlgE4+AlgE6, a.c.f* represents the sample after active coal filtration.

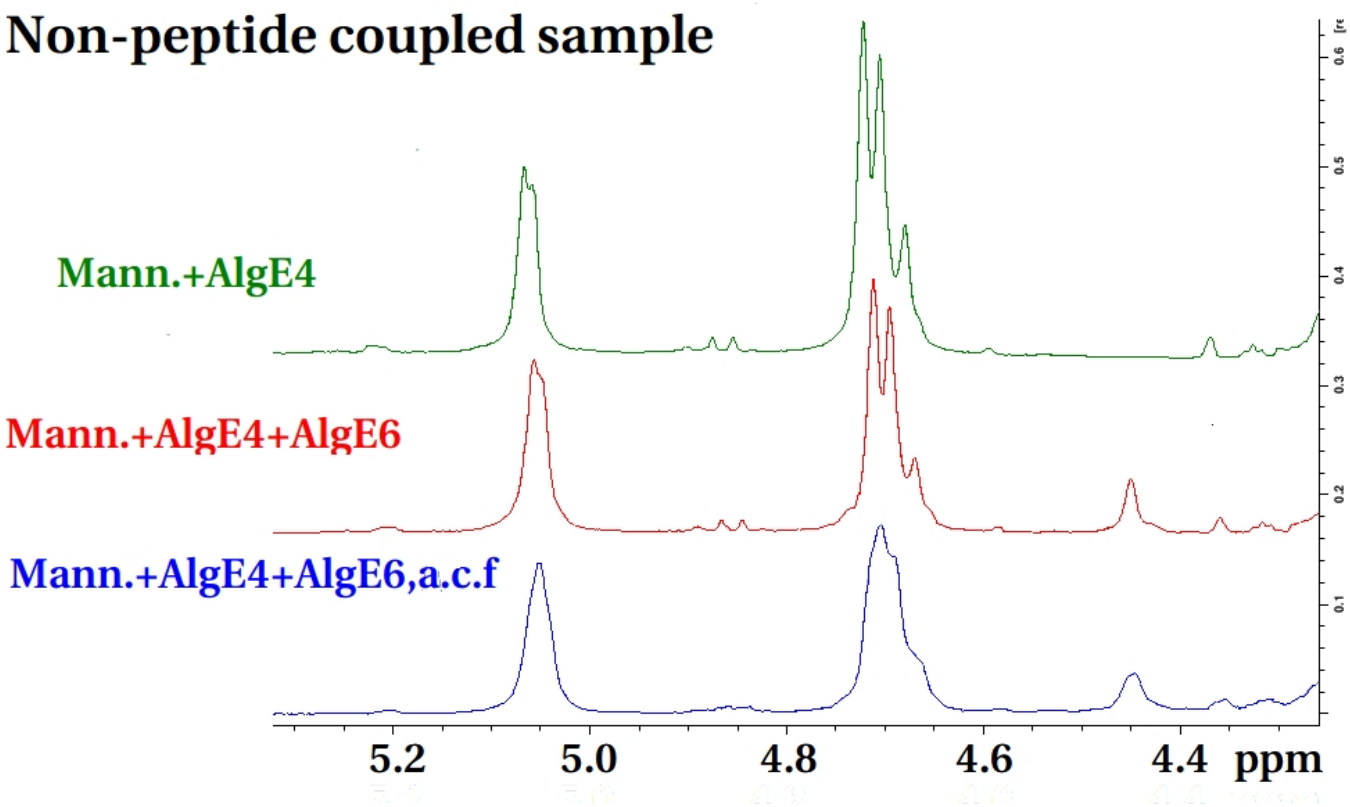

Figure 39: Epimerisation of AlgE4 and AlgE6 for non-peptide coupled sample, ^{1}H NMR spectra. The peak at 4.70 ppm represents the mannuronan protons in the sample, the peak at 5.06 and 4.46 ppm represents guluronic residues. For a full description of the proton peaks, see appendix R. Epimerisation was performed with AlgE4 from *H. polymorpha* in 50mM MOPS buffer (2.5mM $CaCl_2$, 10mM NaCl). AlgE4 was added in an enzyme-mannuronan ration of 2:50, and left to incubate over night at 37 °C. Polyalternating alginate was further epimerised with AlgE6 from *E. coli* in 50mM MOPS-buffer (2.5mM $CaCl_2$, 75mM NaCl) for 2.5 hours. *Mann.+AlgE4* is the mannuronan sample after AlgE4 epimerisation. *Mann.+AlgE4+AlgE6* show the ^{1}H NMR spectrum for the non-coupled sample after epimerisation of AlgE4 and AlgE6. The final ^{1}H NMR spectrum named *Mann.+AlgE4+AlgE6, a.c.f* represents the sample after active coal filtration.

After epimerisation with AlgE4, new peaks at 3.20-3.60 ppm were observed in the ^{1}H NMR spectra of mannuronan with and without RGD, as shown in figure 40.

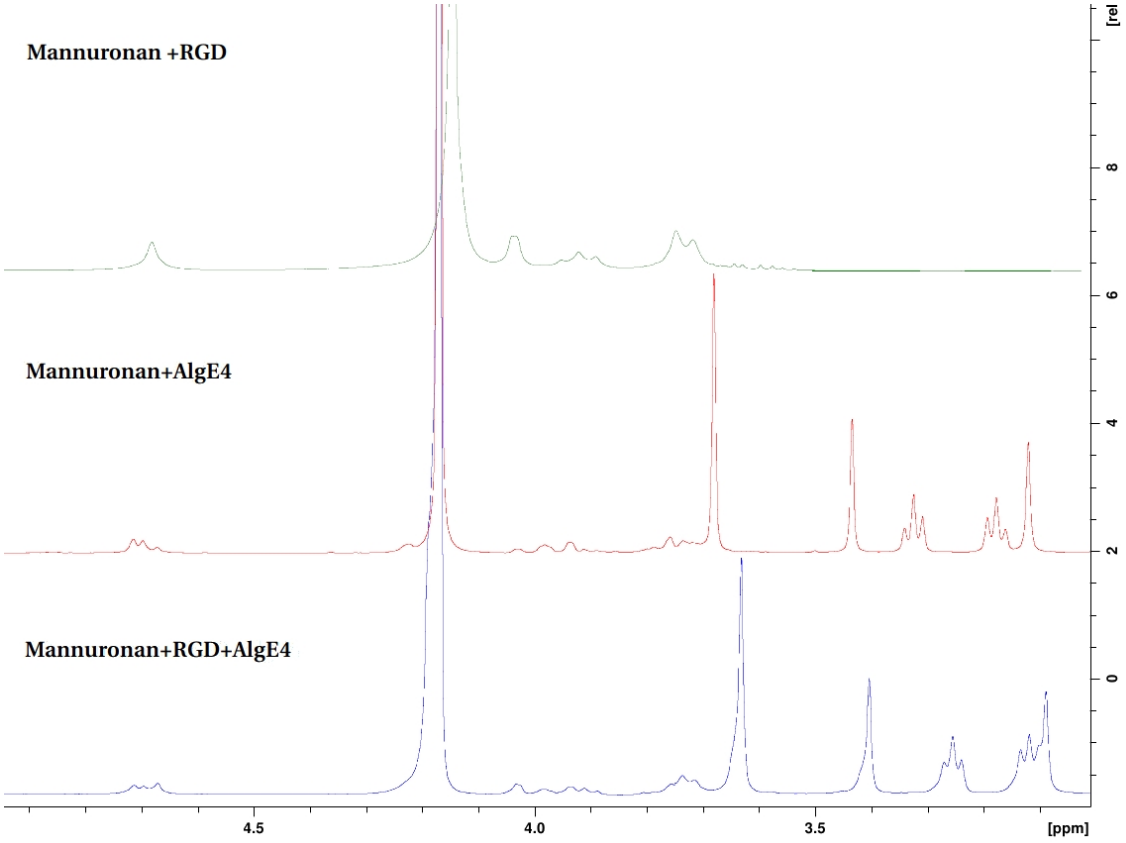

Figure 40: Unknown proton peaks at 3.20-3.60 ppm after epimerisation with AlgE4, ^{1}H NMR spectra. The green line named *Mannuronan+RGD* show the peptide coupled sample before epimerisation. The red line named *Mannuronan+AlgE4* show the non-peptide coupled sample taken after epimerisation with AlgE4. The blue line named *Mannuronan+RGD+AlgE4* show the peptide coupled sample after epimerisation of AlgE4.

The ^{1}H NMR spectra of mannuronan with RGD and the effect on epimerisation, with AlgE4 and AlgE6, and active coal filtration is shown in figure 41.

When inspecting the region from 3.20-3.60 ppm in figure 41, the signal intensities were slightly lower after active coal filtration, but they were still dominating. The proton peaks does not represent adducts form the carbodiimide reaction, MOPS buffer or alginate and their origin or molecular structure is not known.

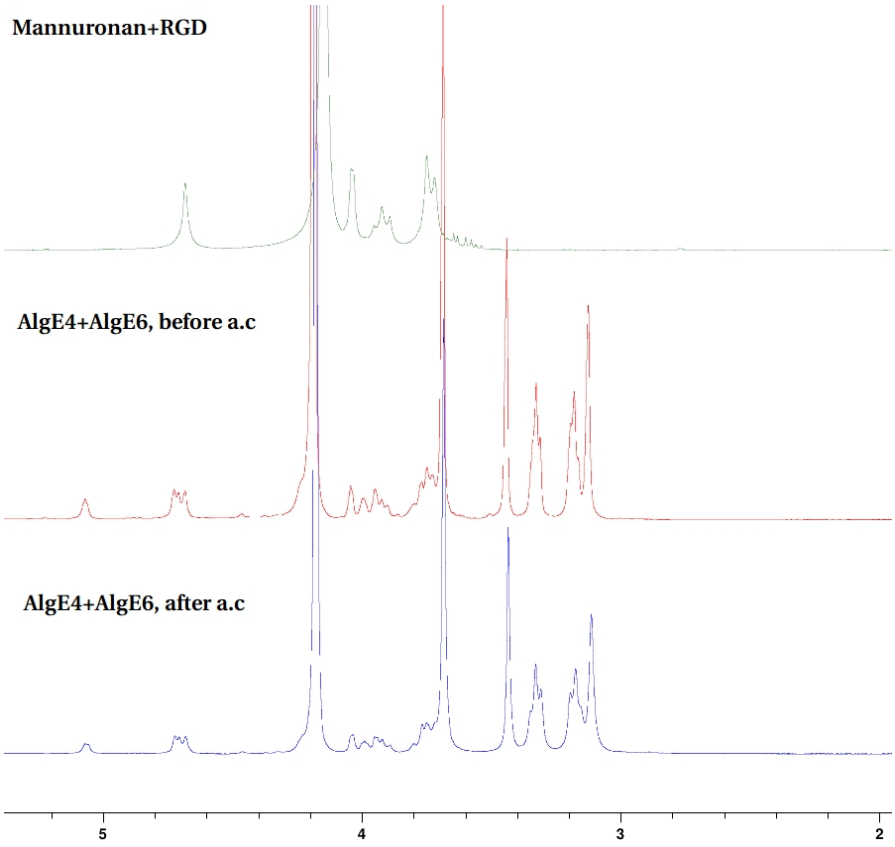

Figure 41: GRGDYP coupled to alginate before and after active coal filtration, ^{1}H NMR. The green line named *Mannuronan+RGD* show the peptide coupled sample before epimerisation. The red line named *AlgE4+AlgE6, before a.c* show the sample taken after epimerisation and before active coal filtration. The blue line named *AlgE4+AlgE6, after a.c* show the epimerised sample after coal filtration.

After epimerisation, the samples were coal filtrated over an activated coal filter and ^{1}H NMR samples were recorded before and after filtration for comparison. The ^{1}H NMR spectra of RGD-coupled alginate before and after active coal filtration are shown in figure 42.

Methyl protons of N-acylurea peaks at 2.90 ppm and 1.15 ppm (see figure 15). As indicated with arrows in figure 42, the coal filtration has had an effect on the intensities of N-acylurea protons. This means that active coal filtration has reduced adducts from the sample.

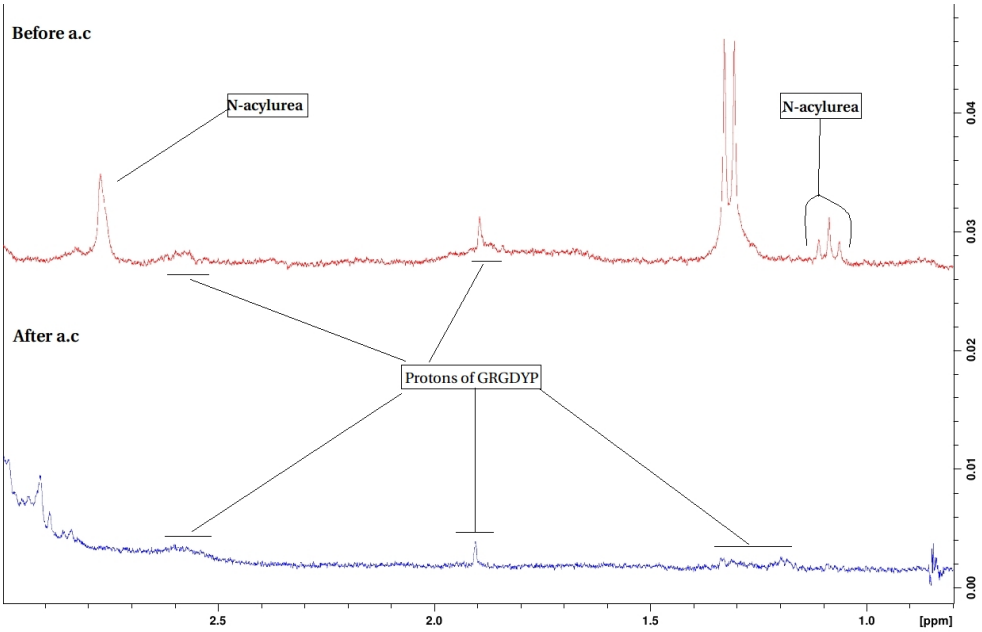

Figure 42: Adducts removed by active coal filtration, ^{1}H NMR spectra. Red line show the sample taken before active coal filtration, while the blue line represent sample after active coal filtration.

A ^{1}H NMR sample was prepared for the peptide coupled sample prior to epimerization to deduce the peptide coupling. The integration and subsequent degree of coupling is shown in table 12.

Table 12: Bound GRGDYP (%) to mannuronan, ^{1}H NMR. The sample named *PolyM+RGD* is a peptide coupled mannuronan sample, prepared before epimerisation and active coal filtration. The sample named *After a.c.f* was epimerised with AlgE4 and AlgE6 and has been filtrated with active coal.

	Integral at ppm			Coupling(%)	
	6.9	7.2	2.8	Me-O-Tyr	Adducts
PolyM+RGD	0.0075	0.0104	0.200	0.45	3.3
After a.c.f	0.0358	0.0258	-	0.39	-

The adducts were not calculated for the coal filtrated sample as the N-acylurea adducts were removed.

For the mannuronan sample, the total amount of mannuronic acids are represented by one peak in the spectrum (4.60-4.80 ppm). The integral for this peak is set as 1. However, the alginate sample that was epimerised could not be represented by one proton peak in the ^{1}H NMR spectra, as it contains G-sequences and polyalternating sequences (compare spectra for *Mann.+RGD* with *Mann.+RGD+AlgE4* and *Mann.+RGD+AlgE4+AlgE6* in figure 38). Therefore, the integrals of all the alginate peaks were summarized and the aromatic peaks were calculated as a relative percentage to these. The width of the integrals for the aromatic peaks after a.c.f, were set based on the width from the aromatic peaks found before epimerisation and a.c.f (figure 43). The calculations of the peptide concentration after coal filtration is therefore overestimated.

Active coal filtration successfully removed adducts, but have also drastically reduced the amount of peptide present, as can be seen from the enhanced spectra of aromatic tyrosine protons below in figure 43.

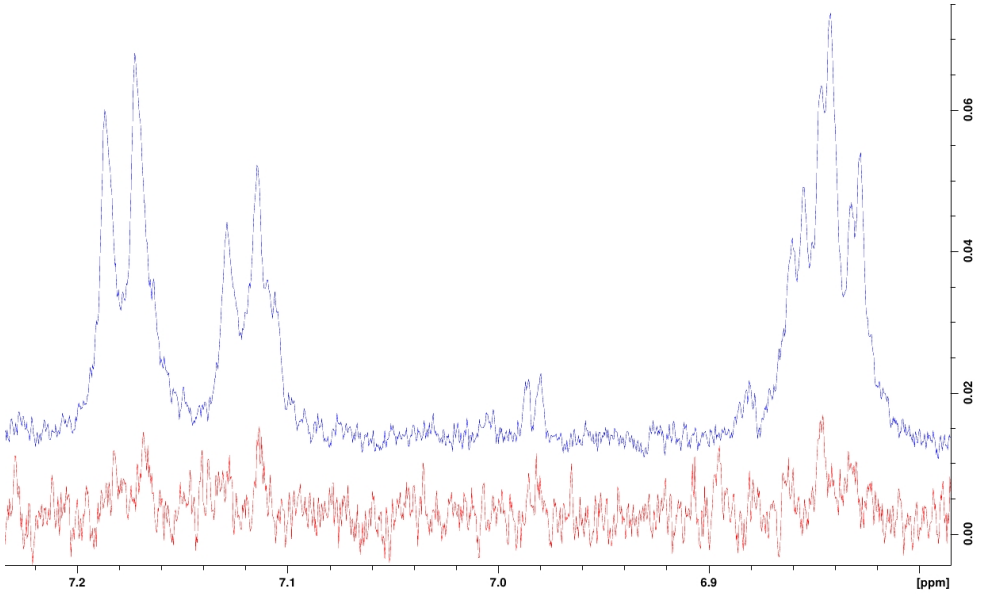

Figure 43: Expansion of GRGDYP signals, before and after active coal filtration, ^{1}H NMR. Blue line show the sample taken before active coal filtration, while the red line represent the spectra after active coal filtration. The spectra were recorded at 600MHz.

In the spectra recorded at 600MHz (figure 43), the water signal was suppressed which affects the alginate proton peaks, causing them to be distorted and small. Thus, integration of the aromatic proton peaks relative to the alginate peaks was not possible. Calculating the amount of GRGDYP coupled was therefore based on spectra recorded at 400MHz, where the water signal was not suppressed, and the relative integrals between alginate and aromatic proton peaks could be calculated. The spectra recorded at 400MHz are included in appendix S.

The effect of coal filtration on absorbance at 280nm was measured. A sample was taken out prior to coal filtration and compared to a sample after coal filtration. The non-filtrated sample gave an absorbance of 0.034 at 280nm which corresponds to a coupling of 0.0065%. However, a greater absorbance was observed for the coal filtrated sample which gave an absorbance of 0.130 at 280nm. This corresponds to a coupling of 0.14%. The change in absorbance is probably caused by a reduction of background noise, giving a higher signal/noise ratio. Figure 44 show the absorbance spectra for two samples of GRGDYP coupled to alginate, one taken before active coal filtration (black) and one after (red).

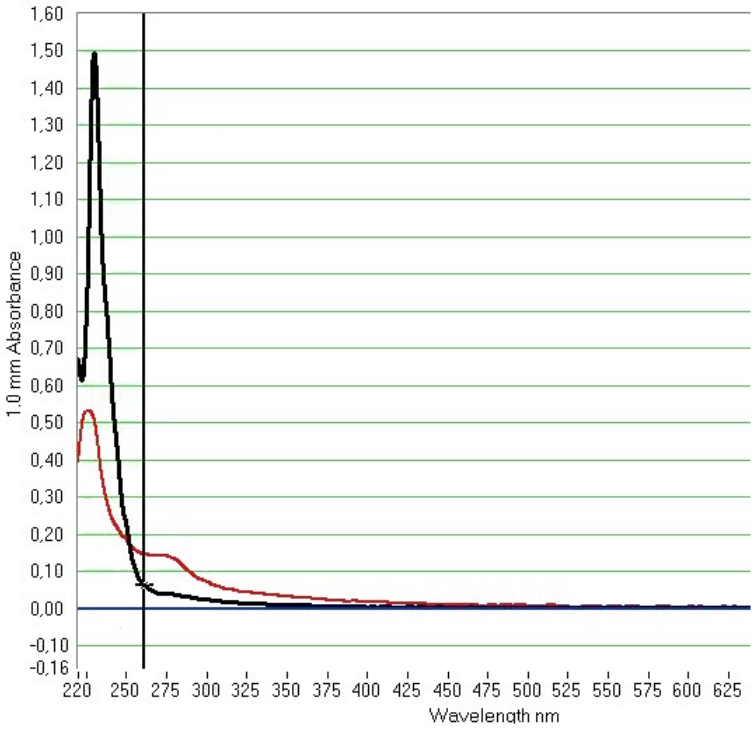

Figure 44: GRGDYP coupled to alginate before active coal filtration (black) and after (red), determined by UV/vis spectroscopy. The absorbance was measured at 280nm. The red line show the absorbance for the sample taken after active coal filtration, while the black line show the sample taken out before active coal filtration.

A ^{1}H diffusion spectroscopy was recorded of the peptide coupled sample before and after active coal filtration and is shown in figure 45.

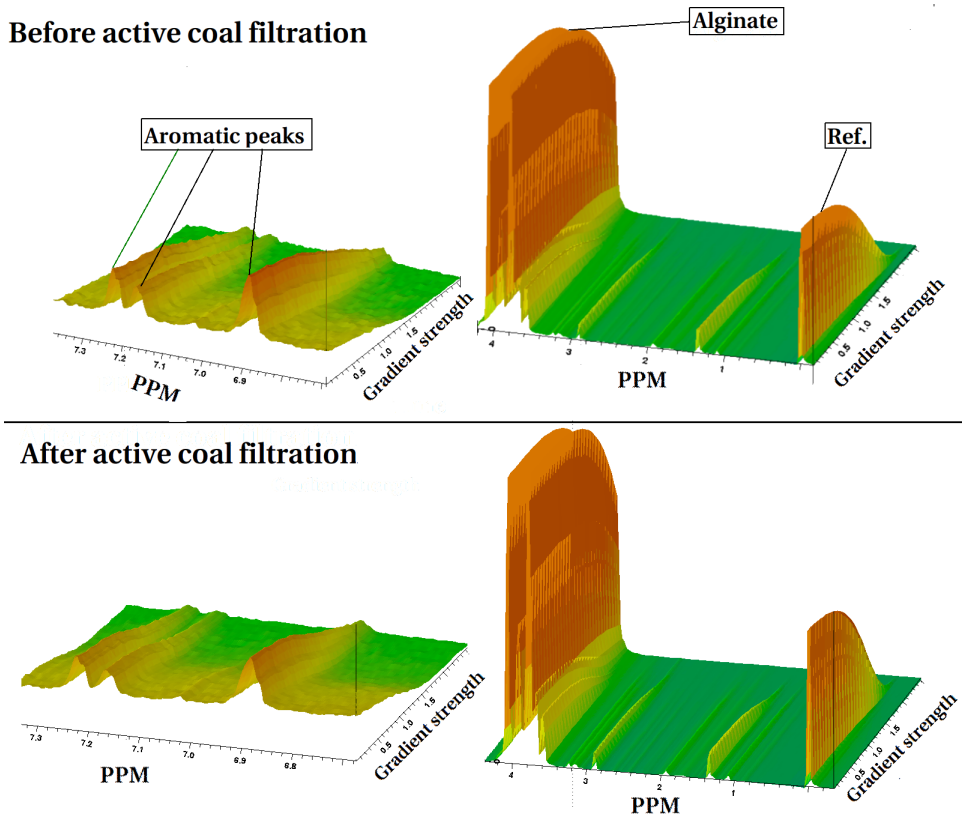

Figure 45: Diffusion ordered spectroscopy, before and after coal filtration. The ^{1}H diffusion spectroscopy spectra show the signal decay as a function of gradient strength and the chemical shift of the species present in the sample. Smaller molecules have faster signal decay than large molecules as they diffuse faster in the solution. Proton signals from alginate and aromatic peaks of tyrosine seems to have similar signal decay, indicating that the peptide is associated with alginate both before and after active coal filtration. The height of the aromatic peaks are lower after coal filtration, indicating that some fraction of the peptide has been removed. This is also observed in the ^{1}H NMR spectra (figure 43).

3.6 Encapsulation of olfactory ensheating cells

The following results were obtained from master student Marthe Fredheim Fjelldal who performed the encapsulation of olfactory ensheating cells in epimerised alginate with and without peptides produced in this study.

The viability of the cells was monitored by live/dead assay. 3D Z stack projections and cross-sectional images were taken by confocal laser scanning microscopy and the images are included in appendix T.

The peptide coupled alginate and the non-coupled alginate gave no differences in cell viability. No change in morphology was observed, indicating that there was no interaction of cells with the RGD-peptide.

3.7 Coupling of chitosan and insulin

Bovine and porcine insulin were coupled to mannuronan to a theoretical coupling of ∼10% to see if larger molecules could be coupled to mannuronan by using carbodiimide chemistry. Both insulin types have four tyrosines in their A and B-chain which can be identified with ^{1}H NMR spectroscopy[58]. Precipitation was observed for both ^{1}H NMR samples which made detection by ^{1}H NMR and UV/vis spectroscopy impossible. The precipitation may have been caused by hydrolysis in the slightly acidic MES-buffer[58]. The spectra are included in appendix U.

The acetyl side chain of chitosan dimers (AD) can be observed at 2.05 ppm with ^{1}H NMR spectroscopy. Chitosan dimers were succesfully bound to mannuronan in a dose-dependant manner as shown in figure 46. The peaks at 2.02 and 2.04 ppm are protons of the acetyl side chain of N-acetylglucosamine and acetate respectively. The acetate peak is an impurity from the lyophilization pump (personal conversation with Finn L. Aachmann).

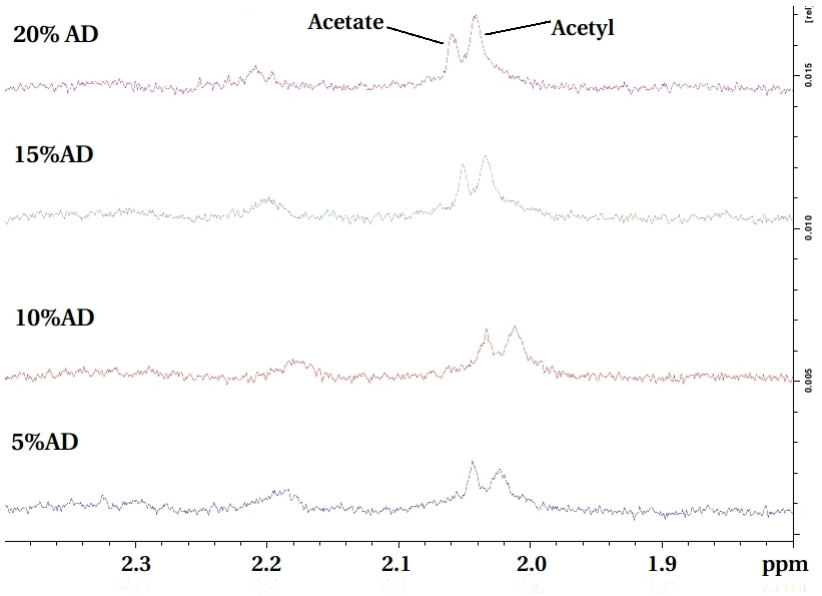

Figure 46: Coupling of chitosan dimer (AD) to mannuronan. The y-axis of the figure show the amount of AD dimer added, shown in relative percentage to the carboxylic acids of mannuronan. The coupling of AD to mannuronan activated with 10% EDC and sulfo-NHS was performed in 0.1M MES-buffer (pH=6.0) at room temperature. One sample was prepared for each 5% increase of AD. The spectra were recorded at 300MHz at 363K.

Table 13 show the calculated amount of chitosan dimer coupled to mannuronan, calculated by integrating proton peaks at 2.02 and 2.04 ppm in the recorded ^{1}H NMR spectra shown in figure 46. The integral was divided by 3, representing the three protons of the methyl group on N-acetylglucosamine (for molecular structure of AD dimer, see appendix U).

Table 13: Bound AD (%) to mannuronan, calculated from ^{1}H NMR spectroscopy

Added AD (%)	Integral at ∼2.0 ppm	Bound AD to mannuronan(%)
5	0.0028	0.093
10	0.0030	0.10
15	0.0037	0.12
20	0.0050	0.17

A diffusion spectroscopy was performed on a sample of AD dimer coupled to mannuronan and the specter is shown in figure 47. The acetyl peak from the chitosan dimer has the same decay as mannuronan, while the acetate group decay faster than the acetyl proton peak, as indicated by the arrow in figure 47. If two molecules have the same decay, they have the same size or they are associated with one another. Since the decay rate of the proton acetyl peaks are the same as the M-1 protons of mannuronan (see appendix R), this indicates that the chitosan dimer is associated with mannuronan.

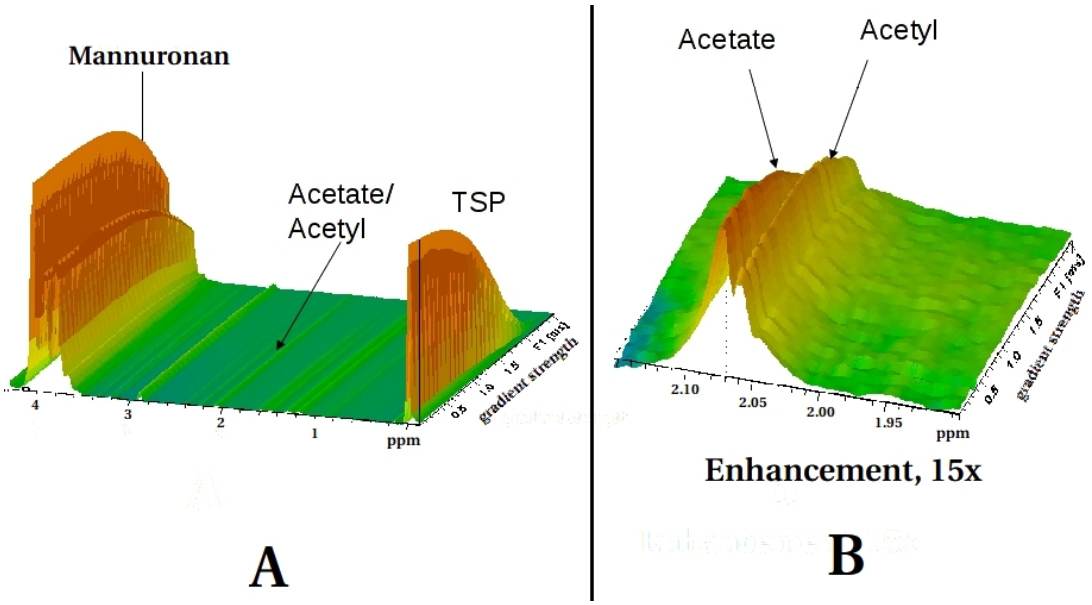

Figure 47: A: Signal intensity as a function of increased gradient strength. B: enhanced spectrum of acetyl peaks of chitosan (AD) dimer. Chitosan was coupled to mannuronan activated with 10% EDC and sulfo-NHS in 0.1M MES-buffer (pH=6.0) at room temperature. The spectra were recorded at 300MHz at 363K.

4 Discussion

Coupling of FA and 4AP to mannuronan

Fluoresceinamine and 4-aminophenol were both tested as model molecules for GRGDYP in the carbodiimide mediated coupling of GRGDYP to mannuronan. Fluoresceinamine is more hydrophobic than GRGDYP and demands a non-polar solvent in order to be properly solvated. When preparing a stock solution of FA in 0.1M MES-buffer, particles of FA were observed in the suspension. Using a stock solution simplifies the procedure when several samples and parallels are being prepared. However, the stock solution of FA in 0.1M MES-buffer was inhomogeneous, which makes it impossible to use for accurate addition of fluoresceinamine to the reaction beaker.

The differences in coupling when adding solvated FA (figure 20) was probably a result of the inhomogeneous stock solution, as different amounts of FA was being added for each parallel. However, addition of dry FA did not seem to give reproducible results either.

Decreasing the polarity of the solvent with addition of *e.g* 50% EtOH was beneficial for making a homogeneous stock solution, as the solubility of FA increased (as was shown in figure 21). However, mannuronan precipitates at higher EtOH concentrations[59] which is not beneficial for the coupling procedure or analysis with ^{1}H NMR. Using FA as a model molecule for GRGDYP is already cumbersome as it demands protection from light. Based on these findings it was decided to change the model molecule to 4AP, which is more soluble in water, is not light-sensitive and detectable by ^{1}H NMR and UV/vis spectroscopy.

Although 4AP gave more promising coupling degrees with reproducible results (see figure 22 and 25) compared to FA, 4AP changed its absorbance characteristics once coupled to mannuronan (see absorbance spectrum in figure 26). This was considered a major drawback as only ^{1}H NMR could be used to compare peptide coupling with coupling of 4AP to mannuronan. Also, 4AP gave higher degrees of coupling than GRGDYP at the same concentrations of EDC, sulfo-NHS and peptide. This indicates that 4AP is easier to couple to mannuronan than GRGDYP, which also makes 4AP not suitable as a model molecule.

Varying pH for coupling

Coupling of 4AP, Me-O-Tyr and GRGDYP to mannuronan was tested in MES-buffers with varying pH in order to determine if the pH value influenced the degree of coupling. For the model molecules, the pH-values 5.5, 6.0 and 6.5 were tested, while the peptide was tested at pH=5.5 and 6.5.

The highest coupling was observed at pH 6.5 for GRGDYP (figure 35), 6.0 for 4AP (figure 25) and 5.5 for Me-O-Tyr (figure 30). A study performed by Rowley *et. al* on pH-optimisation indicated that pH=6.5 is optimal for peptide coupling[8]. The results described here indicate the same.

A qualitative comparison between the formation of adducts indicate that at pH=5.5, the formation is lowest for GRGDYP (figure 35), for Me-O-Tyr it is lowest at pH=6.0 (figure 30) and for 4AP it is lowest at pH=5.5 (figure 25). The pH variations when coupling Me-O-Tyr was performed at 0°C, while the pH variations were performed at 20°C for 4AP and GRGDYP. This means that the results are not fully comparable, as they were not prepared in the same way.

For 4AP, the pK_a of the amine group is 5.5[50],for Me-O-Tyr the pK_a for the amine group is around 7.4[60], while the terminal amine group of GRGDYP is 7.2-7.4[8]. At pH-values below the pK_a, the majority of the amine groups are protonated. This lowers the rate of amide bond formation, as the lone electron pair of the amine is, to a larger extent, bound to a proton. As the pH increases, a proton dissociates from the amine and the amount of amine groups with available lone electron pairs increase. This will in turn cause a higher probability of nucelophilic attack on the formed carboxylic anhydride and in turn product formation (the reaction is shown in figure 6). It is thus expected that optimal coupling occur at the amine groups pK_a and above. Activating EDC with sulfo-NHS in MES-buffer at pH= 5-6, and then raising the pH to 7.2-7.5 with phosphate buffer before adding the amine is beneficial for optimal coupling[46] [47]. However, this may be practical when coupling to solid materials that are easily washed and removed from the reaction beaker, but is not practical when coupling to solubilized alginate. Instead of changing the buffer, the pH can be raised to 7.2-7.5 before adding the amine. The optimal pH value for peptide coupling at $\sim$7 is probably caused by the pK_a of the peptides, but this is not stated in the cited papers[46] [47].

4AP has a pK_a that is approximately two pH-units lower than Me-O-Tyr and GRGDYP. It is therefore expected that optimal coupling for 4AP will take place at lower pH-levels than GRGDYP and Me-O-Tyr. However, the differences in coupling 4AP to mannuronan when varying the pH from 5.5 to 6.5 were small, and all pH-values

gave coupling degrees of 0.7%. This indicates that coupling of 4AP to mannuronan with carbodiimide chemsitry can be performed in the pH interval 5.5-6.5 without any differences in coupling.

Although the pK_a of Me-O-Tyr is closer to GRGDYP compared to 4AP, comparing the results from Me-O-Tyr and GRGDYP does not give any obvious correlation between pH and coupling. For GRGDYP, the highest coupling was achieved at pH=6.5 wile for Me-O-Tyr the higest coupling was at pH=5.5. These are also the pH-values that had the highest peaks at 2.90 ppm, indicating that some of the detected Me-O-Tyr and GRGDYP are associated in adducts.

When varying the pH in the MES-buffer for coupling 4AP to mannuronan, the highest coupling was obtained at pH=6.0 with a degree of coupling of 0.73% (figure 25). When coupling Me-O-Tyr to mannuronan, the degree of coupling is approximately 0.2% (figure 30), which is close to the results when coupling GRGDYP($\sim$0.2%, figure 35). This suggests that Me-O-Tyr is a better model molecule for peptide coupling as the coupling degrees are similar. The degree of coupling 4AP was more than three times larger than coupling of Me-O-Tyr and GRGDYP. Increased reactivity of 4AP can be explained by its hydroxyl group. This functional group can act as a nucleophile towards the protonated O-acylisourea, and thus increase the degree of coupling (see 2^{nd} *carbocation* in figure 8). However, Me-O-Tyr also contain this active site and the pK_a of the hydroxy group of Me-O-Tyr and 4AP is approximately the same[50] [60]. This may indicate that the pK_a and the reactivity of the amine group is more important for coupling efficiency than the hydroxyl group of the model molecule.

For Me-O-Tyr, the pH with the largest degree of coupling had the parallels with the largest degree of adducts, which is also the case for GRGDYP. This indicates that Me-O-Tyr can be associated with adducts, contributing to the aromatic peaks and giving an overestimated degree of coupling. The parallels with the lowest amount of adducts may thus give a better representation of the actual amount coupled to mannuronan, as the contribution from adducts are smaller. As mentioned earlier, Rowley *et. al*[8] showed that the optimal peptide coupling was achieved at pH=6.5, and no active coal filtration was performed. However, the method used for determining the amount of peptide coupled was based on radiolabelled peptides. By comparing the radioactivity before and after coupling and taking into account the decay, the degree of coupling was calculated. If there are no quantification of the amount of adducts formed, it is likely that the pH with the highest radioactivity represent the sample with the highest amount of adducts formed.

Since the carbodiimide reaction is most efficient at low pH-values, a higher produc-

tion of adducts can be expected as the pH increase[13]. The mannuronic acids were incubated with EDC at pH=4.2 and the pH was increased to 5.8 before adding the peptide (figure 34). However, incubating the mannuronic acids with EDC and sulfo-NHS at pH=4.2 did not give an increased product formation. This may be caused by a lower amount of deprotonated amine groups in the solution, causing a decreased nucleophilic attack on the carboxylic anhydride. At low pH-values, there are more protons that can form the first carbocation which is necessary for O-acylisourea formation (see figure 8). The carbocation is highly reactive, and may hydrolyse to a non-reactive urea derivate if the concentration of carboxylate ions is too low (figure 10). If this happens, increasing the pH will not cause an increased reaction between carboxylate ions and EDC as a fair portion of EDC has been formed into urea derivates. However, sulfo-NHS is supposed to reduce hydrolysis by forming a stable intermediate.

Wether the reaction rate of hydrolysis is faster than O-acylurea formation at low pH is a target for further studies, but the results indicate that coupling at pH=4.2 is not beneficial for increased peptide coupling.

Samples with increasing amounts of peptide and constant amounts of EDC and sulfo-NHS were prepared at pH= 4.0 and 6.0 to determine any differences in peptide coupling when the pH and amounts of GRGDYP was varied (figure 36). When deducing the coupling by ^{1}H NMR, the highest coupling was achieved at pH 6.0 when the added sulfo-NHS, EDC and GRGDYP was 20%. The results from these experiments questions the influence of the pH on the coupling reaction as no clear differences in coupling could be observed at pH 4.0 and 6.0. At pH=4.0 and pH=6.0, the trend is increased peptide coupling and the coupling degrees are quite similar, except for the coupling at 3.4% observed at pH=6.0 and 20% Me-O-Tyr added. The results indicate that the coupling efficacy og GRGDYP is equal at pH 4.0 and 6.0, which is not in accordance with the discussion above.

For both pH-values, the amount of adducts was higher at lower concentrations of added peptides. The high amounts of adducts questions the efficacy of sulfo-NHS at pH=4.0 and at pH=6.0 as adduct formation is seen at these pH-levels.

When comparing the proton peaks for this experiment (figure 37) with the calculated results (figure 36), there are discrepancies. In the spectra, the coupling seems higher at pH 4.0, but the calculations show a higher coupling at pH 6.0. When inspecting the peaks in figure 37, the aromatic peaks at pH 4.0 are more distinct compared to the parallels prepared at pH 6.0. The peaks at pH 6.0 are broader, which makes the integration difficult. At approximately 7.21 ppm when the pH is 6.0, there is a broad peak that was included in the integrations. Wether this in fact is an aromatic

peak of GRGDYP or not is difficult to determine. Since a broadening of the peaks happened for all samples prepared at pH=6.0, it is believed that the integrations should include the broadened peak at 7.21 ppm. However, if this is not correct, the resulting integrations will be lower for all parallels at pH 6.0.

Since all the samples referred to here were not rinsed further than dialysis, adducts may still be present (for structure of adducts, see figure 14). Presence of adducts influence the estimated coupling to mannuronan, as an unknown portion of the model molecule or peptide are associated in adducts [44] [61]. As a compromise between adducts and product, an intermediate pH of 6.0 was chosen for further Me-O-Tyr and peptide coupling.

As has been mentioned in section 1.6.1, controlling the formation of by-products and adducts is difficult and it may be that the differences in by-product and adduct formation is not a result of the pH-level, as was indicated when coupling GRGDYP at pH 4.0 and 6.0 (figure 36). In order to determine at which pH the lowest amount of adducts are formed, or if the pH is important at all, a larger more thourough study has to be performed. Here, only two parallels were prepared for each pH-value, which is too low to predict or conclude on how the pH influence the reactions.

Varying the temperature

Coupling of Me-O-Tyr to mannuronan was performed at 0°C and 20°C. No obvious changes in adduct or product formation was observed (figure 27). The litterature [13] suggests that letting sulfo-NHS, EDC and mannuronan react at 0°C before adding the amine would lower the amount of unwanted adducts as the rate of adduct formation is lower. Since the mannuronan in this experiment was not cooled before adding sulfo-NHS and EDC, the results may not represent a true coupling at 0°C and may explain the deviation from litterature [13].

When varying the incubation time at 0°C (figure 29), mannuronan was cooled before adding sulfo-NHS and EDC, giving a more representative description of the reaction at 0°C.

The results from this latter experiment show that the level of adducts are higher at 20 and 40 minutes compared to 60 minutes (figure 29). This suggests that the incubation time at 0°C affects the formation of adducts. The peptide coupling and adduct formation was reduced from 20°C to 0°C. A reduced amount of peptide coupling is not desirable, and it was decided not to cool mannuronan before coupling.

Cooling a large sample of 500mg high molecular weight mannuronan is quite different from cooling down parallels of mannuronan that has a degree of polymerisation of 40-50 when it comes to the viscosity. The viscosity depends on the molecular size,[2] and is also temperature dependent[62]. As the molecular size increase and the temperature decrease, the viscosity of the solution increase. Thus, applying low temperatures to a high molecular weight alginate solution may cause a lower coupling as the polymer chains are moving less.

Increased incubation time at 20°C

Increasing the incubation time of coupling 4AP was beneficial for increased coupling (figure 23). The percentage bound 4AP increased rapidly from 15 min to 4-6 hours and then levelled off towards 24 hours incubation time. Incubation times described by Westhrin was set to two hours when coupling FA[49].

However, as noted in the discussion above in *Varying pH for coupling*, the coupling degree may be higher when using 4AP compared to GRGDYP. Still, the trend of the kinetic experiment is thought to be applicable to peptide coupling.

By inspecting the singlet at 2.90 ppm in figure 24, it can be observed that the peak intensity increase up to four hours, but is quite stable from four hours and above. This has probably affected the reported results, as the calculated coupling degree does not separate product from adducts containing 4AP. Determining how much of the adducts are associated with 4AP is difficult to deduce without active coal filtration.

The reaction time was extended to eight hours or more for coupling GRGDYP to mannuronan. Although the adduct formation increase with reaction time, the amount of RGD-coupled mannuronan may also increase. Filtrating these samples with active coal would have purified the samples and the calculated amount of peptide coupled would give a more representative number than an unfiltrated sample due to the removal of adducts. However, active coal filtration would have complicated the procedure. First, all samples would have to be larger than 1mL in order to perform pH-adjustments for acid degradation and coal filtration. Second, the starting point would be high molecular weight mannuronan in order to pass the sample through the active coal without being retarded. In the filtration set-up described here, only two samples are filtrated at the same time. After filtration, the samples would have to be degraded by acid hydrolysis before ^{1}H NMR analysis. These steps seem few, but would have caused an increase in the experimental time, resulting in fewer performed experiments. The starting point for the optimalised experiments has been a batch of

already degraded high molecular weight mannuronan that before analysis was rinsed with dialysis and filtrated after peptide coupling.

Varying amount of reactants

Testing the ratio between EDC and added Me-O-Tyr gave the highest coupling when adding 20% EDC, sulfo-NHS, and Me-O-Tyr. At these concentrations, the coupling was approximately 0.5% (figure 31). A similar experiment was conducted with GRGDYP, and adding 10% EDC and sulfo-NHS and 20% peptide gave the highest coupling of 3.4% (figure 36).

For the peptide coupled samples, the adduct formation decreased rapidly when the amount of added GRGDYP exceeded the amount of EDC in the reaction beaker. This indicates that optimal coupling of GRGDYP happens when the amounts of GRGDYP are above EDC. For Me-O-Tyr, a marked increase in adduct formation was observed when adding 10% EDC and 15% Me-O-Tyr. When adding 20% EDC, a more constant level of adducts was observed for all samples. This indicates that the adduct contribution is larger as the concentration of Me-O-Tyr exceeds the EDC-concentrations, but is quite stable when concentrations are equal, or when the concentration of Me-O-Tyr is less than EDC.

The reason for the discrepancies in N-acylurea adduct formation between adding 10% EDC and sulfo-NHS and varying the amounts of Me-O-Tyr and GRGDYP is quite difficult to adress, as the only differences between the experiments were the coupled molecule. However, when GRGDYP was coupled, two parallels were prepared for each concentration of GRGDYP while only one sample was prepared for each Me-O-Tyr concentration. This questions the reliability of the Me-O-Tyr results, as no interparallel comparisons can be discussed.

Samples containing higher ratios of Me-O-Tyr:EDC were prepared in order to establish if the coupling of Me-O-Tyr to mannuronan increased with increasing Me-O-Tyr. The results indicate that the coupling decreased when the Me-O-Tyr:EDC ratio exceeded 2:1 (figure 32). Here, the maximum yield was calculated to 6% (see appendix B for calculating yields) when coupling 20% Me-O-Tyr in 10% EDC (figure 32). For any greater concentrations of Me-O-Tyr, the degree of coupling decreased. The presence of adducts did not seem to be affected by the amount of Me-O-Tyr added as they were all varying between ∼0.3-0.5%. This reduce the adduct formation to the efficacy of EDC and/or sulfo-NHS. However, when comparing the adduct formation when the Me-O-Tyr concentrations was varied up to 20% (figure 31), the adduct formation were ten times larger compared to the adducts when coupling up to 100%

Me-O-Tyr (figure 32). It was expected that the adduct formation would continue to increase as the Me-O-Tyr concentration exceeded the EDC concentrations, this however, was not the case. The apparent random formation of adducts illustrate how difficult it is to predict the amounts of adducts formed.

Sulfo-NHS is added in order to prevent N→O displacement of O-acylisourea, still the amount of N-acylurea adducts formed far exceeds the product formation. This is a major drawback of utilising carbodiimide chemistry as expensive peptides are dialysed out and thrown away. If sulfo-NHS was in fact effective, no peaks at 2.9 ppm would be observed. Still, a large portion of adducts are observed for all samples, indicating that N→O displacement of O-acylisourea readily occur in the reaction beaker. A comparison of a carbodiimide mediated coupling with and without added sulfo-NHS would have indicated to which extent the sulfo-NHS prevents formation of N-acylurea adducts. A more precise conclusion on sulfo-NHS activity could have been drawn from this comparable study.

For the large scale peptide-coupled sample, 10% EDC and 5% GRGDYP were chosen as appropriate amounts. This was due to the cost and availability of the peptide. 5% added peptide to 500mg mannuronan corresponds to 200mg peptide. When the same ratio was tested on Me-O-Tyr (figure 31), a coupling of 0.24% was obtained. For coupling GRGDYP, an average coupling of 0.63% (one parallel had 0.48%, the other parallel had 0.77%) was achieved (figure 36). Although the adducts were quite high for the peptide (figure 36), it was still not clear how much of the peptide was associated in unwanted adducts. However, testing concentrations of EDC and GRGDYP that were known to give higher levels of adducts, offer a possibility to deduce how much of the peptides are associated in adducts.

Rowley *et. al* [7] [8] reports molar EDC:Alginate ratios of 1:20, meaning an activation of every 20 carboxylic acids of alginate, or 20%. Sulfo-NHS is added in the molar ratio 1:2 to EDC, which corresponds to 10% to the alginic acids. Their reported incorporation of peptides ranges from 55% [7] to above 80% [8]. In this study, the amounts of EDC and sulfo-NHS were always added in a 1:1 molar ratio with a maximum yield of 17% (For calculating the yield, see appendix B, equation 5). The amounts of peptides added is not reported by Rowley *et. al*, which makes it very difficult to compare their reported results with the results attained in this study.

Choice of detection methods

As has been discussed above, the presence of adducts influence the calculated amount of peptide or model molecule coupled to mannuronan. This illustrates that only investigating the amide coupling is not sufficient, as an unknown amount is coupled in adducts. Thus, using a detection method where adducts and peptide coupled to mannuronan are identified and quantified is important for a comprehensive understanding of the carbodiimide mediated coupling.

Different analytical methods have been applied for determining the incorporation of peptides to various surfaces. The use of radiolabelled ^{125}I- GRGDYP [7] [8] [63] has been reported. These studies offer no quantification of the amounts of adducts present. By using radiolabelled peptides for quantification, Rowley *et al.* [8] reports coupling efficiencies of ∼80%. This is remarkably different from the yields attained here. The highest coupling reported in this study was 3.4% coupling of peptide (see appendix S, table 36), which corresponds to a yield of 17% (see appendix B for calculations of yields). This is substantially lower to yields reported elsewhere, where the coupling yield is up to 60% [7] and 80% [8] [64]. However, Rowley *et al.* [7] reports a maximum peptide incorporation of 400μmol peptides/L when adding 1000μmol peptides/L. In this study, adding 5% GRGDYP to 10 mg mannuronan (in 1mL MES-buffer) corresponds to 2520μmol/L added peptide, and reaching a peptide coupling of *e.g* 3.4% calculated from ^{1}H NMR, corresponds to 1713.6μmol peptides/L. This means that, although Rowley *et. al* reports a higher yield, the incorporated amount of peptides is higher in this study compared to results reported by Rowley *et. al* [7].

Another approach is indirect quantification with HPLC where the amount of unreacted soluble peptides are measured. This value is subtracted from the initial value and the difference is set as incorporated peptide [64]. Also, HPLC/UV and UV quantifications can be employed [11]. Coupling a chromophore to the peptide can enable spectrophotometric detection [44]. However, these methods does not offer a quantification of adducts.

Amide bonds on solid surfaces can be detected via IR at 1650 and 1530 cm^{-1} [11], but these may also include N-acylurea [12].

Using ^{1}H NMR to deduce N-acylurea adducts will give a more comprehensive understanding of the formation of peptide coupled mannuronan as well as adduct formation. In addition, ^{1}H NMR, and diffusion spectroscopy enables not only a quantification and identification of all species present but can also indicate if the peptide is associated with mannuronan or not.

Although ^{1}H NMR can quantify the amount of adducts present, the method can not quantify the amount of peptide associated in unwanted adducts. Purification by *e.g* active coal filtration can remove unwanted hydrophobic side products, and ^{1}H NMR can again be performed on the sample. As has been shown here, purification with active coal reduced the amount of adducts, and integration of aromatic peaks of the filtrate is thought to represent the wanted product.

The aromatic peaks at 7.20 and 6.90 ppm recorded by ^{1}H NMR are very small compared to the adjacent mannuronan peak (*e.g* in figure 35). Setting the baseline is a source of high error, as only small changes in baseline settings can drastically change the integral. The spectra of mannuronan in D_2O display large peaks in the area 3-5 ppm due to residual water. These peaks cause a distortion of the baseline, pulling up smaller adjacent peaks. The aromatic peaks are further from the central peaks compared to N-acylurea at 2.90 ppm. As a consequence of this, the peaks at 2.90 ppm may be overestimated when integrated. Setting the baseline when integrating with respect to the products and adducts is difficult due to the large central peaks, as the baseline needs to be bent in order to perform integration. Thus, the integrations based on ^{1}H NMR is not without error.

There is a large deviation between results calculated from ^{1}H NMR and UV/vis spectroscopy. The absorbance measurements were performed several months after the initial experiments which may have influenced the absorbance properties. The samples were resuspended prior to measurements, but particles may have been present in the solution or there might have been bacterial growth in the NMR tubes. This may have caused an inhomogeneous solution creating scattering of the light beam and thus a greater source of error. The samples were kept refrigerated and sealed in NMR tubes, but water may have evaporated from the samples causing a higher concentration of the sample. This complicates the comparison between ^{1}H NMR and UV/vis spectroscopy. In retrospect, the samples should have been analysed by UV/vis spectroscopy immediately after ^{1}H NMR spectroscopy in order to have comparable results.

Large scale production of RGD-coupled alginate

The results from the large scale epimerisation of mannuronan by AlgE4 and AlgE6 gave a lower G-composition than wanted for the peptide-coupled sample. The incubation times and enzyme concentrations were based on previous work performed by master student Kristin Karstensen[54] who optimized epimerisation of mannuronan by AlgE4 from *H. polymorpha* and AlgE6 from *E. coli*. Even though the procedure for AlgE6 epimerisation was followed as described by Karstensen[54], the same results were not obtained.

Karstensen prepared several batches of mannuronic acids that were epimerised with AlgE4 and AlgE6 to produce alginates with high and low G content. The two batches prepared for low G with and without RGD coupling is compared to the results described here, as the same incubation time of AlgE6 was used in both studies.

Karstensen incubated mannuronan samples in AlgE4 for 48 hours and attained F_{MGM} ranging from 0.1 to 0.3. The F_{MGM} for the study described here was calculated to ∼0.3-0.4 after 10 hours incubation time with AlgE4 epimerisation for the peptide coupled sample, and 0.5 for the non- coupled sample (table 40). This indicates that the AlgE4 activity has been higher for the non-coupled sample.

Incubation of AlgE6 was performed under the same conditions as Karstensen[54]. In the study described here, F_{GGG} was calculated to 0.05 before active coal filtration for the RGD-coupled alginate, and 0.08 for the non-coupled sample (table 40). It may seem that the activity of AlgE6 described here has been affected by the peptide coupling, as the F_{GGG} and F_{GG} were higher for the non-coupled sample. Karstensen reported less variability and higher values for both coupled and non-coupled alginates (F_{GGG} ∼0.1-0.2).

The average block length ($N_{G>1}$, table 40) was calculated to four or less after incubation with AlgE6. The longest average block was obtained for the non-peptide coupled sample with an average block length of four. The short G-blocks may eventually lead to softer gels that may influence the encapsulation and cell viability. However, MG-junctions also participate in gel formations[19] and it is believed that the produced alginate will have the proper geling abilities for cell encapsulation. Karstensen reports average block lengths ranging from 4 to 7 and no specific differences between peptide-coupled and non-coupled samples were observed. In the study reported here, the geling abilities of RGD-coupled alginate was tested before cell encapsulation by dripping the alginate in a 50mM $CaCl_2$-solution. Gel formation was observed and was considered strong enough for further cell encapsulation.

Karstensen had a lower peptide coupling than what was reported here, with reported couplings of ∼0.1 and >0.20%. The percentage coupling of RGD to the peptide-coupled sample described here, was calculated to 0.45% before active coal filtration, which is close to the test coupling of 5% GRGDYP and 10% EDC (figure 36). The percentage coupling is more than twice the amount of the largest coupling described by Karstensen. UV/vis measurements taken from the large scale experiment show an absorbance corresponding to 0.1% peptide after coal filtration (figure 44). The same value was calculated by ^{1}H NMR to be approximately 0.45%. The absorbance measurements were performed a week after ^{1}H NMR, and no bacterial growth or any other impurities were observed. Thus, the UV/vis measurement is assumed to represent a less erroneous value compared to previous UV/vis measurements shown in this study. The coupling of ∼0.4% calculated from ^{1}H NMR is likely overestimated, as the width of the integrals were set based on the spectra recorded before active coal filtration. Thus, the coupling after active coal filtration is likely below 0.45% and is probably in the range of 0.1-0.4%.

The results obtained by Marthe Fredheim Fjelldal on encapsulation of olfactory ensheating cells gave no enhanced cell viability or morphology changes in the RGD-coupled alginate hydrogels. As was concluded by Karstensen[54], the gel rigidity seemed to affect the viability and metabolic activity of encapsulated C2C12 myoblast cells, more than the prescence of RGD on the alginate surface. The cells encapsulated by Karstensen in low-G alginate had higher viability and metabolic activity compared to capsules prepared with higher G-content. The low-G alginate capsules prepared by Karstensen had higher F_G, F_{GG}, F_{GGM}/F_{MGG}, F_{GGG} and $N_{G>1}$ than the peptide coupled sample described here. This indicates that an increased AlgE6 epimerisation in the peptide-coupled alginates would have been beneficial for increased cell viability and morphology changes.

The differences in peptide coupling compared to Karstensen, may in fact explain why there is a lower AlgE6 activity in this study. The bound peptides may have sterically hindered AlgE6 epimerisation to a larger extent compared to Karstensens results. This is however only speculations, and there may be several reasons for lowered AlgE6 epimerisation. Another reason for the low epimerase activity can be explained by the dry weight of the enzyme. In the peptide coupled sample there are several small organic molecules in addition to the peptide that can interfere with the enzyme. These are sulfo-NHS, N-acylurea and possibly several other by-products of EDC that were not removed by dialysis. These molecules may inactivate the enzyme by *e.g.* blocking the active site. If the peptide coupled sample was subjected to extensive dialysis, and possibly active coal filtration prior to epimerisation this would

have indicated whether components from the carbodiimide reaction influenced the enzyme activity. Also, the dry weight of AlgE4 contain salt and other proteins that in turn would lead to a lower concentration of enzymes. However, the same weighing procedures were performed for the peptide and non-peptide coupled sample.

The stiffness of the gel seem to be of importance, depending on the type of cells that are encapsulated[42]. This underlines the importance of being able to produce epimerised RGD-coupled alginates with varying stiffness. Considering the low activity of the enzymes in the epimerisation described here, it is tempting to suggest a starting point that is not mannuronan. Coupling an alginate sample that already has the correct M- and G-frequencies, will remove the epimerisation procedure but active coal filtration should still be performed as it has been shown to remove unwanted adducts. A similar attempt was performed in this study, by attaching Me-O-Tyr to alginate beads. Unfortunately, the amount of adducts far exceeded the amounts of Me-O-Tyr coupled. Coupling to alginate beads is further discussed later.

Figure 40 compares peptide coupled mannuronan with AlgE4 epimerised samples. After epimerisation with AlgE4, new peaks are visible at 3.0-3.6 ppm for both the peptide coupled and non-coupled sample. These peaks are not known by-products, adducts, MOPS buffer or alginate. The peaks are still present after AlgE6 epimerisation (figure 41). However, active coal filtration seem to have lowered the intensity of the peaks. These peaks represents small molecules, and the singlet at $\sim$2.5 ppm is most likely methyl protons. Since the molecule(s) are not removed by active coal, this indicates that the molecule(s) are hydrophilic (personal conversation with Finn L. Aachmann).

From which step in the procedure the molecules originate from is difficult to say, as the samples taken out for ^{1}H NMR were not handled with sterile equipment. The impurities may have entered the samples during epimerisation, acid degradation or from impurities in the NMR tubes. It is therefore not possible to say if the ^{1}H NMR sample truly represents the large scale sample, as the former was not degraded and handled with utter care to avoid any contaminations. If contaminants are in fact present in the large scale samples, it is difficult to deduce how or if these molecules will affect the geling or cell attachement properties of the alginate hydrogels.

Active coal filtration gave an effect on the N-acylurea peak at 2.90 ppm (figure 42), and also had an effect on the amount of peptide present (figure 43). The UV/vis measurements of the peptide coupled sample before and after coal filtration (figure 44), show an enhanced peak at 280nm after active coal filtration, which is probably due to a purification of the sample. This may support the hypothesis that a portion of the peptides are coupled in adducts, and that a substantial amount is removed by

active coal filtration.

Filtrating the alginate samples with active coal is necessary because of the bacterial origin of the enzymes and because it removes a substantial amount of the N-acylurea adducts (figure 42). Rowley *et. al* use alginate with high G-content when optimising their carbodiimide coupling[8]. When the starting point is alginate with high G-content, introducing G-blocks by epimerases is not necessary and no coal filtration is thus reported. By not filtrating the samples with active coal, it is believed that the alginate material will contain a substantial amount of impurities. If the RGD-sequence is associated with adducts in such a way that its conformation is intact, it may be that the adducts contribute to the cell adhesion. When encapsulating myoblasts, Rowley *et. al* used active carbon to remove any by-products. Still, the reported incorporated yields of peptides were 55-60%[7]. These yields correspond to 400μmol peptide/L. 1% incorporated peptide to a 10mg mannuronan (50.5μmol mannuronan) sample in 1mL corresponds to 505μmol peptide/L, meaning that 400 μmol peptide/L corresponds to 0.79% coupled peptide to alginate. This is higher than the calculated peptide incorporations after active coal filtration described here, which was set to 0.1-0.4.

Coupling to alginate beads

Coupling Me-O-Tyr directly to alginate beads were performed in order to determine if this procedure could be considered a novel approach to peptide coupling. 10% sulfo-NHS and EDC, and 20% Me-O-Tyr were added to the beads. These concentrations were previously shown to give high degrees of coupling (figure 31).

The coupling in this study was performed with the model molecule Me-O-Tyr, and it is believed that coupling a peptide sequence in the same way would render the same results as for Me-O-Tyr. Coupling a peptide sequence directly to alginate beads has three advantages: first, the coupling will occur at non-geling residues, secondly, the coupling is performed in organic solvents which is thought to increase the peptide coupling, and third, epimerisation with enzymes are not necessary. Alginate precipitates in organic solvents such as EtOH and formamide, making it difficult to perform the coupling in these solvents. However, when the alginate is chelated with divalent cations, the precipitation is lower and the coupling can still be performed (personal communication with Berit L. Strand). After coupling, the beads are dissolved with EDTA, dialysed and filtrated with active coal before lyophilization. The peptide-coupled alginate is solvated and prepared for cell encapsulation.

As an alternative to coupling directly to a bead, the coupling could have been per-

formed on alginate before cross-linking. However, the peptide can couple to guluronic carboxylic acids which may affect the geling properties. Rowley *et. al* use this approach, and does not report any problems with geling[7] [8].

One major drawback of starting with alginate is quantification of the peptide coupling with ^{1}H NMR. The mannuronic protons peaks as a singlet which is easy to integrate, while the alginate peaks at several different chemical shifts. This makes deduction of the coupling in ^{1}H NMR easier with mannuronan than alginate, and the calculations are less prone to errors.

5 Further studies

The peptide-, sulfo-NHS and EDC concentrations used in the large scale batch described here was known to give a larger quantity of unwanted adducts. Thus, producing a large scale batch of 20% EDC, sulfo-NHS and GRGDYP would probably result in a higher peptide coupling after active coal filtration, as the amount of adducts were shown to be smaller at these concentrations (figure 36). This would in turn lead to a higher cell adhesion, as more adhesive peptides are present at the alginate surface[7].

Activating EDC with sulfo-NHS in MES-buffer at pH=5.0-6.0, and then raising the pH to 7.2-7.5 before adding the amine may be beneficial for optimal coupling[46] [47], and further studies should try to incorporate this.

Coupling on cross-linked alginates was investigated in this study, but with undetectable results in ^{1}H NMR. Future studies could involve coupling to alginates with the desired M:G ratios, as is described by Rowley *et. al*[7] [8]. A comparative cell viability study could be performed on coupling performed directly on beads, and on alginates purified with active coal, and alginate samples not purified with active coal filtration. This would determine if the adducts in fact participate in cell survival or not.

The variable degradability of alginate beads in the body (as discussed in subsection 1.4) should also be adressed for tissue engineering applications. Alginates prepared by periodate oxidation have better prerequisits for degradation, which are important properties in biomedical applications where biodegradability is necessary[65]. One example is where alginates are used as drug vehicles for proteins that promote regeneration of mineralized tissue[8]. Oxidation of alginates is performed by periodate in aqueous solutions. The oxidation results in ring cleavage between C2 and C3 as the hydroxy groups on these carbon atoms are oxidised to keton groups[66] [67]. Sodium borohydride ($NaBH_4$) is added to reduce the keton groups to hydroxyl groups[68]. This ring cleavage enables an easier degradation of the alginate backbone[5], and offer a controlled degradability by varying the oxidation[67]. In addition to enhanced biodegradability, oxidised alginates have more reactive groups due to the keton groups[65] [66] and the geling properties are retained[5]. However, the degree of oxidation needs to be in the range of 1-5% in order to avoid reduced gelation[66], and the biocompatibility is also believed to be affected at higher oxidation degrees due to the aldehyde groups on the sugar residues[67]. Interestingly, periodate oxidised alginates can be modified by peptide attachement by the familiar carbodiimide chemical approach described in this study, or with reductive amination using sodium

cyanoborohydride. Bouhadir *et. al* performed coupling of GRGDY to poly periodated guluronic acids with both these methods and attained peptide incorporations of 60% for the carbodiimide approach, and peptide incorporations of 68% when using $NaBH_4$[69]. In the study reported by Bouhadir *et. al*, 0.641μmol peptide was added to a batch of polyguluronate. The yields were calculated by measuring the amount coupled by radiolabelled ^{125}I GRGDY and dividing with the initial amounts of peptide added[69]. 68% incorporation corresponds to 0.436μmol peptide, which again corresponds to 0.86% coupled peptide (see *Large scale production of RGD-coupled alginate* for calculations). The results reported by Bouhadir *et.al*, is close to the results reported by Rowley *et.al*[7] where 400μmol peptide/L were incorporated, corresponding to 0.79% coupled peptide. The slightly increased degrees of coupling on periodate oxidised alginate implies that $NaBH_4$ is an attractive approach for producing degradable alginates with cell adhesion peptides.

Coupling of amino acids with bulky side chains, such as *e.g* arginine, is less favourable because of steric hindrance[70]. The adjacent bulky side chain of arginine may impair the ability of the terminal glycine to react with EDC. Therefore, using a peptide with a longer spacer arm can be favourable, and other amino acids, such as glycine, can be used as a spacer[11]. Spacers have been shown to increase cell adhesion[5] [71] [64] [11], and it is believed that the spacer makes the RGD-motif more available for integrin interaction. A spacer arm lifts the RGD sequence up from its attached surface, making it easier for the integrin receptors to bind to the motif[11]. Results published by Lee *et. al* when coupling RGD-motifs with varying spacer arm lengths to alginate, concluded that at least four glycine units, but less than twelve, was beneficial for growth of human fibroblasts[41]. However, there are reports of succesfull cell adhesion when no spacer was used, but here the scaffold for peptide coupling was not alginate, but glass[10]. Hersel[11] arguments that spacers may compensate for surface roughness and that the use of spacers must be tested for each system. As indicated by Lee *et. al*[41], spacers may be beneficial when using alginate as scaffold.

Chitosan was coupled to mannuronan by carbodiimide chemistry. Linking a D-A-D dimer to mannuronic acids and further linking a peptide to the amine group of the terminal D-glucosamine by carbodiimide chemistry can introduce chitosan trimers as novel spacer molecules. A chitosan trimer has a lower degree of freedom compared to glycine chains, meaning that chitosan trimers offer a different rotational stability as spacers compared to glycine spacers (personal conversation with Finn L. Aachmann).

Optimalising the coupling of the peptide sequence is the most essential part of this study, but properties of the peptide sequence may have impaired its reactivity. A property of the RGD sequence that may impair its cellular interactions, is the positive

charge of the arginine side chain. It may be that the arginine side chain can associate with the negatively charged carboxylate ions of alginate and that a spacer can reduce this interaction. This ionic interaction will probably distort the structure of the sequence and impair its ability to attach to integrin receptors[11]. However, with a saline concentration of 0.3M as used in this study, the electrostatic effects are believed to be cancelled out[72] [9].

Further studies should therefore involve coupling of peptides with various spacer arm lengths, to determine how this affects cell adhesion for *e.g* olfactory ensheating cells. The reaction conditions for the peptide sequence with the proper spacer arm length could be further optimalised, *e.g* in the same way as described for Me-O-Tyr and GRGDYP in this study. Other peptides, such as cyclic RGD should also be investigated, as they are resistant to proteolysis and have higher affinities for integrin interactions compared to linear RGD sequences[73].

6 Conclusions

Carbodiimide chemistry offer the possibility of amide bond formation between mannuronan and the peptide GRGDYP in a concentration-dependent manner. The amount of incorporated peptide depends on the amount of activation of the mannuronic acids and the amount of peptide added. The highest coupling of GRGDYP to mannuronan was achieved when the EDC and sulfo-NHS concentrations were 10% and the peptide concentration was 20%, relative to the carboxylic acids of mannuronan. It is deduced, based on coupling with excess Me-O-Tyr, that the GRGDYP:EDC ratio should not exceed 2:1 for optimal coupling, as a decrease in coupling percentages were observed for Me-O-Tyr above these ratios.

The results found in this study, show higher coupling percentages compared to Rowley*et.al*[7] [8] and Boonthekul *et.al*[67]. Compared to previous work by Karstensen, where the peptide coupling was reported to a maximum 0.2%[54], the peptide incorporation described here has been increased to 0.45% for the large scale production of RGD-coupled alginate before active coal filtration.

This study show that the adduct formation decrease as the peptide concentrations are increase, which indicate purer samples at reactant concentrations above 10% sulfo-NHS, EDC and peptide. At reactant concentrations below these values, the formation of adducts seem to overestimate the amount of peptide coupled to mannuronan. Comparing samples before and after active coal filtration, with ^{1}H NMR spectroscopy, showed that a substantial amount of peptides were removed from the sample along with N-acylurea adducts. Purification with active coal filtration is thus necessary to remove the unwanted adducts from the sample, but also demonstrates that peptides can be associated in adducts.

Encapsulation of olfactory ensheating cells in RGD-coupled alginate gave no morphology changes or increased cell viability when compared to non-peptide coupled alginate. This may have been caused by low AlgE6 epimerisation, low peptide concentrations or a combination of both. In order to enhance the peptide coupling after active coal filtration, high molecular weight mannuronan can be activated with 10% EDC and 20% added GRGDYP. At these concentrations the formation of N-acylurea adducts were shown to be below 6%, and the peptide couplings were shown to be above 1%. However, this material is more expensive to produce as a higher concentration of peptides is added. The use of sodium borohydride in combination with periodate oxidised alginates for peptide coupling can be assessed as a novel approach for increased peptide yields at lower peptide concentrations.

References

[1] Mørch, Y., Strand, B. and Skjåk-Bræk, G. (2009). *Alginate structure function relationship relevant to their use for cell encapsulation*. In *The bioartificial pancreas and other biohybrid therapies (Hallè, J.P. and de Vos, P. and Rosenberg, L. (eds))*, Chapter 4. Transworld Research Network, Kerala, India, pp. 51–66.

[2] Smidsrød, O. and Skjåk-Bræk, G. (March 1990). *Alginate as immobilization matrix for cells*. TIBTECH, vol. 8, pp. 71–78.

[3] Monalbetti, C. and Falque, V. (August 2005). *Amide bond formation and peptide coupling*. Tetrahedron, vol. 61, iss. 740, pp. 10827–10852. DOI:10.1016/J.tet.2005.08.031.

[4] Andersen, T., Strand, B., Formo, K., Alsberg, E. and Christensen, B. (2011). *Alginates as biomaterials in tissue engineering*. In *Carbohydrate chemistry vol. 37: Chemical and biological approaches; Glycosciences for human health and disease (Rauter, P. and Lindhorst, T.K (eds))*, Chapter 1. Royal Society of Chemistry, London, England, pp. 1–55.

[5] Lee, K. and Mooney, D. (June 2011). *Alginate: Properties and biomedical applications*. Progress in Polymer Science, vol. 37, iss. 1, pp. 106–126. DOI:10.1016/j.progpolymsci.2011.06.003.

[6] Draget, K., Smidsrød, O. and Skjåk-Bræk, G. (2005). *Alginates from algae*. In *Polysaccharides and polyamides in the food industry. Properties, production and patents(Steinbüchel, A. and Rhee, S.K. (eds))*, Chapter 1. Wiley Verlag GmbH and Co., Weinheim,Germany, pp. 1–30.

[7] Rowley, J. and Mooney, D. (May 2002). *Alginate type and RGD density control myoblast phenotype*. Journal of Biomedical Materials Research, vol. 60, iss. 2, pp. 217–223.

[8] Rowley, J., Madlambayan, G. and Mooney, D. (April 1999). *Alginate hydrogels as synthetic extracellular matrix materials*. Biomaterials, vol. 20, iss. 1, pp. 45–53.

[9] Pawar, S. and Edgar, K. (January 2012). *Alginate derivatization: A review of chemistry, properties and applications*. Journal of Biomaterials, vol. 33, iss. 11, pp. 3279–3305. DOI:10.1016/j.biomaterials.2012.01.007.

[10] Massia, S. and Hubbell, J. (September 1991). *An RGD Spacing of 440 nm is sufficient for integrin $\alpha_v \beta_3$ mediated fibroblast spreading and 140 nm for focal contact and stress fiber formation.* The Journal of Cell Biology, vol. 114, iss. 5, pp. 1089–1100.

[11] Hersel, U., Dahmen, C. and Kessler, H. (November 2003). *RGD modified polymers: biomaterials for stimulated cell adhesion and beyond.* Biomaterials, vol. 24, iss. 24, pp. 4385–4415.

[12] Nakajima, N. and Ikada, Y. (January 1995). *Mechanism of amide formation by carbodiimide for biconjugation in aqueous media.* Biconjugate Chemistry, vol. 6, iss. 1, pp. 123–130.

[13] Monalbetti, C. and Falque, V. (August 2005). *Amide bond formation and peptide coupling.* Tetrahedron, vol. 61, iss. 740, pp. 10827–10852. DOI:10.1016/J.tet.2005.08.031.

[14] Rokstad, A. and Donati, I. t. (May 2006). *Cell-compatible covalently reinforced beads obtained from a chemoenzymatically engineered alginate.* Journal of Biomaterials, vol. 27, iss. 27, pp. 4726–4737. DOI: 10.1016/j.biomaterials.2006.05.011.

[15] Smidsrød, O. (January 1974). *Molecular basis for some physical properties of alginates in the gel state.* Faraday Discussions of the Chemical Society, vol. 57, pp. 263–274. DOI:10.1039/DC9745700263.

[16] Augst, A., Kong, H. and Mooney, D. (August 2006). *Alginate hydrogels as biomaterials.* Macromolecular Bioscience, vol. 6, iss. 8, pp. 623–633.

[17] Smidsrød, O. and Moe, S. (2008). *Biopolymer Chemistry*, 2^{nd} *edition.* Tapir Academic Press, Trondheim, Norway, p. 44 and 87 and 185.

[18] Cathell, M., Szewczyk, J. and Schauer, C. (February 2010). *Organic modification of the polysaccharide alginate.* Mini-Reviews in Organic Chemistry, vol. 7, iss. 1, pp. 61–67.

[19] Donati, I., Holtan, S., Mørch, Y., Borgogna, M., Dentini, M., and Skjåk-Bræk (January 2005). *New hypothesis on the role of alternating sequences in calcium-alginate gels.* Biomacromolecules, vol. 6, iss. 2, pp. 1031–1040.

[20] Cathell, M., and Schauer, C. (August 2007). *Structurally colored thin films of Ca^{2+}-cross-linked alginate.* Biomacromolecules, vol. 8, iss. 1, pp. 33–41. DOI:10.1021/bm060433f.

[21] Skjåk-Bræk, G., Grasdalen, H. and Larsen, B. (October 1986). *Monomer sequence and acetylation pattern in some bacterial alginates.* Carbohydrate Research, vol. 154, iss. 1, pp. 239–250.

[22] Høidal, H., Ertesvåg, H., Skjåk-Bræk, G., Stokke, B. and Valla, S. (April 1999). *The recombinant Azotobacter vinelandii mannuronan C-5-epimerase AlgE4 epimerizes alginate by a nonrandom attack mechanism.* The Journal of Biological Chemistry, vol. 274, iss. 18, pp. 12346–12322.

[23] Blatny, J., Ertesvåg, H., Nes, I. and Valla, S. (August 2003). *Heterologous gene expression in Lactococcus lactis; expression of the Azotobacter vinelandii AlgE6 gene product displaying mannuronan C-5 epimerase activity.* FEMS Microbiology, vol. 227, iss. 2, pp. 229–235. DOI:10.1016/S0378-1097(03)00685-2.

[24] Donati, I. and Paoletti, S. (2009). *Material Properties of Alginates.* In *Alginates: Biology and applications (Rehm, B.H.A (eds))*, 1^{st} *edition*, Chapter 1. Springer-Verlag, Berlin Heidelberg, pp. 1–55.

[25] Hine, R. (2008). *Oxford Dictionary of Biology*, 6^{th} *edition.* Oxford University Press, Oxford, p. 28 and 29 and 238 and 647.

[26] Al-Shamkhani, A. and Duncan, R. (January 1995). *Radioionidation of alginate via covalently-bound tyrosinamide allows monitoring of its fate in vivo.* Journal of Bioactive and Compatible Polymers, vol. 10, iss. 1, pp. 4–13.

[27] Alberts, B., Johnson, A. and Lewis, J. (2002). *Molecular Biology of the Cell*, 4^{th} *edition.* Garland Science, New York, USA, p. 87 and 185.

[28] Geiger, B., Bershadsky, A., Pankov, R. and Yamada, K. (November 2001). *Transmembrane extracellular matrix-cytoskeleton crosstalk.* Nature Reviews: Molecular Biology, vol. 2, iss. 11, pp. 793–805.

[29] Dvir, T., Timko, B., Kohane, D. and Langer, R. (December 2010). *Nanotechnological strategies for engineering complex tnumbers.* Nature Nanotechnology, vol. 6, iss. 13, pp. 13–22. DOI: 10.1038/NANO.2010.246.

[30] Palecek, S., Loftus, J., Ginsberg, M., Lauffenburger, D. and Horwitz, A. (February 1997). *Integrin-ligand binding properties govern cell migration speed through cell-substratum adhesiveness*. Letters to nature, vol. 385, pp. 537–540.

[31] Lanza, R., Langer, R. and Vacanti, J. e. (2007). *Principles of Tnumber Engineering, 3^{rd} edition*. Elsevier Academic Press, Burlington, pp. 81–99 and 287 and 300.

[32] Shibayama, M. and Tanaka, T. (1993). *Volume phase transition and related phenomena of polymer gels*. Advances in Polymer Science, vol. 109, pp. 1–62. DOI:10.1007/3-540-56791-71.

[33] Lehenkari, P. and Horton, M. (June 1999). *Single integrin molecule adhesion forces in intact cells measured by atomic force microscopy*. Biochemical and Biophysical Research Communications, vol. 259, iss. 3, pp. 645–650.

[34] Massia, S. and Hubbell, J. (December 2006). *Covalently attached GRGD on polymer surfaces promotes biospecific adhesion of mammalian cells*. Annals of the New York Academy of Sciences, vol. 589, iss. 1, pp. 261–270.

[35] Hotchin, N. and Hall, A. (December 1995). *The assembly of integrin adhesion complexes requires both extracellular matrix and intracellular rho/rac GTPases*. The Journal of Cell Biology, vol. 131, iss. 6, pp. 1857–1865.

[36] Meredith, J. and Schwartz, M. (April 1997). *Integrins, adhesion and apoptosis*. Trends in Cell Biology, vol. 7, iss. 4, pp. 146–150.

[37] Nelson, D. and M.M., C. (2008). *Lehninger Principles of Biochemistry, 5^{th} edition*. W.H. Freeman and Company, New York, p. 455.

[38] Shin, H. and Jo, A., S. Mikos (November 2003). *Biomimetic materials for tnumber engineering*. Biomaterials, vol. 24, iss. 24, pp. 4353–4364.

[39] Jell, G., Minelli, C. and Stevens, M. (2009). *Biomaterial-Related Approaches: Surface Structuring*. In *Fundamentals of Tissue Engineering and Regenerative Medicine (Meyer, U. and Handschel, J. and Meyer, T. and Wiesmann, H.P. (eds))*, 1^{st} *edition*, Chapter 35. Springer-Verlag, Berlin Heidelberg, pp. 469–484.

[40] Hern, D. and Hubbell, J. (February 1997). *Incorporation of adhesion peptides into nonadhesive hydrogels useful for tissue resurfacing*. Journal of Biomedical Materials Research, vol. 39, iss. 2, pp. 266–276.

[41] Lee, J., Park, Y. J., Lee, S., Lee, S. and Lee, K. (July 2010). *The effect of spacer arm length of an adhesion ligand coupled to an alginate gel on the control of fibroblast phenotype*. Journal of Biomaterials, vol. 31, iss. 21, pp. 5545–5551. DOI:10.1016/j.biomaterials.2010.03.063.

[42] Augst, A., Kong, H. and Mooney, D. (August 2006). *Alginate hydrogels as biomaterials*. Macromolecular Bioscience, vol. 6, iss. 8, pp. 623–633.

[43] Sehgal, D. and Vijay, I. (April 1994). *A method for the high efficiency of water-soluble carbodiimide-mediated amidation*. Analytical Biochemistry, vol. 218, iss. 1, pp. 87–91.

[44] Darr, A. and Calabro, A. (July 2009). *Synthesis and characterization of tyramine-based hyaluronan hydrogels*. Journal of Materials Science: Materials in Medicine, vol. 20, iss. 1, pp. 33–44. DOI: 10.1007/s10856-008-3540-0.

[45] Timkovich, R. (1977). *Detection of the stable addition of carbodiimide to proteins*. Analytical Biochemistry, vol. 79, pp. 135–143.

[46] Grabarek, Z. and Gergely, J. (February 1990). *Zero-length crosslinking procedure with use of active esters*. Analytical Biochemistry, vol. 185, iss. 1, pp. 131–135.

[47] Staros, J., Wright, R. and Swingle, D. (July 1986). *Enhancement by N-hydroxysulfosuccinimide of water-soluble carbodiimide-mediated coupling reactions*. Analytical Biochemistry, vol. 156, iss. 1, pp. 220–222.

[48] Subirós-Funosas, R., Prohens, R., Barbas, R., El-Faham, A. and Albericio, F. (July 2009). *Oxyma: An efficient additive for peptide synthesis to replace the benzotriazole-based HOBt and HOAt with a lower risk of explosion*. Chemistry: A European Journal, vol. 15, iss. 37, pp. 9394–9403. DOI:10.1002/chem.200900614.

[49] Westhrin, M. (2010). *A novel alginate matrix for tissue engineering, Student work*. Norwegian University of Science and Technology, Institute of Biotechnology.

[50] Kroschwitz, J. (2004). *Kirk-Othmer Encyclopedia of Chemical Technology*, 5^{th} *edition*, vol. 2. John Wiley and Sons Inc., Hoboken, N.J, pp. 652–664. DOI: 10.1002/0471238961.

[51] Creighton, T. (2007). *Proteins, structures and molecular properties*, 2^{nd} *edition*. W.H Freeman and Company, Heidelberg, pp. 14–17.

[52] Strand, B., Gåserød, O., Kulseng, B., Espevik, T. and Skjåk-Bræk, G. (January 2002). *Alginate-polylysine-alginate microcapsules: effect of size reduction on capsule properties.* Journal of Microencapsulation, vol. 19, iss. 5, pp. 615–630.

[53] Thu, B., Gåserud, D., O. Paus, Mikkelsen, A., Skjåk-Bræk, G., Toffanin, R., Vittur, F. and R., R. (January 2000). *Inhomogeneous alginate gel spheres: An assessment of the polymer gradients by synchrotron radiation-induced X-ray emission, magnetic resonance microimaging, and mathematical modeling.* Biopolymers, vol. 53, iss. 1, pp. 60–71.

[54] Karstensen, K. (2010). *Novel alginate matrix for tissue engineering, Master Thesis.* Norwegian University of Science and Technology, Department of Biotechnology.

[55] Mørch, Y., Donati, I., Strand, B. and Skjåk-Bræk, G. (August 2007). *Molecular engineering as an approach to design new functional properties of alginate.* Biomacromolecules, vol. 8, iss. 9, pp. 2809–2814.

[56] Mørch, Y. (February 2008). *Novel alginate microcapsules for cell therapy, Doctoral Theses*, p. 37. Norwegian university of Science and Technology, Department of Biotechnology.

[57] Millipore-Corporation (2004). *Activated Carbon Clarification Filters.* Millipore Corporation.

[58] Brange, J. and Langkjær, L. (1993). *Insulin Structure and Stability.* In *Stability and characterization of protein and peptide drugs: case histories (Wang, J. Y. and Pearlman, R. (eds))*, 1^{st} *edition*, Chapter 11. Plenum Press, New York, p. 317.

[59] Ertesvåg, H. and Skjåk-Bræk, G. (1999). *Modification of alginate using mannuronan C-5 epimerases.* In *Carbohydrate biotechnology protocols(Bucke, C.(ed))*, vol. 10, Chapter 11. Humana Press, Totowa, NJ, pp. 71–78.

[60] *National industrial chemicals notification and assessment scheme(NICNAS): Full public report on L-Tyrosine methyl ester*. Published October 2004, Downloaded from www.nicnas.gov.au.

[61] Mojarradi, H. (March 2011). *Coupling of substances containing a primary amine to hyaluronan via carbodiimide- mediated amidation, Master Thesis.* Uppsala University, ISSN: 1650-8297 UPTEC K11 002.

[62] Painter, P. and Coleman, M. (1997). *Fundamentals of Polymer Science*, 2^{nd} *edition*. CRC Press, Boca Raton, p. 296.

[63] Genes, N., Rowley, J. and Mooney, L., D.J. Bonassar (February 2004). *Effect of substrate mechanics on chondrocyte adhesion to modified alginate surfaces*. Archives of Biochemsitry and Biophysics, vol. 422, iss. 2, pp. 161–167.

[64] Beer, J.-H., Springer, K. and Coller, B. (January 1992). *Immobilized Arg-Gly-Asp (RGD) peptides of varying lengths as structural probes of the platelet glycoprotein IIb/IIIa receptor*. Blood, vol. 12, iss. 1, pp. 117–128.

[65] Balakrishnan, B., Lesieur, S., Labarre, D. and Jayakrishnan, A. (February 2005). *Periodate oxidation of sodium alginate in water and in ethanol-water mixture: a comparative study*. Carbohydrate Research, vol. 340, iss. 7, pp. 1425–1429. DOI:10.1016/j.carres.2005.02.028.

[66] Gomez, C., Rinaudo, M. and Villar, M. (February 2007). *Oxidation of sodium alginate and characterization of the oxidized derivatives*. Carbohydrate Polymers, vol. 67, iss. 3, pp. 296–304.

[67] Boontheekul, T., Kong, H. and Mooney, D. (June 2005). *Controlling alginate gel degradation utilizing partial oxidation and bimodal weight distribution*. Biomaterials, vol. 26, iss. 15, pp. 2455–2465. DOI:10.1016/j.biomaterials.2006.06.044.

[68] Vold, I. and Kristiansen, C. B., K.A (2006). *A study of the chain stiffness and extensions of alginates, in vitro epimerized alginates, and periodate-oxidised alginates using size-exclusion chromatopgraphy combined with light scattering and viscosity detectors*. Biomacromolecules, vol. 7, iss. 7, pp. 2136–2146. DOI: 10.1021/bm060099n.

[69] Bouhadir, K., Hausman, D. and Mooney, D. (June 1999). *Synthesis of cross-linked poly(aldehyde guluronate) hydrogels*. Polymer, vol. 40, iss. 12, pp. 3575–3584.

[70] Besselink, G., Beugeling, T. and Bantjes, A. (May 1993). *N-hydroxysuccinimide-activated glycine-sepharose*. Applied Biochemistry and Biotechnology, vol. 43, iss. 3, pp. 227–246.

[71] Salinas, C. and Anseth, K. (May 2008). *The influence of the RGD peptide motif and its contextual presentation in PEG gels on human mesenchymal stem cell viability*. Journal of tissue engineering and regenerative medicine, vol. 2, pp. 296–304. DOI: 10.1002/term.95.

[72] Hiemenz, P. and Rajagopalan, R. (1997). *Principles of Colloid and Surface Chemistry*, 3^{rd} *edition*. CRC Press, Boca Raton, p. 512.

[73] Bubenikova, S., Stancu, I., Kalinovska, L., Schacht, E., Lippens, E., Declerq, H., Cornelissen, M., Santin, M., Amblard, M. and Martinez, J. (February 2012). *Chemoselective cross-linking of alginate with thiol-terminated peptides for tissue engineering applications*. Carbohydrate Polymers, vol. 88, iss. 4, pp. 1239–1250. DOI:10.1016/j.carbpol.2012.01.089.

[74] Grasdalen, H., Larsen, B. and Smidsrød, O. (January 1979). *A P.M.R. study of the composition and sequence of uronate residues in alginate*. Carbohydrate Research, vol. 89, iss. 1, pp. 25–31.

[75] Grasdalen, H., Larsen, B. and Smidsrød, O. (January 1983). *High field, H-n.m.r spectroscopy of alginate: sequential structure and linkage conformations*. Carbohydrate Research, vol. 118, pp. 255–260.

[76] Madihally, S. and Matthew, H. W. (June 1999). *Porous chitosan scaffolds for tissue engineering*. Biomaterials, vol. 20, iss. 12, pp. 1133–1142.

List Of Appendices

A Degree of polymerisation

The average degree of polymerisation is determined by dividing the sum of the total signal of the internal protons, $I_{M1-intern}$, and the reducing ends, I_{red}, with I_{red}. The definition is shown in equation 1

$$\overline{DP_n} = \frac{I_{M1-intern} + I_{red}}{I_{red}} \tag{1}$$

$I_{M1-intern}$ refers to all the protons in M except the end groups.

The average degree of polymerisation can be determined from ^{1}H NMR by setting the mannuronan peak at ∼4.7 as a reference peak, and integrating the two peaks named α and β in figure 48.

The reducing ends equals the sum of the anomeric protons of the reducing end, α and β. As a rule of thumb, the integral of β is half the integral of α for mannuronan. This is often seen as the conformation of M favours the β conformation of the reducing end. A flat baseline is crucial for quantification of signal intensities. However, small peaks that are adjacent to larger peaks will be enlarged because of a non-linear baseline. The β-integral is often overestimated due to the vicinal mannuronan peak. If the β-signal is more than half of the α-signal, I_{red} can be calculated, from the α-signal alone, as shown in equation 2.

$$I_{red} = \alpha + \frac{1}{2}\alpha \tag{2}$$

As shown in figure 48, the integral for the β-signal equals 0.0159 which is more than half of the α signal which was estimated to 0.0128. Thus, the average degree of polymerisation is calculated from the α signal.

$$\overline{DP_n} \approx \frac{1 + 0.0128 + (0.5x0.0128)}{0.0128(0.5x0.0128)} \approx 53 \tag{3}$$

Calculating the average degree of polymerisation using the β-integral gives a value of 36. Therefore, the average degree of polymerisation can be said to lie between approximately 40-50.

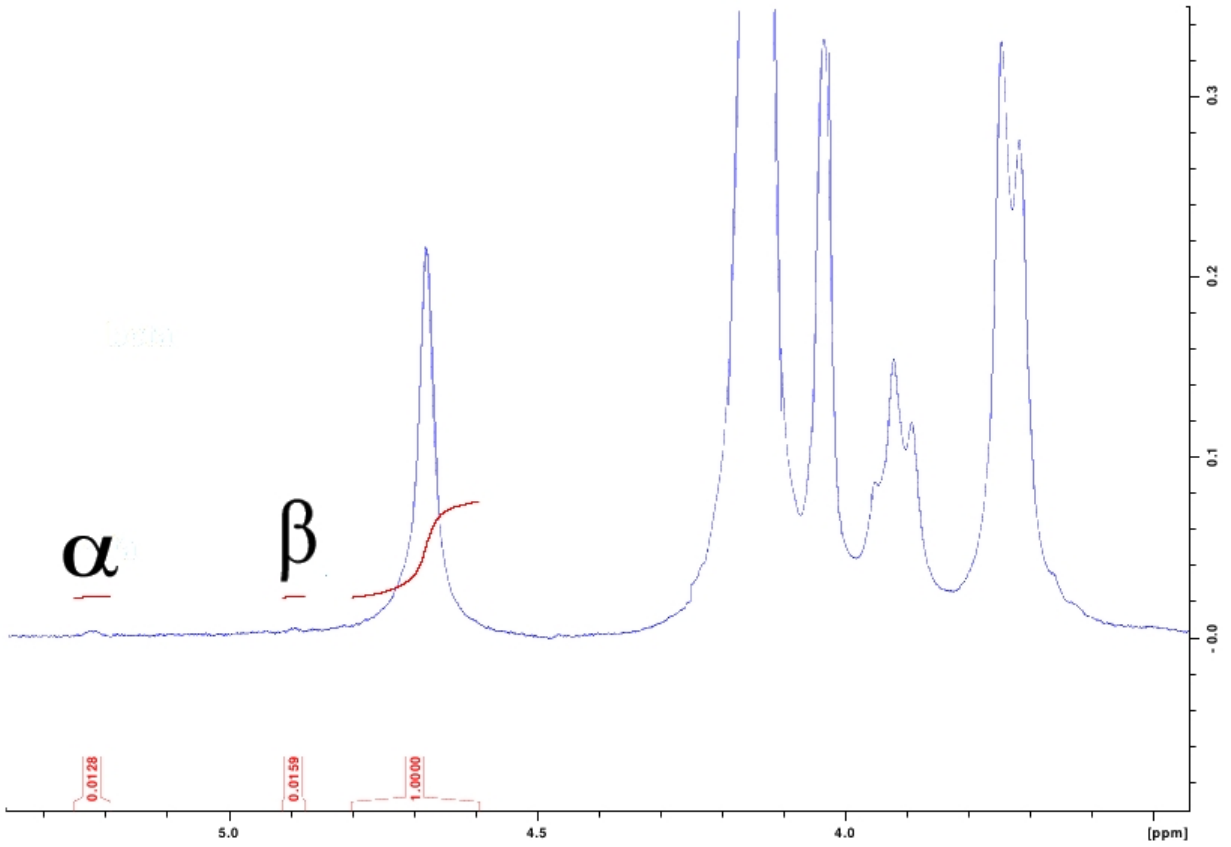

Figure 48: Determination of average degree of polymerisation. The spectra were recorded at 300MHz.

B Calculating the degree of coupling from ^{1}H NMR

Figure 49 show the ^{1}H NMR spectrum of Me-O-Tyr coupled to mannuronan.

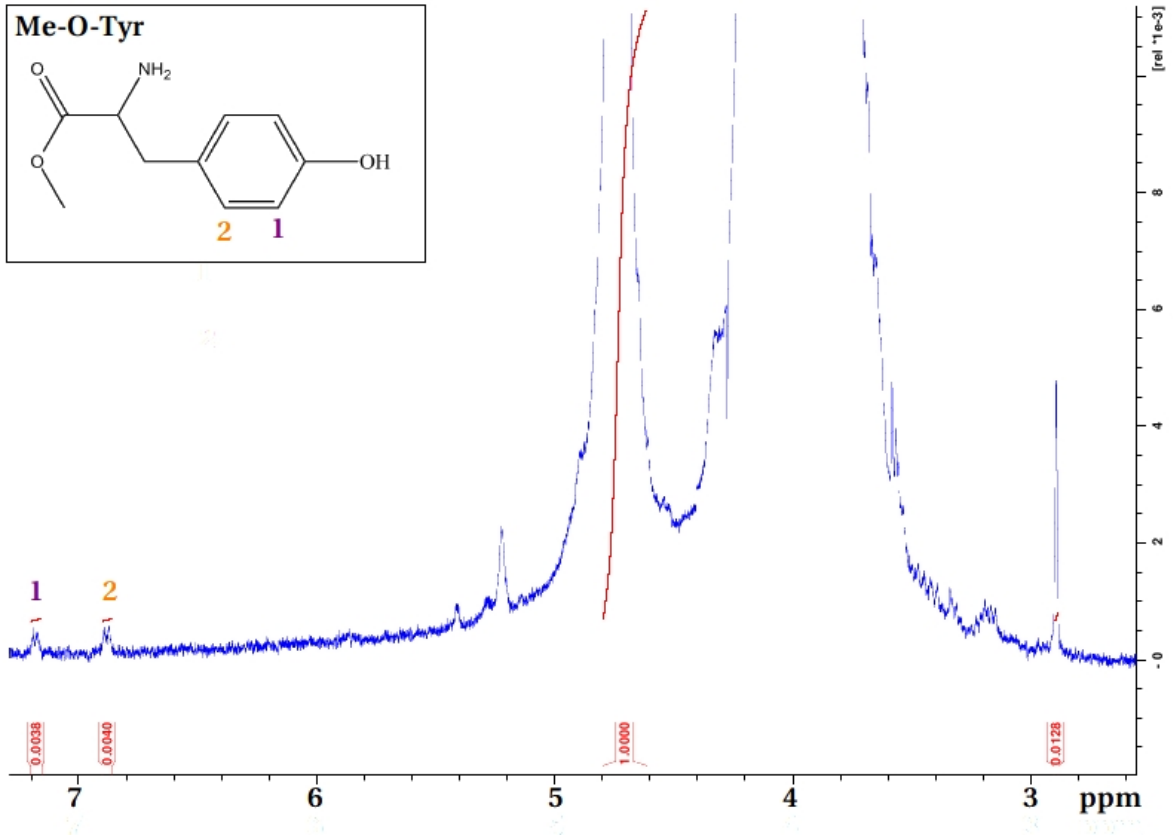

Figure 49: Determination of degree of coupling. Proton 1 and 2 represent the aromatic protons of the tyrosine residue in Me-O-Tyr. Each peak represents two protons, giving a total of four aromatic protons. The sample shown in the spectrum was coupled to mannuronan at pH=5.5 and at 0°C. See appendix J, table 27, parallel number 2.

The mannuronan peak at 4.60-4.80 ppm represents proton number 1 in mannuronan. This proton peak is set as reference with the integral 1.000. The sum of the integrals of the aromatic protons represent 4 protons. The degree of coupling, DC, is calculated as shown below:

$$DC \approx \frac{0.0038 + 0.0040}{4} x100\% \approx 0.2\% \tag{4}$$

The amount of adducts is estimated by using the integrals at 2.90 ppm. The peak at 2.90 ppm represents 6 protons. See figure 15 for shift assignments for N-acylurea.

The integration of samples containing FA was performed by Wenche I. Strand. When calculating the amount of FA coupled, the reference peak (integral=1.0000) was set at 6.70ppm. This proton peak was divided by four, as it represents four aromatic protons of FA, and further divided by the integral of the mannuronan peak. Multiplying the dividend with 100 gives the coupling degree in percentage.

The yield for a sample having a coupling degree of 0.2% ME-O-Tyr in a sample where 5% Me-O-Tyr was added, is calculated as shown in equation 5.

$$Yield = \frac{0.2\%}{5\%} x 100\% = 4\% \tag{5}$$

C Coupling fluoresceinamine to mannuronan

Table 14 show the amount of fluoresceinamine coupled to mannuronan in percentage and yield calculated by ^{1}H NMR. The yield was calculated from a theoretical coupling of 5% FA. For calculations of yield, see appendix B, equation 5.

The fluoresceinamine peak was observed at ∼6.7 ppm and set as reference integral. Proton number 1 of mannuronan was observed at ∼4.7 ppm. Sample 1 was prepared by adding dry fluoresceinamine to the reaction beaker, while sample 2 was prepared by adding solvated fluoresceinamine.

Table 14: Bound FA(%) to mannuronan, ^{1}H NMR

Sample	Parallel	Integral at ∼4.7ppm	Bound FA (%)	Yield (%)
1	1	31.73	0.79	0.16
	2	27.98	0.89	18
	3	35.24	0.71	14
	4	145.57	0.17	3.4
	5	71.57	0.35	7.0
2	2	104.24	0.24	4.8
	3	149.49	0.17	3.3
	4	130.81	0.19	3.8
	5	103.89	0.24	4.8

Parallel number 1 in sample 2 did not show any peaks of interests in the ^{1}H NMR and the percentage coupling could not be calculated.

Table 15 show the calculated standard deviations for the coupling of fluoresceinamine to mannuronan based on the integrals in table 14.

Table 15: Averages and standard deviations for coupling FA to mannuronan

Sample	Average bound FA (%)	Average yield	Std. deviation (%)	Std. deviation, yield
1	0.58	12	0.20	5.5
2	0.21	4.2	0.032	0.63

Figure 50 show the entire spectra for coupling of fluoresceinamine, sample 1 and sample 2.

Figure 51 show the proton peaks for coupling of fluoresceinamine, sample 1 and sample 2.

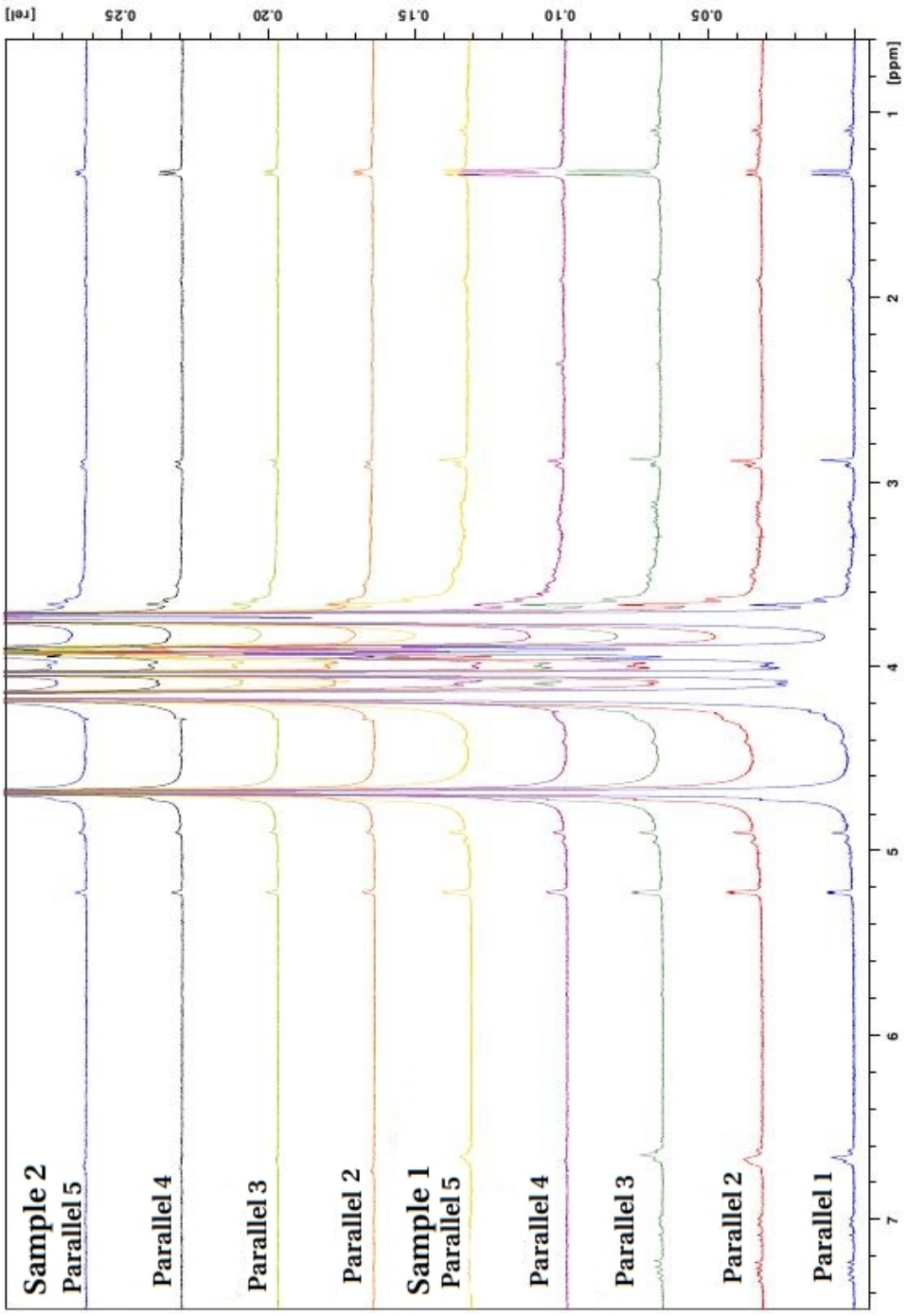

Figure 50: Coupling of fluoresceinamine.

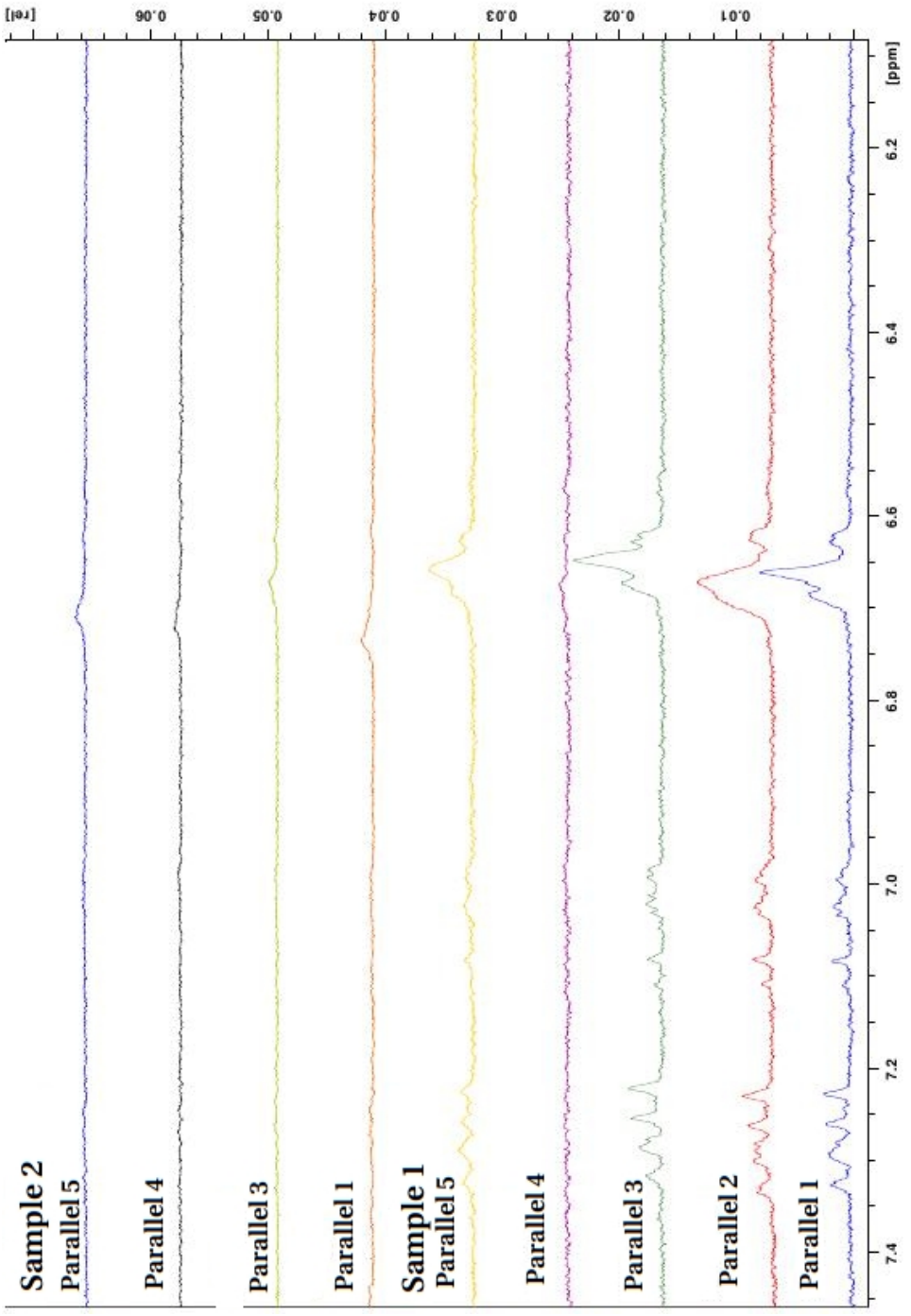

Figure 51: Coupling of fluoresceinamine. The spectra were recorded at 300MHz.

D Coupling 4AP in MES-buffer or PBS

Table 16 show the percentage amount of 4AP coupled to mannuronan calculated by ^{1}H NMR. The mannuronan peak is at ∼4.7 ppm and set as reference point. The aromatic protons of 4AP were observed at ∼6.9 and ∼7.3 ppm. The theoretical coupling of 4AP is 5% and the yield is calculated based on this. For calculating the yield, see appendix B, equation 5.

Table 16: Bound 4AP (%) to mannuronan, ^{1}H NMR

Buffer	Sample	Integral at 6.90 ppm	Integral at ∼7.3 ppm	Bound 4AP (%)	Yield (%)
MES	1	0.017	0.017	0.85	17
	2	0.017	0.017	0.85	17
	3	0.017	0.018	0.88	18
PBS	1	0.0083	0.0093	0.44	8.8
	2	0.0082	0.0096	0.45	9.0
	3	0.0090	0.011	0.49	9.8

Table 17 show the calculated averages and standard deviations for coupling 4AP to mannuronan in MES-buffer and PBS.

Table 17: Averages and standard deviations for coupling 4AP to mannuronan

Buffer	Average bound 4AP(%)	Average yield (%)	Std. deviation (%)	Std. deviation, yield
MES	0.86	17.2	0.01	0.28
PBS	0.46	9.2	0.02	0.43

Figure 52 show the entire spectra of proton peaks for coupling of 4AP to mannuronan in MES-buffer and PBS. Figure 53 show the proton peaks of the aromatic protons of 4AP at ∼7.5 and ∼7.9

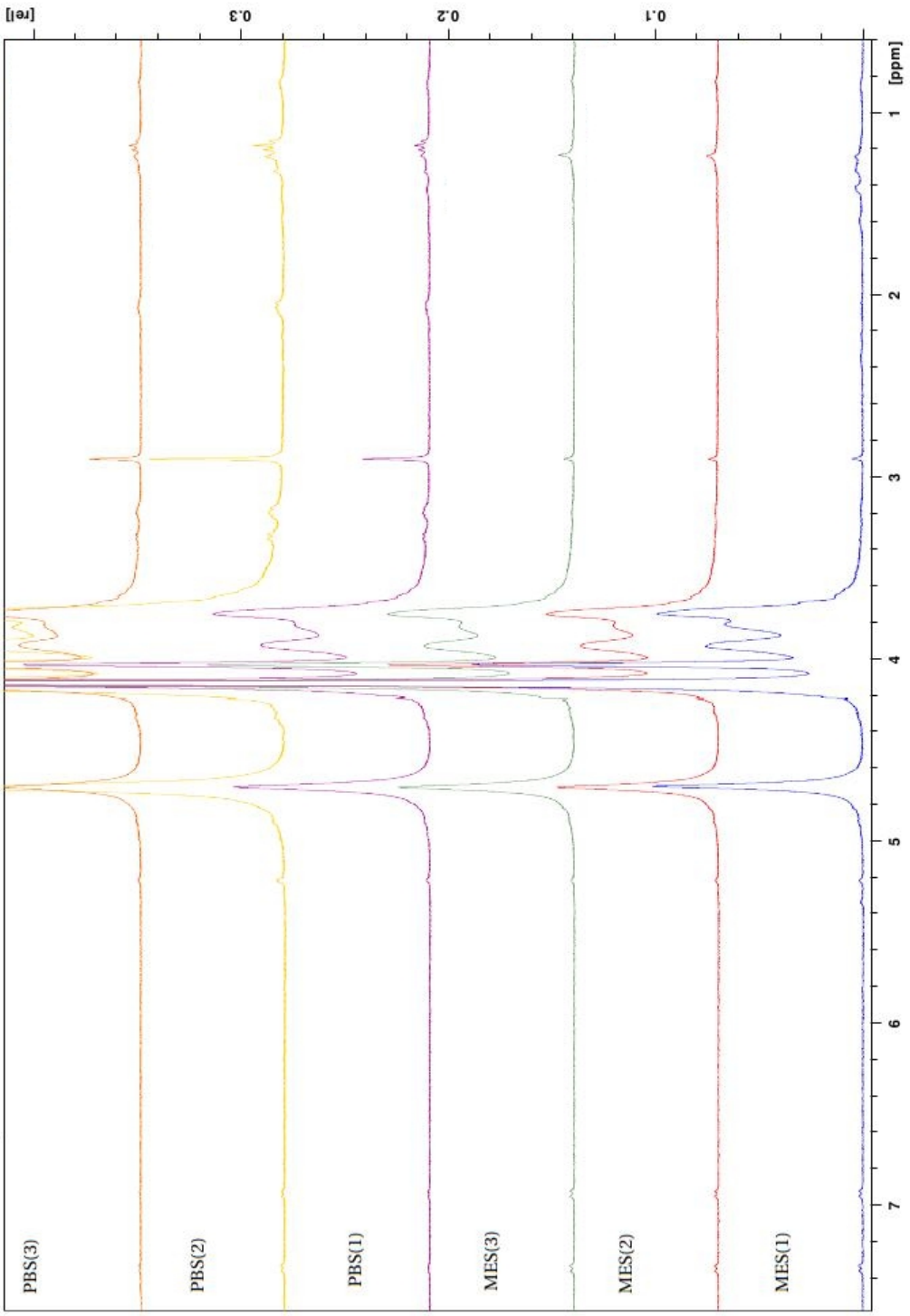

Figure 52: Coupling of 4AP in MES-buffer and PBS. The spectra were recorded at 300MHz.

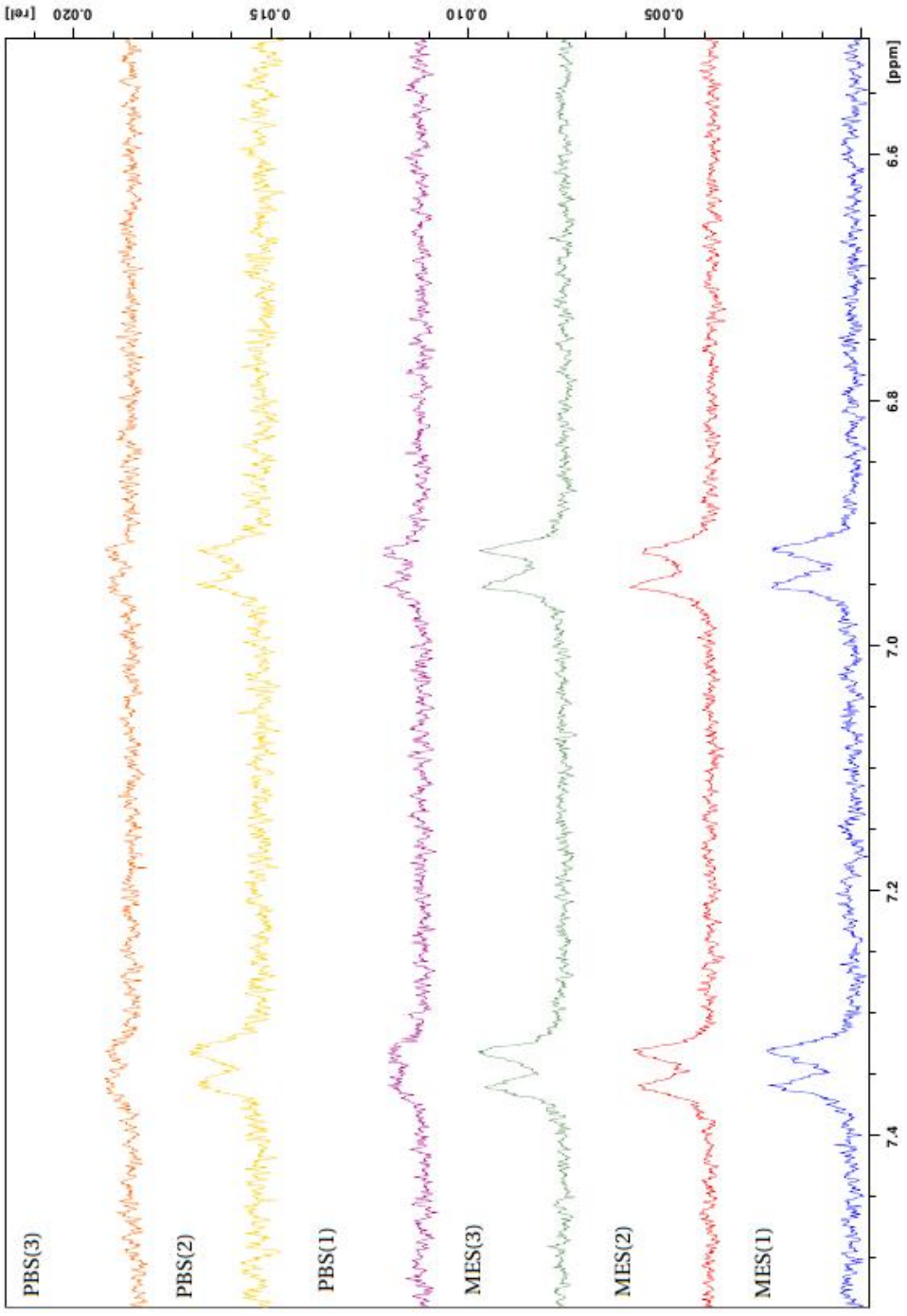

Figure 53: Molecular peaks of 4AP in MES-buffer and PBS. The spectra were recorded at 300MHz.

E Kinetics of coupling 4-AP

Table 18 show the percentage amount of 4AP coupled to mannuronan calculated by ^{1}H NMR. The mannuronan peak is at ∼4.7 ppm and set as reference point. The aromatic protons of 4AP were observed at ∼6.9 and ∼7.3 ppm. For calculating the yield, see appendix B, equation 5.

Table 18: Time dependant binding of 4AP (%) to mannuronan

Time (hours)	Parallel	Integral 6.90 ppm	Integral ∼7.3ppm	Bound 4AP (%)	Yield (%)
0.25	1	0.0121	0.0103	0.56	11.2
	2	0.0123	0.0107	0.575	11.5
0.50	1	0.0152	0.0140	0.730	14.6
	2	0.0144	0.0137	0.703	14.1
1	1	0.0178	0.0171	0.873	17.5
	2	0.0169	0.0162	0.828	16.6
2	1	0.0238	0.0227	1.163	23.3
4	1	0.0238	0.0236	1.185	23.7
	2	0.0292	0.0278	1.425	28.5
8	1	0.0263	0.0258	1.303	26.1
	2	0.0260	0.0259	1.298	26.0
24	1	0.0251	0.0254	1.263	25.3
	2	0.0204	0.0187	0.978	19.6

Table 19 show the calculated averages and standard deviations of the time dependent coupling of 4AP to mannuronan.

Table 19: Average bound 4AP to mannuronan and standard deviations for time dependent experiment

Time (hours)	Av. bound 4AP(%)	Av. yield (%)
0.25	0.57	11.4
0.50	0.72	14.3
1	0.85	17
2	1.16	23.3
4	1.29	25.8
8	1.30	26.0
24	0.14	25.3

Figure 54 show the proton peaks of the aromatic protons of 4AP at ∼7.28 and ∼6.88. Figure 55 show the entire spectra of time dependent coupling of 4AP to mannuronan.

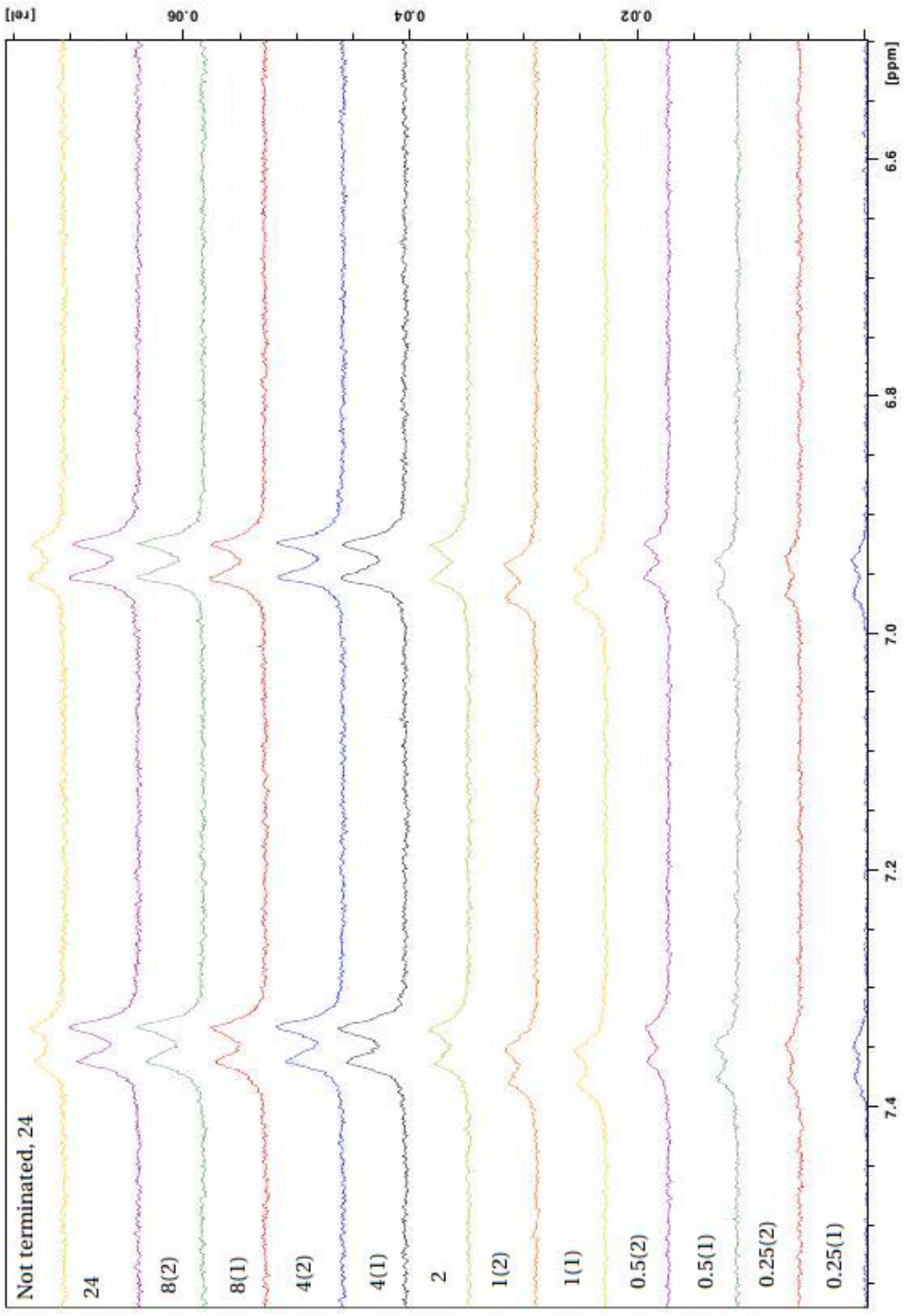

Figure 54: Molecular peaks of 4AP in MES at different reaction times. The spectra were recorded at 300MHz.

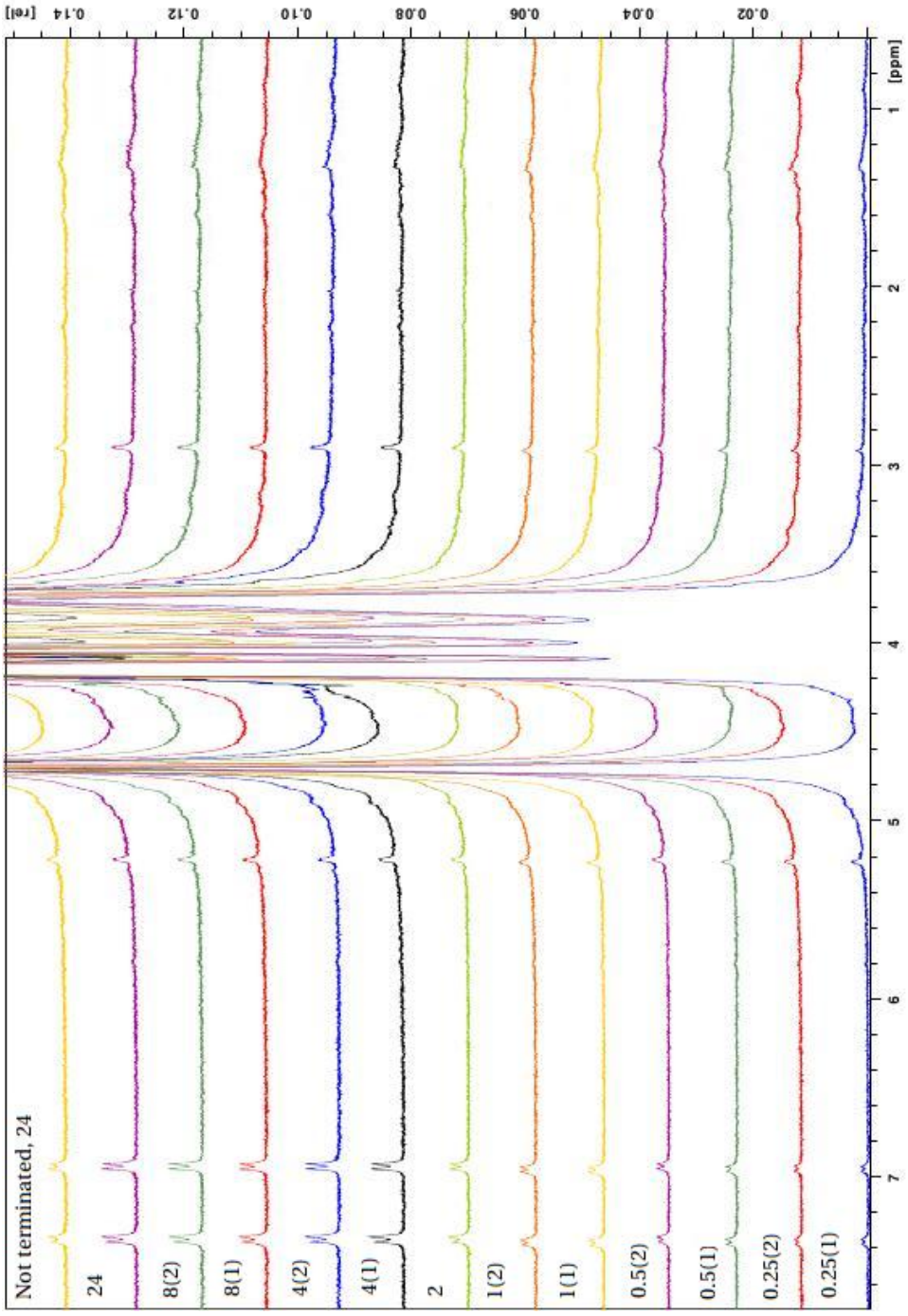

Figure 55: Coupling of 4AP in MES-buffer at different reaction times. The spectra were recorded at 300MHz.

F Varying pH for coupling 4AP

Table 20 show the calculated percentage bound 4AP in MES-buffer at pH-values 5.5, 6.0 and 6.5 and the calculated yield calculated by ^{1}H NMR. For calculating the yield, see appendix B, equation 5.

Table 20: Bound 4AP (%) to mannuronan, ^{1}H NMR at different pH-values

pH	Parallel	Integral at 6.90 ppm	Integral at ∼7.3 ppm	Bound 4AP (%)	Yield (%)
5.5	1	0.013	0.014	0.68	13.6
	2	0.014	0.014	0.72	14.4
6.0	1	0.014	0.015	0.73	14.6
	2	0.014	0.015	0.73	14.6
6.5	1	0.013	0.014	0.68	13.6
	2	0.012	0.014	0.67	13.4

Table 21 show the calculated standard deviations for coupling 4AP to mannuronan when the pH is varied.

Table 21: Averages and standard deviations for coupling 4AP to mannuronan at different pH-values

pH	Av. bound 4AP (%)	Av. yield (%)
5.5	0.70	14
6.0	0.73	14.6
6.5	0.68	13.5

Figure 56 show the entire spectra of proton peaks for coupling of 4AP to mannuronan in MES-buffer.

Figure 57 show the proton peaks of the aromatic protons of 4AP at ∼7.5 and ∼7.9

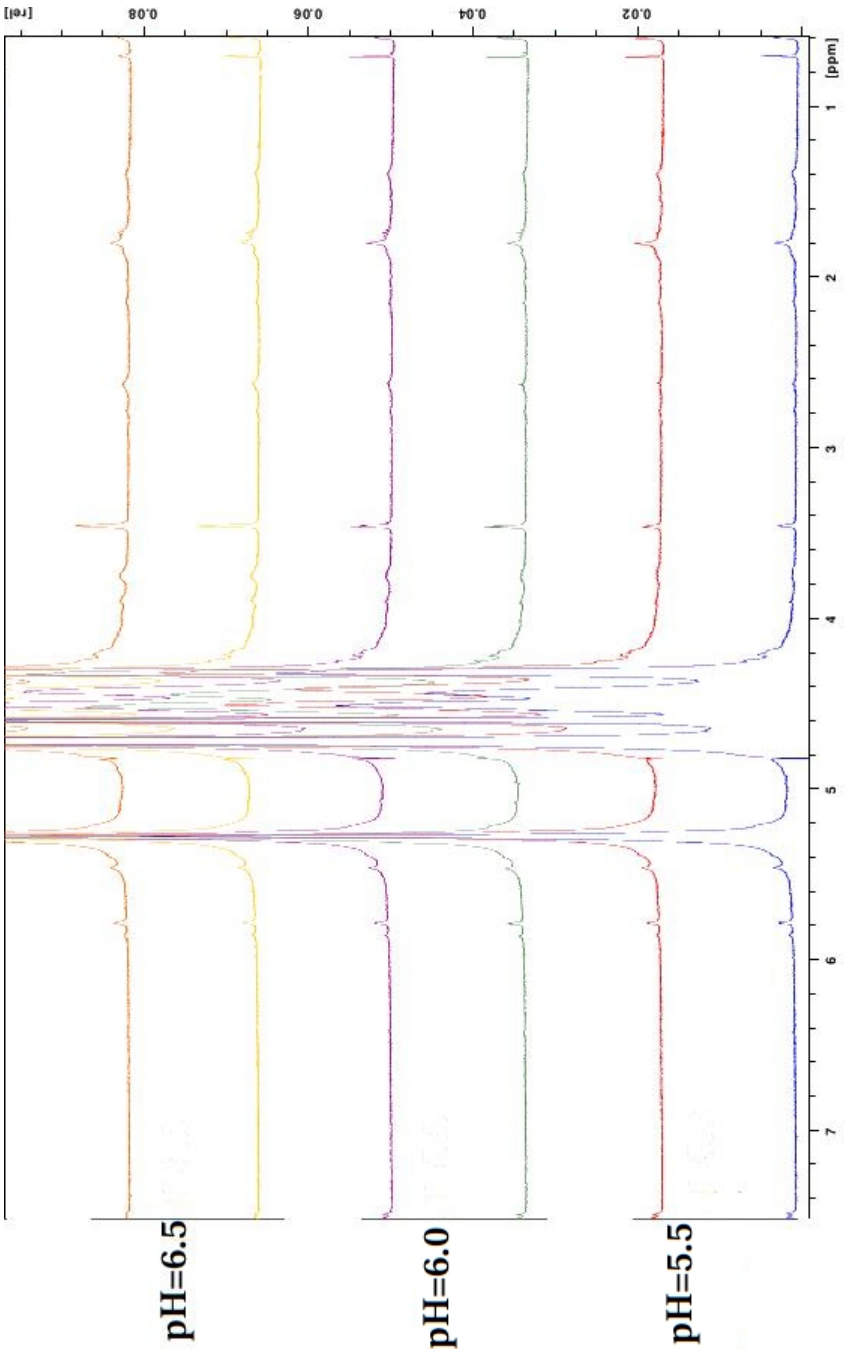

Figure 56: Coupling of 4AP in MES-buffer with different pH.

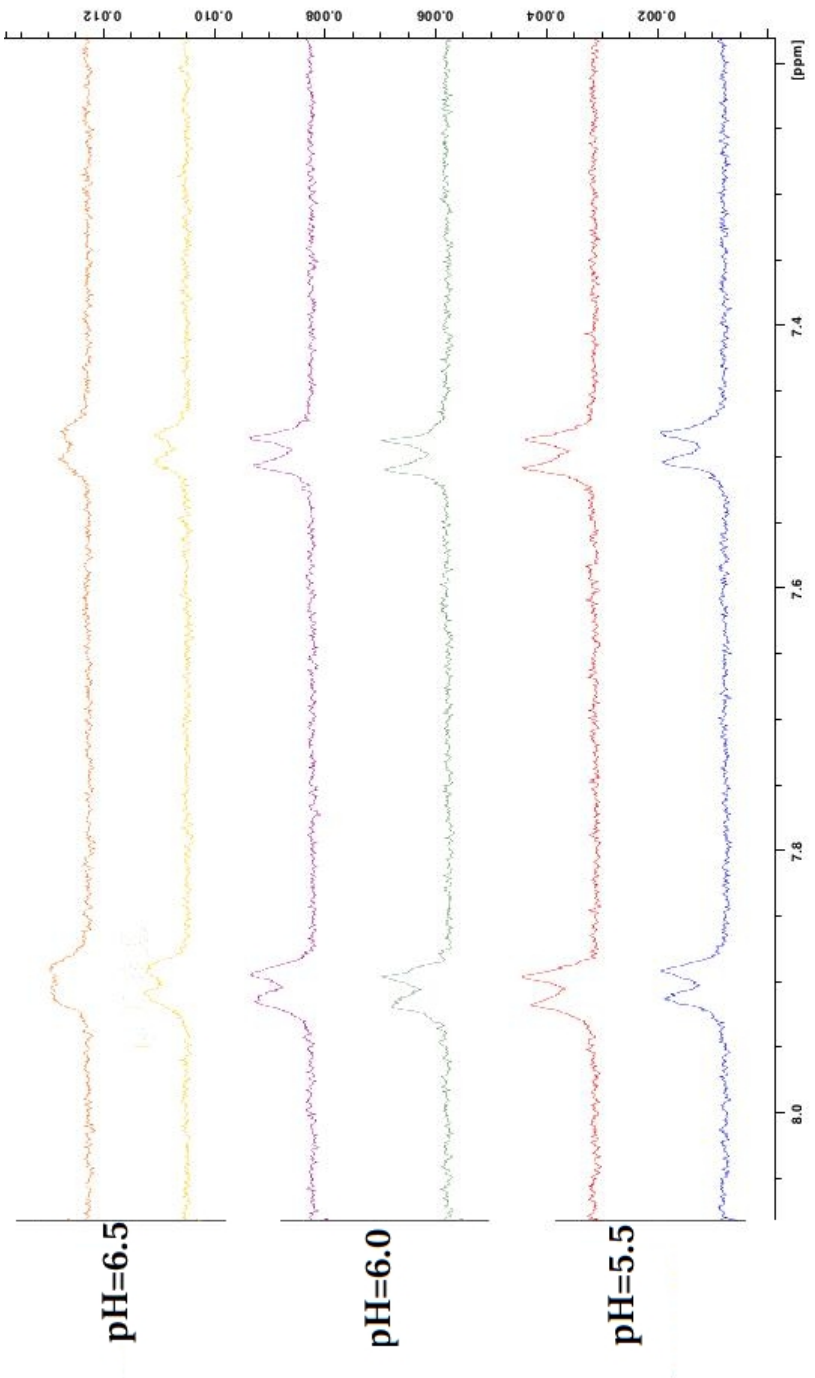

Figure 57: Molecular peaks of aromatic protons in 4AP.

G Standard curve for absorbance measurements, Me-O-Tyr

The percentage coupling of Me-O-Tyr was calculated based on a standard series of Me-O-Tyr, with 0.25, 0.50, 0.75 and 1mM solutions. The absorbance was measured at 280nm. Two measurements were performed for each parallel, if the absorbance deviated much a third measurement was performed.

Figure 58 show the absorbance spectra for the standard series of Me-O-Tyr.

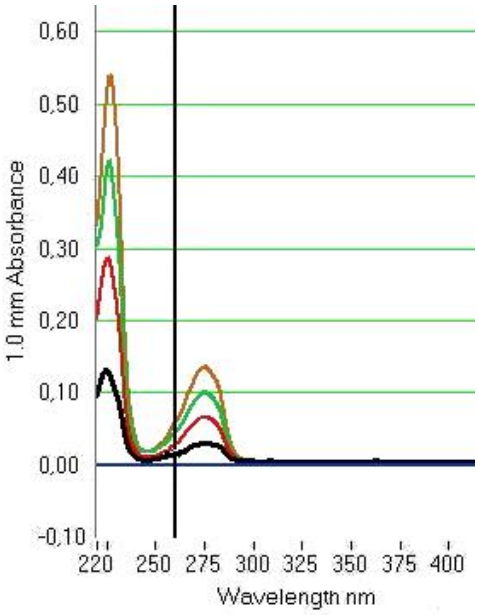

Figure 58: Absorbance spectra of standards. The highest absorbance at 280nm is observed for 1mM Me-O-Tyr, and the lowest for 0.25mM.

Lambert-Beers law states that, at low concentrations, the absorbtion, A, of a specie is linear with its concentration, C, and the distance the light travels through the material, l multiplied by a extinction coefficient, ε. The law is shown in equation 6.

$$A = \varepsilon lc \tag{6}$$

Figure 59 show the relationship between absorbance and concentration.

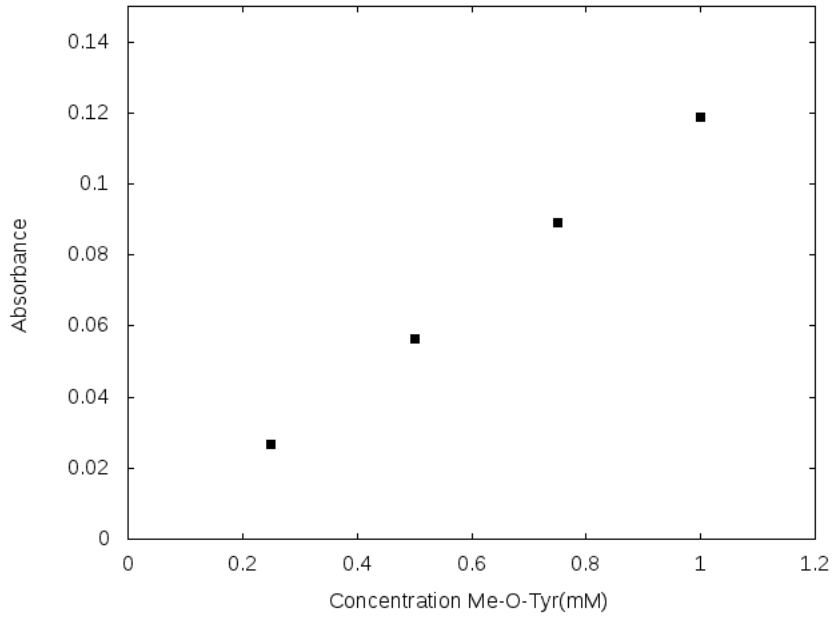

Figure 59: Absorbance as a function of Me-O-Tyr concentration.

The approximated linear relationship between the absorbance (f(x)) of standarized samples of Me-O-Tyr of different concentrations (x) at λ=280nm is given in equation 7:

$$f(x) = 0.1234x - 0.0045 \tag{7}$$

The R^2 for this trendline is 0.999. Equation 7 was used to calculate the concentration of Me-O-Tyr coupled to alginate for all Me-O-Tyr samples.

Example:

A parallel has an average absorbance of 0.200. The concentration is calculated in equation 8:

$$Me - O - Tyr(mM) = (0.1234x0.200) - 0.0045 = 0.0202mM \tag{8}$$

The concentration of mannuronan is calculated from its dry weight after lyophilization. The molecular weight of mannuronan is set as 176.124 g/mol. For a parallel weighing 6.8mg dissolved in 600μL D_2O, the concentration is calculated as shown in equation 9.

$$polyM(mM) = \frac{6.8mg}{176.124g/mol} x \frac{1}{0.006dm^3} = 6.43mM \tag{9}$$

To find the relative percentage amount of Me-O-Tyr in the parallel, the concentration of Me-O-Tyr is divided by the polymannoronan concentration as shown in equation 10.

$$BoundMe - O - Tyr(\%) = \frac{0.0202mM}{6.43mM} x100\% = 0.31\% \tag{10}$$

H Varying temperature for Me-O-Tyr coupling

The calculated percentage bound Me-O-Tyr was calculated by integration of aromatic Me-O-Tyr protons at ∼6.9 and 7.20 ppm. The yield was calculated from a theoretical coupling of 5%. For calculating the yield, see appendix B, equation 5. The results are summarized in table 22.

Table 22: Bound Me-O-Tyr(%) to mannuronan, ^{1}H NMR

Temp.(°C)	Parallel	Integral ∼6.9	Integral ∼7.2	Coupling (%)	Yield (%)
20	1	0.0046	0.0037	0.21	4.2
	2	0.0042	0.0037	0.20	4.0
0	1	0.0035	0.0038	0.18	3.6
	2	0.0044	0.0049	0.23	4.6

The ^{1}H NMR spectra of the parallels are shown in figure 60

Table 23 show the average absorbance (av. abs) and bound Me-O-Tyr based on UV/vis spectrometry.

Table 23: Bound Me-O-Tyr(%) to mannuronan

Temperature (°C)	Parallel	Av. abs. λ=280 nm	Bound Me-O-Tyr (%)	Yield (%)
20	1	0.193	0.30	6.0
	2	0.252	0.43	8.6
0	1	0.314	0.51	10.2
	2	0.266	0.42	8.4

Table 24 show the calculated standard deviations and averages calculated from UV-vis and ^{1}H NMR measurements.

Table 24: Standard deviations and averages of bound Me-O-Tyr(%) to mannuronan

	Average (%)	
Temperature (°C)	^{1}H NMR	UV/vis
20	0.21	0.36
0	0.21	0.47

Figure 61 show the absorbance spectra of Me-O-Tyr.

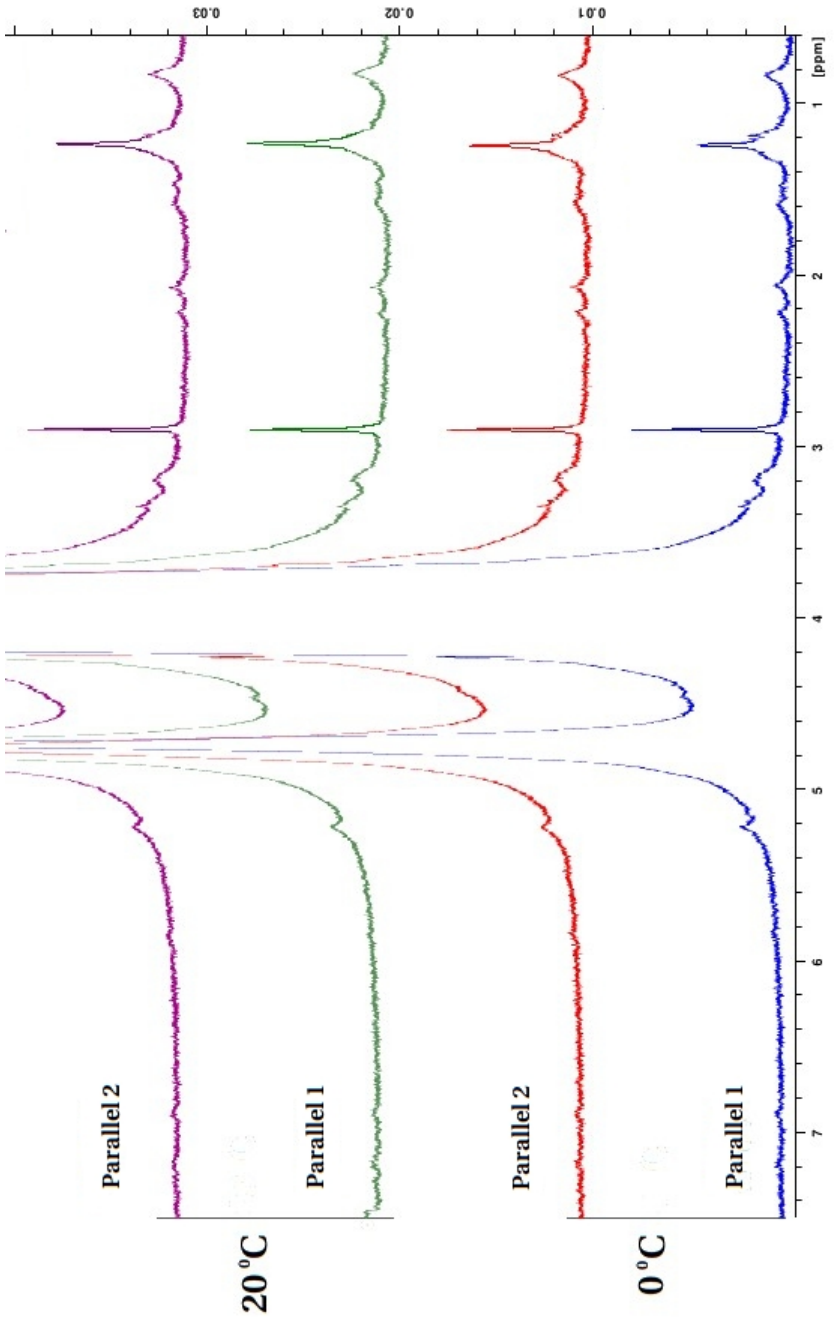

Figure 60: ^{1}H NMR spectra for Me-O-Tyr when the temperature is varied.

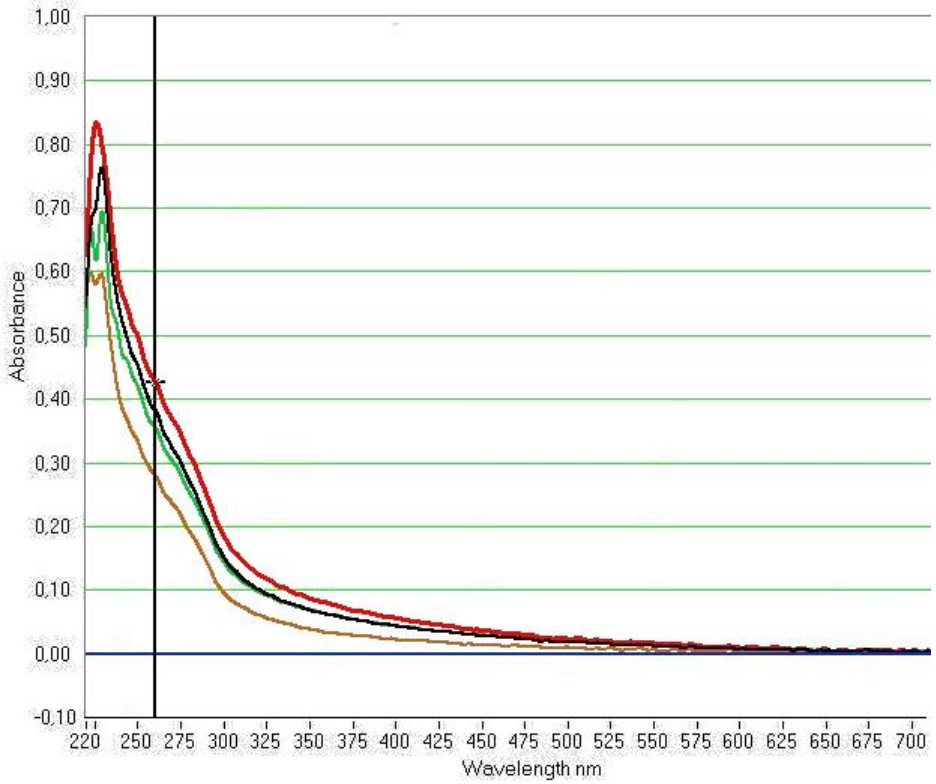

Figure 61: Absorbance spectra for Me-O-Tyr when the temperature is varied. The red line represents parallel 1 at 0°C, black line is parallel 2 of 0°C. The green and brown lines represents parallel 2 and 1 of 20°C, respectively.

I Optimal reaction time at 0 °C

The degree of coupling Me-O-Tyr to mannuronan at 0°C was examined by ^{1}H NMR and UV/vis spectroscopy.

The percentage bound Me-O-Tyr to mannuronan based on ^{1}H NMR is shown in table 25. The integral at 6.9 and 7.2 represents the benzen protons of Me-O-Tyr. Parallel number 1 for the 60 minute sample was lost during the experiment. For calculating the yield, see appendix B, equation 5.

Table 25: Bound Me-O-Tyr(%) to mannuronan, ^{1}H NMR

Time (min)	Parallel	Integral 6.90 ppm	Integral 7.20 ppm	Bound Me-O-Tyr (%)	Yield (%)
20	1	0.0053	0.0054	0.27	5.4
	2	0.0057	0.0054	0.28	5.6
40	1	0.0049	0.0049	0.25	5.0
	2	0.0044	0.0036	0.20	4.0
60	2	0.0053	0.0049	0.26	5.2

Table 26 show the bound Me-O-Tyr calculated from the absorbance measured at 280nm.

Table 26: Bound Me-O-Tyr(%) to mannuronan, determined by UV/vis spectroscopy

Time(min)	Parallel	Av. abs. λ=280 nm	Bound Me-O-Tyr(%)	Yield(%)
20	1	0.191	0.28	5.6
	2	0.190	0.28	5.6
40	1	0.239	0.41	8.2
	2	0.174	0.24	4.9
60	2	0.167	0.24	4.8

Figure 62 show the absorbance spectra for Me-O-Tyr at 0°C when the time is varied.

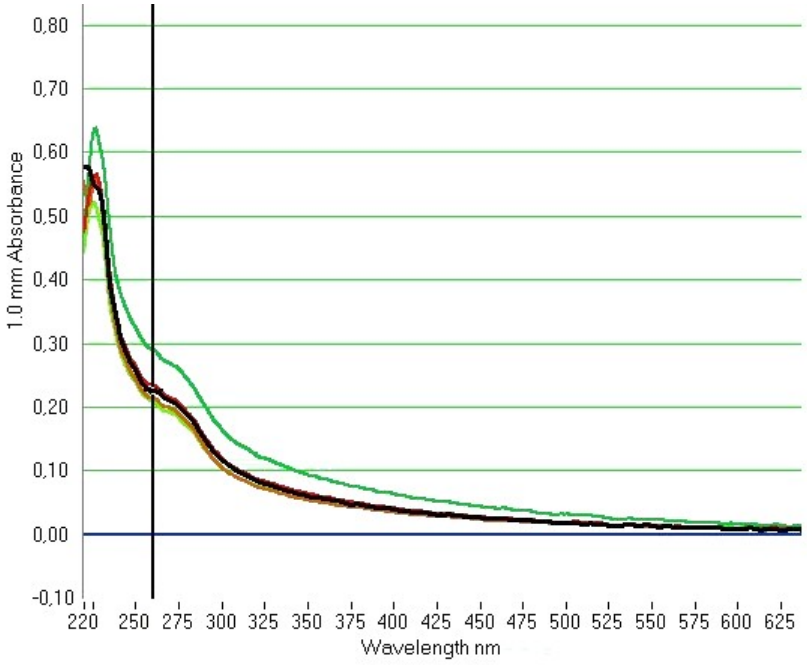

Figure 62: Absorbance spectra for Me-O-Tyr when the time at 0° is varied. The highest absorbance at 280nm represents parallel 1 of the 40 minute sample, and is shown as a green graph. The absorbance for the 20 minute sample was the same, of 0.19 at 280nm, while the 60 minute sample had the lowest absorbance of 0.17 at 280nm and is shown as the light green graph.

J Varying pH at 0°C for Me-O-Tyr coupling

The coupling percentage and yield of coupling Me-O-Tyr to mannuronan when the pH was varied was calculated by ^{1}H NMR spectroscopy. The calculated percentage bound Me-O-Tyr was calculated by integration of aromatic Me-O-Tyr protons at ∼6.9 and 7.20 ppm. The yield was calculated from a theoretical coupling of 5%. For calculating the yield, see appendix B, equation 5. The results are shown in table 27.

Table 27: Bound Me-O-Tyr(%) to mannuronan, ^{1}H NMR

pH	Sample	Integral 6.90 ppm	Integral 7.20 ppm	Bound Me-O-Tyr(%)	Yield (%)
5.0	1	0.0040	0.0044	0.21	4.0
	2	0.0040	0.0038	0.20	4.2
6.0	1	0.0038	0.0033	0.18	3.6
	2	0.0047	0.0040	0.22	4.2
6.5	1	0.0040	0.0029	0.17	3.4
	2	0.0043	0.0034	0.19	3.8

Figure 63 show the spectra for Me-O-Tyr coupled to mannuronan at 0°C when the pH is varied.

The realtionship between absorbance and percentage coupling of Me-O-Tyr to mannuronan at different pH-values at 0°C was calculated based on UV/vis spectroscopy. The calculations are shown in table 28.

Table 28: Bound Me-O-Tyr(%) to mannuronan, UV/vis spectroscopy

pH	Parallel	Av. abs λ=280nm	Bound Me-O-Tyr (%)	Yield (%)
5.5	1	0.293	0.42	8.5
	2	0.243	0.38	7.5
6.0	1	0.120	0.16	3.1
	2	0.352	0.58	11.6
6.5	1	0.235	0.39	7.7
	2	0.215	0.33	6.6

Figure 64 show the absorbance spectra for Me-O-Tyr coupled to mannuronan when the pH is varied.

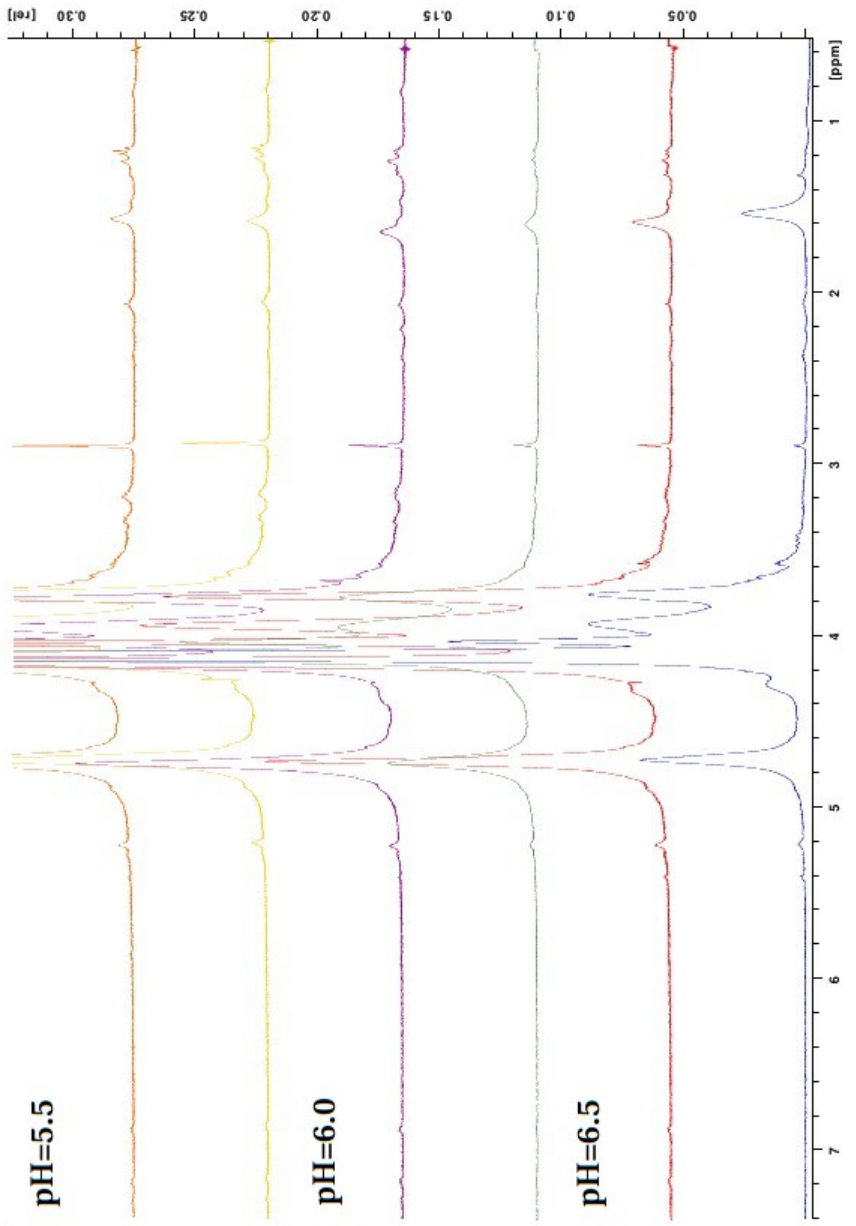

Figure 63: ^{1}H NMR spectra for Me-O-Tyr coupled to mannuronan when the pH is varied. The spectra were recorded at 300MHz.

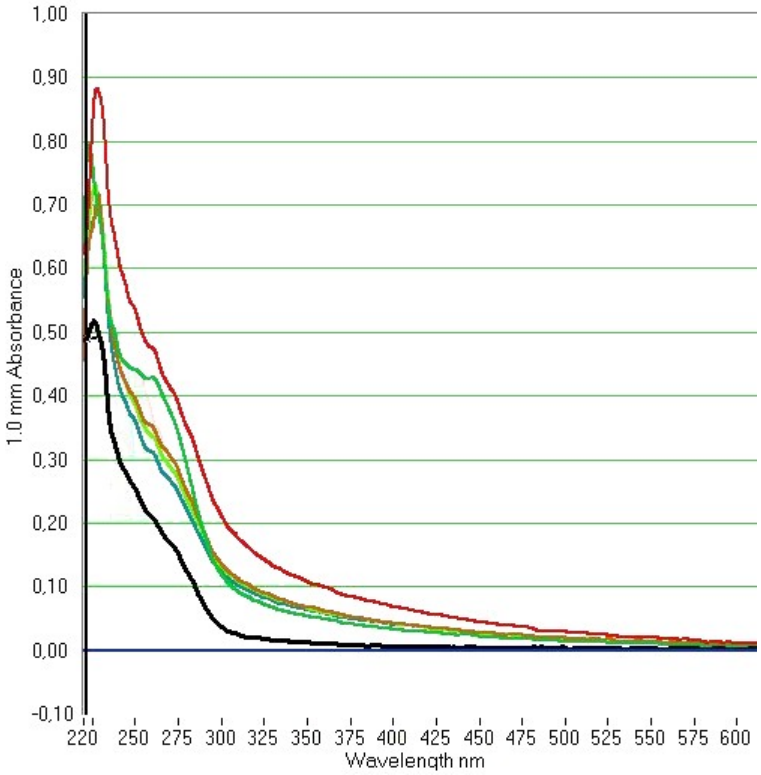

Figure 64: Absorbance spectra of Me-O-Tyr coupled to mannuronan at different pH-values. The red line show the curve for parallel 2 of the 6.0 sample. The absorbance decrease in the following manner: sample 5.5, parallel 1 > sample 6.5, parallel 1 > sample 5.5, parallel 2 > sample 6.5, parallel 2 > sample 6.0, parallel 1.

K Coupling Me-O-Tyr to alginate beads

Table 29 show the average absorbance at 280nm for Me-O-Tyr bound to alginate beads.

Table 29: Bound Me-O-Tyr(%) to mannuronan, determined by UV/vis spectroscopy

Absorbance at λ=280 nm	Bound Me-O-Tyr (%)
0.119	0.09

Figure 65 show the absorbance specter of Me-O-Tyr coupled to alginate beads.

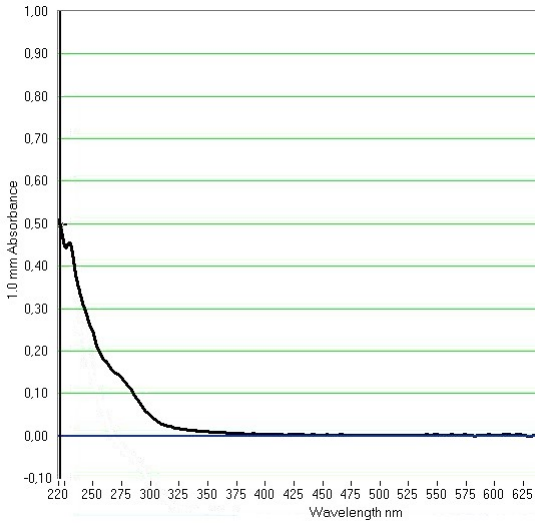

Figure 65: Me-O-Tyr coupled to alginate beads, UV/vis spectroscopy.

Figure 66 show the ^{1}H NMR spectra for Me-O-Tyr coupled to alginate beads.

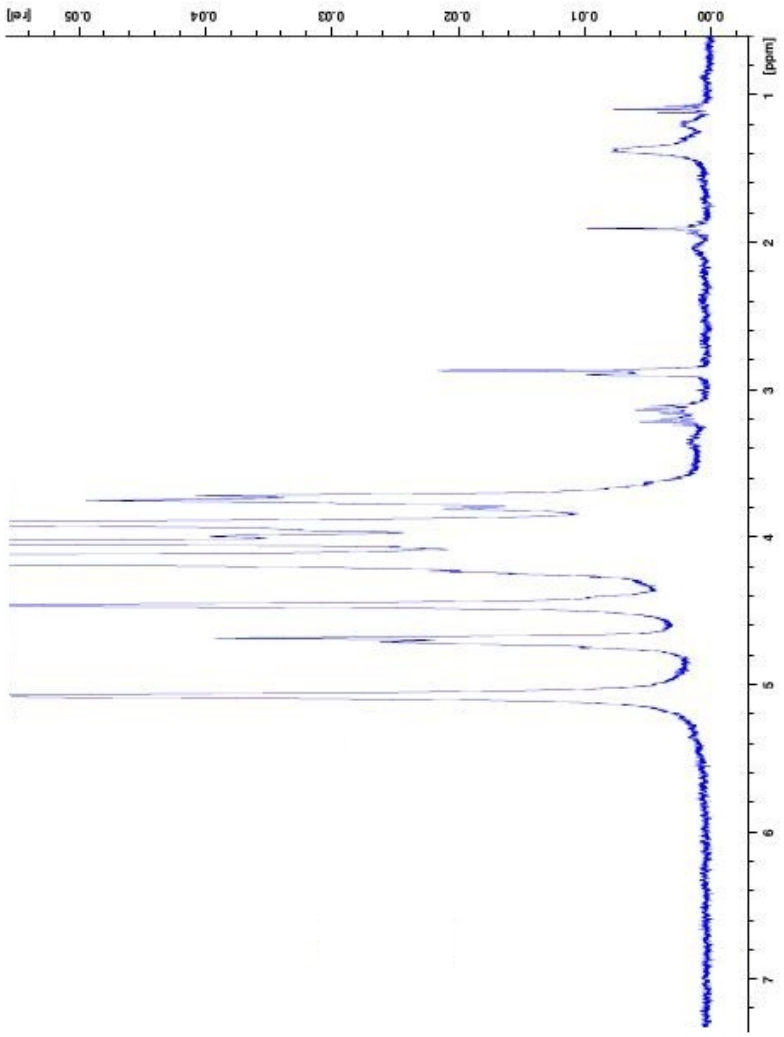

Figure 66: Me-O-Tyr coupled to alginate beads.

L Varying amount of EDC and Me-O-Tyr added

The calculated percentage bound Me-O-Tyr was calculated by integration of aromatic Me-O-Tyr protons at ∼6.9 and 7.20 ppm. Table 30 show the integrals and the calculated amount of bound Me-O-Tyr and presence of adducts calculated by ^{1}H NMR.

Table 30: Bound Me-O-Tyr (%) to mannuronan, ^{1}H NMR

		Integral at ppm			Coupling (%)	
sulfo-NHS&EDC (%)	Me-O-Tyr (%)	6.9	7.2	2.9	Me-O-Tyr	Adducts.
10	5	0.0057	0.0061	0.0238	0.24	0.40
	10	0.0044	0.0039	0.0184	0.27	0.31
	15	0.0069	0.0063	0.0228	0.37	3.8
	20	0.0067	0.0078	0.0270	0.36	4.5
20	5	0.0039	0.0034	0.0159	0.18	0.27
	10	0.0051	0.0050	0.0153	0.25	0.26
	15	0.0076	0.0067	0.0251	0.36	0.42
	20	0.0103	0.0090	0.0285	0.48	0.48

Figure 67 show the ^{1}H NMR spectra for 10% added EDC and s-NHS with increasing amount of Me-O-Tyr added.

Figure 68 show the ^{1}H NMR spectra for 20% added EDC and s-NHS with increasing amount of Me-O-Tyr added.

Table 31 show the calculated amount of Me-O-Tyr calculated by UV/vis spectroscopy.

Figure 69 show the absorbance spectra for 20 and 10% added EDC and s-NHS with increasing amount of Me-O-Tyr added.

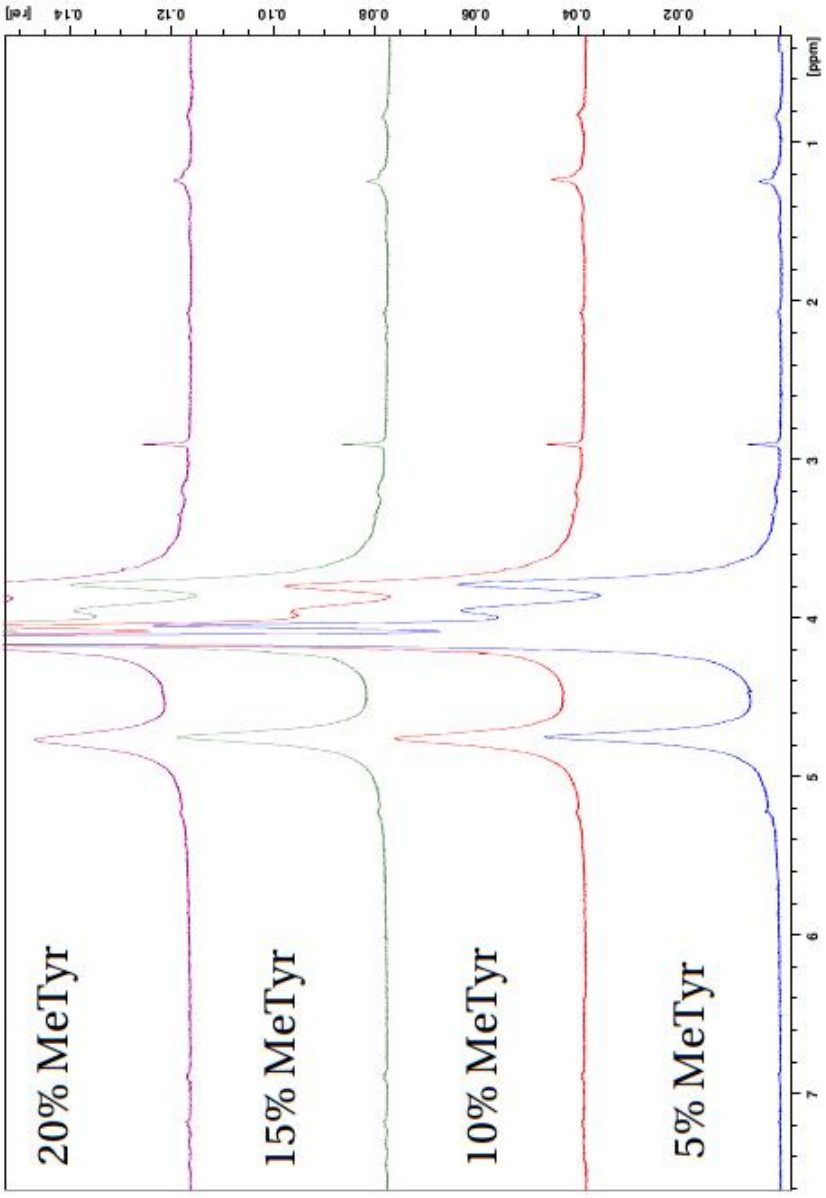

Figure 67: 10% activation with EDC

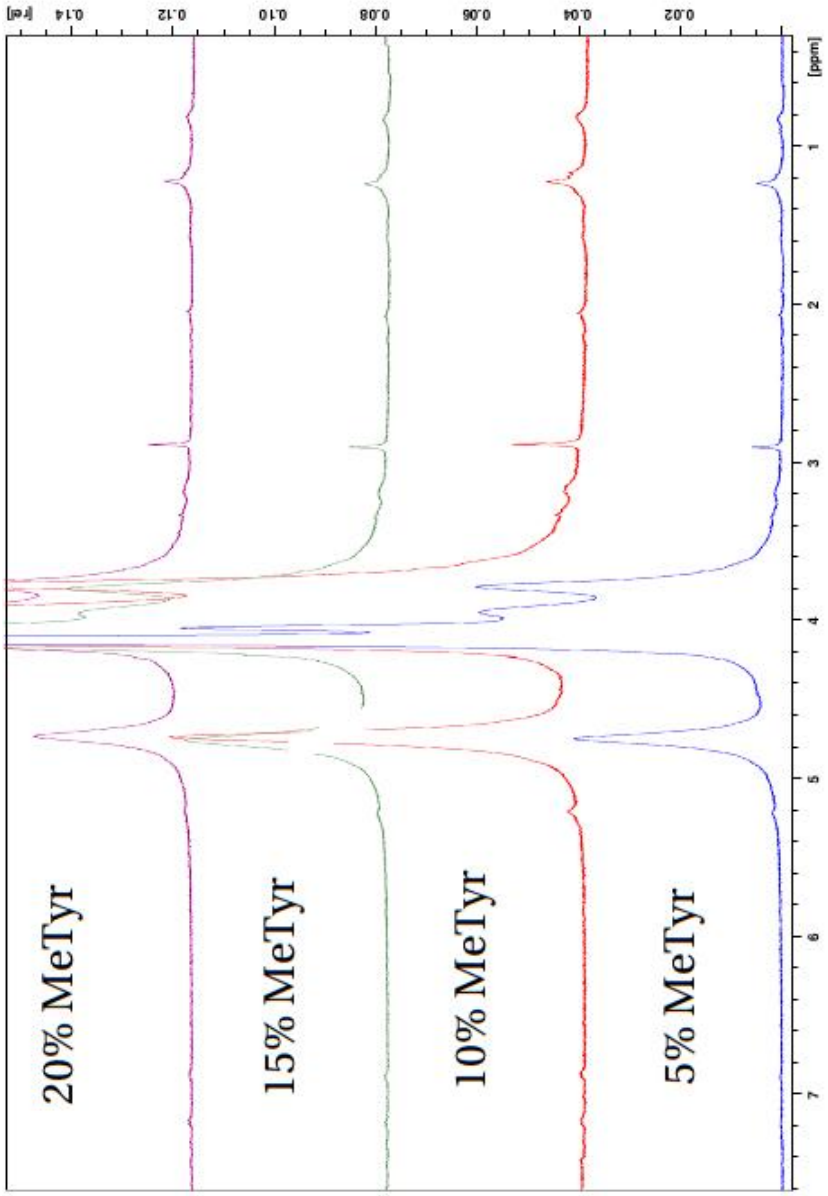

Figure 68: 20% activation with EDC

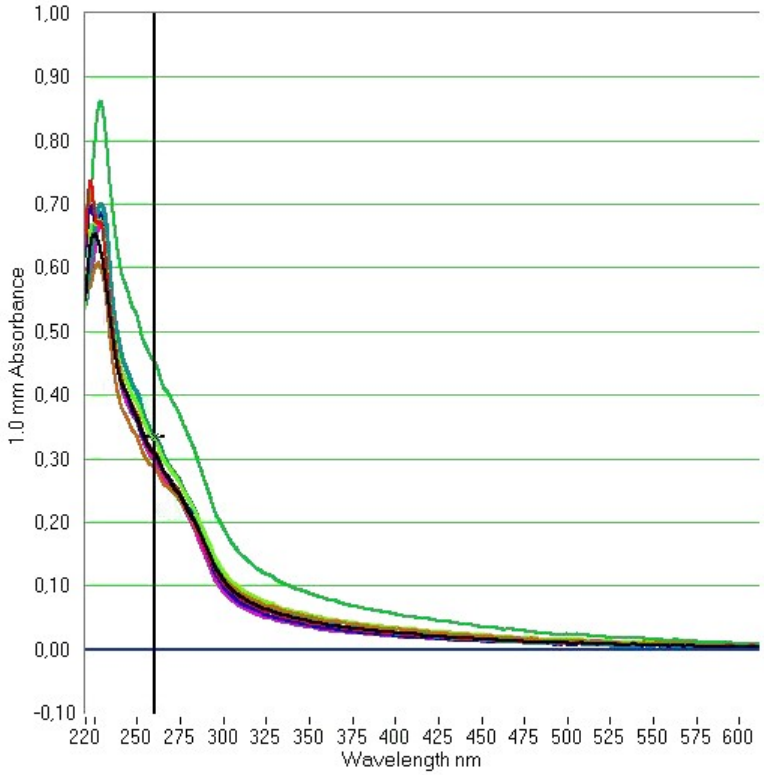

Figure 69: 20 and 10% activation with EDC. The samples are identified as *Amount EDC(Amount Me-O-Tyr)*, meaning that a sample named 20(5) has been added 20% EDC and Sulfo-NHS and 5% Me-O-Tyr, relative to the carboxylic acids in mannuronan. The absorbance at 280nm decreased as following: 10(15) > 20(5) > 20(10) > 10(20)=10(5) > 20(15)=20 (2)=10(10)

Table 31: Bound Me-O-Tyr(%) to mannuronan, determined by UV/vis spectroscopy

sulfo-NHS&EDC (%)	Me-O-Tyr (%)	Av. abs λ=280 nm	Bound Me-O-Tyr (%)
10	5	0.218	0.32
	10	0.215	0.31
	15	0.330	0.47
	20	0.216	0.32
20	5	0.231	0.36
	10	0.234	0.35
	15	0.216	0.31
	20	0.203	0.31

M Coupling with excess Me-O-Tyr

The calculated percentage bound Me-O-Tyr was calculated by integration of aromatic Me-O-Tyr protons at ∼6.9 and 7.20 ppm. Table 32 show the integrals and the calculated amount of bound Me-O-Tyr and presence of adducts calculated by ^{1}H NMR.

Table 32: Bound Me-O-Tyr (%) to mannuronan, ^{1}H NMR

		Integral at ppm			Coupling (%)	
Me-O-Tyr(%)	Parallel	6.9	7.2	2.9	Me-O-Tyr	Adducts
20	1	0.0069	0.0057	0.0216	0.32	0.36
	2	0.0071	0.0062	0.0256	0.33	0.43
40	1	0.0067	0.0056	0.0211	0.31	0.35
	2	0.0067	0.0060	0.0255	0.32	0.38
60	1	0.0057	0.0047	0.0228	0.26	0.38
	2	0.0068	0.0052	0.0324	0.30	0.54
80	1	0.0052	0.0037	0.0238	0.22	0.40
	2	0.0053	0.0037	0.0198	0.23	0.33
100	1	0.0046	0.0035	0.0291	0.20	0.49
	2	0.0040	0.0033	0.0231	0.18	0.39

Table 33 show the calculated amount of Me-O-Tyr calculated by UV/vis spectroscopy.

Table 33: Bound Me-O-Tyr(%) to mannuronan, determined by UV/vis spectroscopy

Me-O-Tyr(%)	Parallel	Av. abs λ=280 nm	Bound Me-O-Tyr (%)
20	1	0.218	0.34
	2	0.213	0.38
40	1	0.216	0.31
	2	0.213	0.32
60	1	0.245	0.37
	2	0.192	0.29
80	1	0.207	0.30
	2	0.187	0.26
100	1	0.201	0.28
	2	0.205	0.29

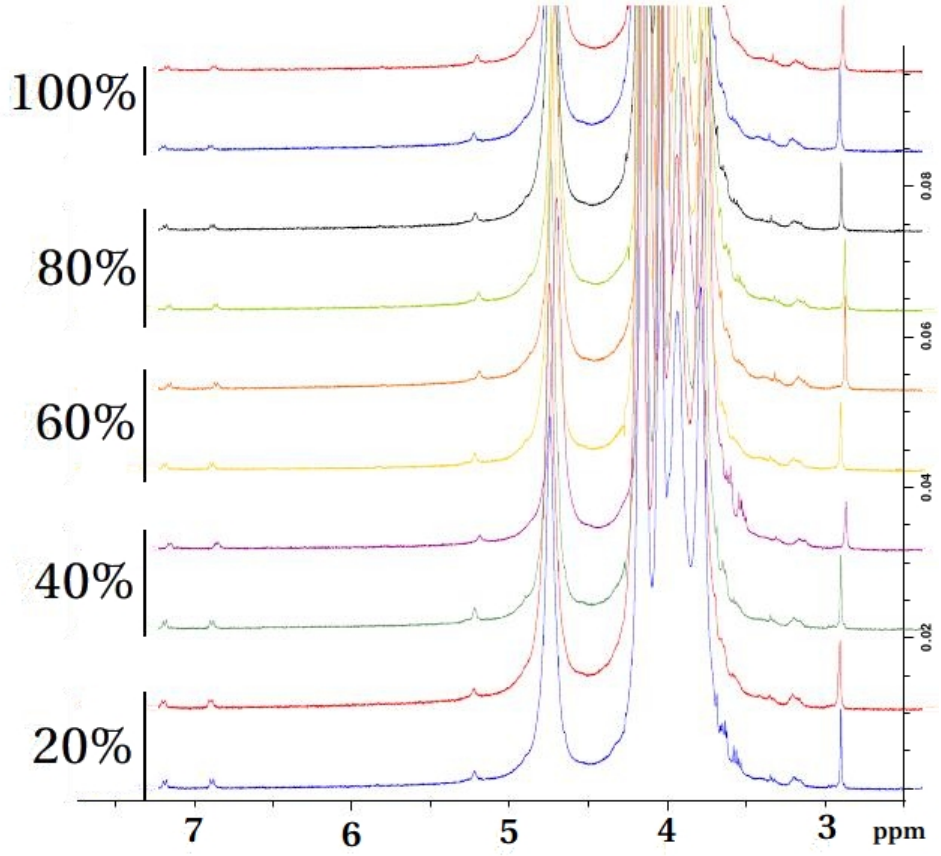

Figure 70: Formation of adducts when coupling with excess Me-O-Tyr. The percentage indicate the amount of Me-O-Tyr added. The integral of the singlet at 2.90 ppm was used to calculate the amount of adducts present, and the integrals at 6.90 and 7.20 ppm were used to deduce the amount of Me-O-Tyr coupled.

Figure 70 show the ^{1}H NMR spectra for coupling of excess Me-O-Tyr.

Figure 71 show the absorbance spectra for coupling with excess Me-O-Tyr.

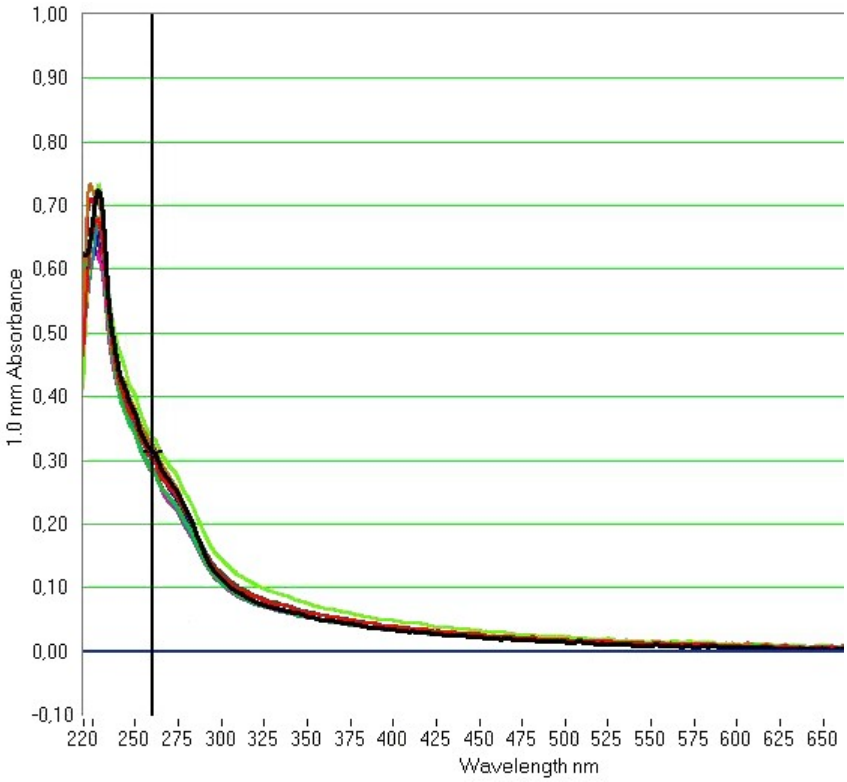

Figure 71: Coupling with excess Me-O-Tyr. The samples are identified as *Amount Me-O-Tyr added(parallel)* and decrease as following: 20(2) > 60(1) > 20(1) > 40(2) > 40(1) > 80(1) > 60(2)=100(2) > 100(1) > 80(2).

N Standard curve for absorbance measurements, GRGDYP

The percentage coupling of GRGDYP was calculated based on a standard series of GRGDYP, with 0.25, 0.50, 0.75 and 1mM solutions. The absorbance was measured at 280nm. Two measurements were performed on each sample, if the absorbance deviated much a third measurement was performed.

Figure 72 show the absorbance spectra for the standard series of GRGDYP.

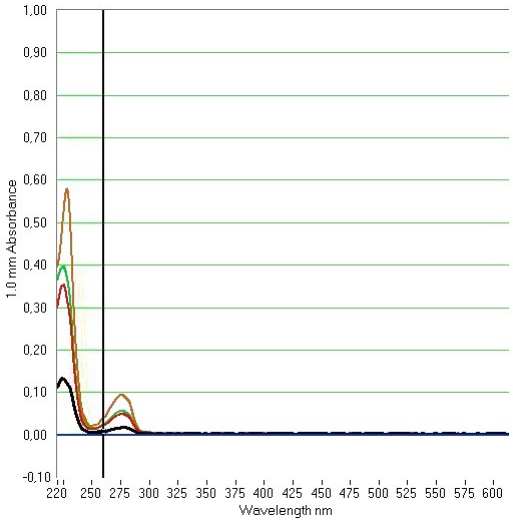

Figure 72: Absorbance spectra of standards for GRGDYP. The highest absorbance at 280nm was observed for 1mM GRGDYP, and the lowest absorbance for 0.25mM.

Lambert-Beers law states that, at low concentrations, the absorbtion, A, of a specie is linear with its concentration, C, and the distance the light travels through the material, l multiplied by a extinction coefficient, ε. The law is shown in equation 11.

$$A = \varepsilon lc \tag{11}$$

Figure 73 show the relationship between absorbance and concentration.

The approximated linear relationship between the absorbance (f(x)) of standarized samples of GRGDYP of different concentrations (x) at λ=280nm is given in equation 12:

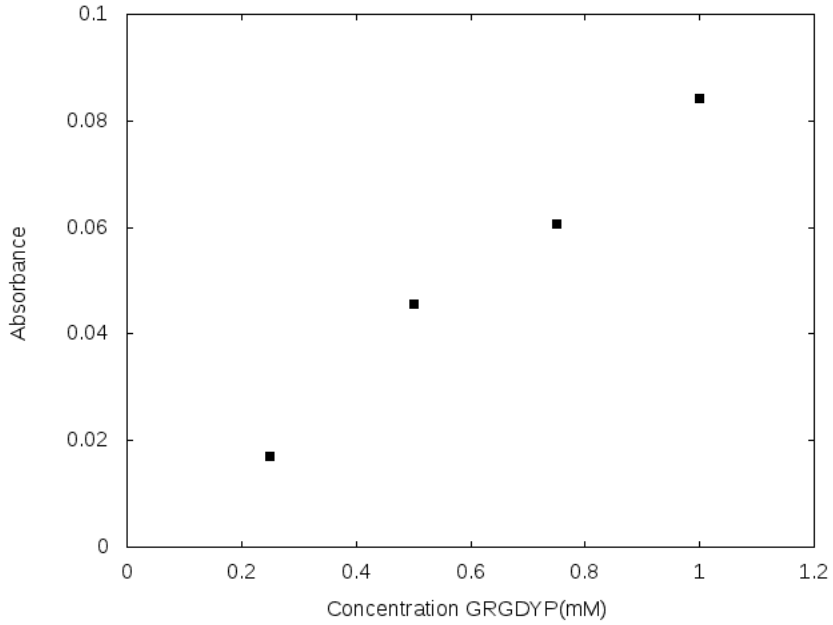

Figure 73: Absorbance as a function of GRGDYP concentration.

$$f(x) = 0.0868x - 0.00233 \tag{12}$$

The R^2 for this trendline is 0.987. Equation 12 was used to calculate the concentration of GRGDYP coupled to alginate for all GRGDYP samples. An example of how this is calculated is shown in appendix G.

O Activating mannuronan at pH=4.2

Integration of the proton peaks at 7.20 and 6.90 gave an area of 0.0014 and 0.0018 respectively. This was calculated to correspond to 0.08% coupling.

Figure 74 show the spectra for Me-O-Tyr coupled to mannuronan.

The average absorbance of the sample at 280nm was 0.231 which corresponds to 0.24% coupling.

Figure 75 show the absorbance spectra for Me-O-Tyr coupled to mannuronan at pH=4.2.

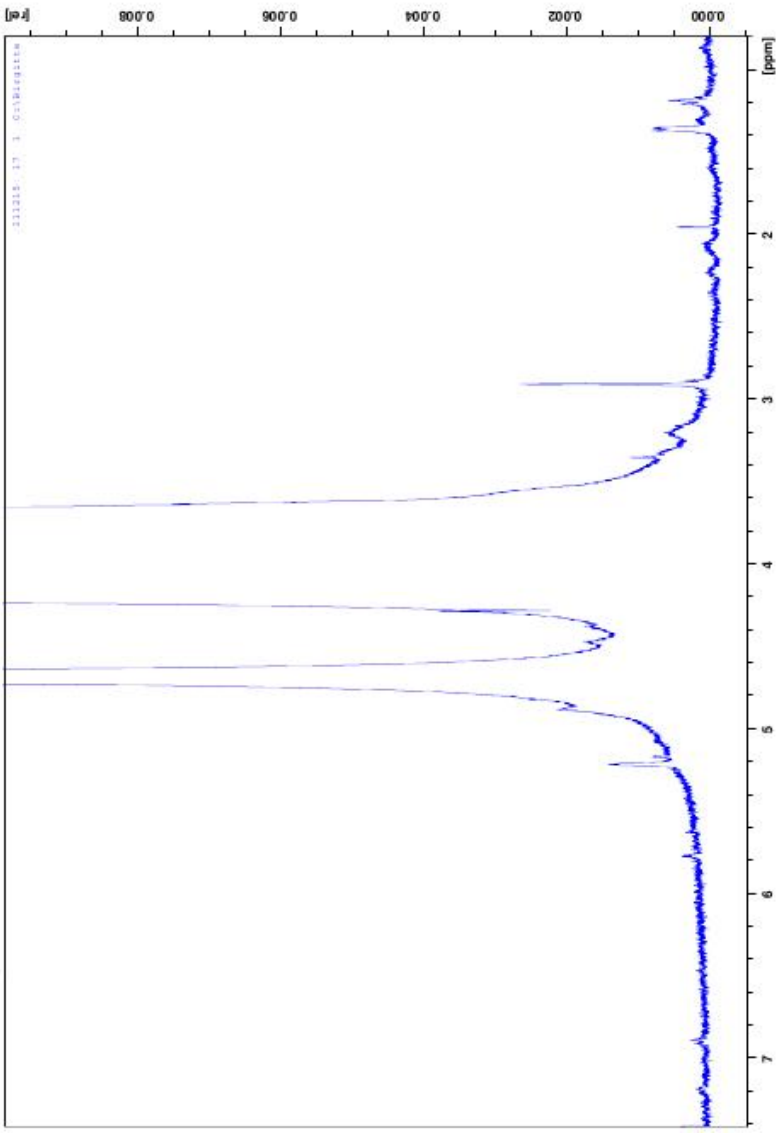

Figure 74: Me-O-Tyr coupled to mannuronan activated at pH=4.2

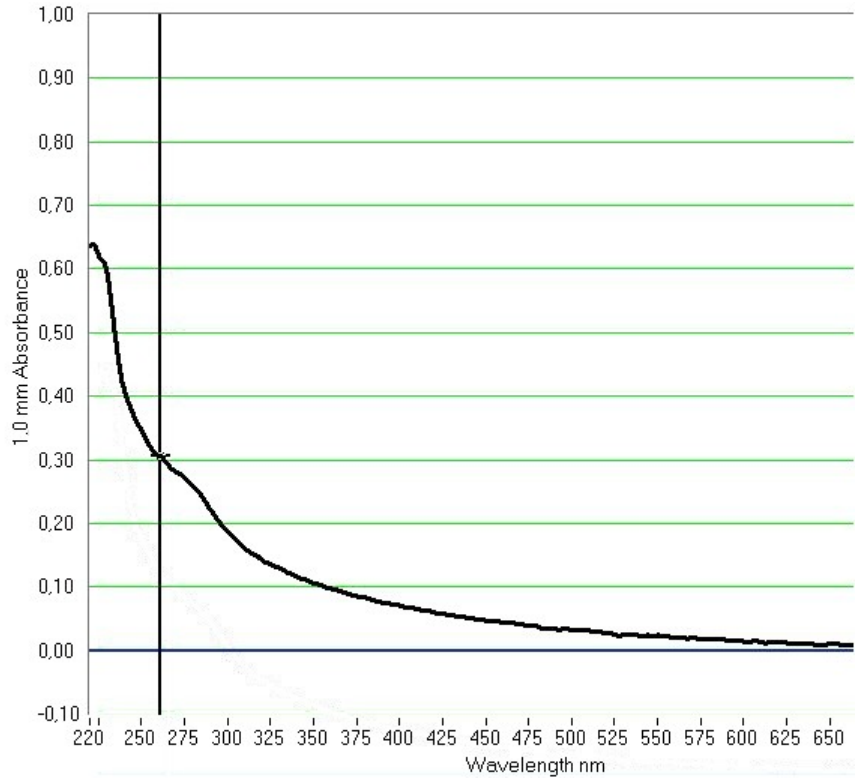

Figure 75: Absorbance spectra for coupling Me-O-Tyr to mannuronan activated at pH=4.2

P Varying pH for GRGDYP coupling

The coupling of GRGDYP to mannuronan when the pH was varied was calculated by ^{1}H NMR spectroscopy. The results are shown in table 34.

Table 34: Bound GRGDYP(%) to mannuronan, ^{1}H NMR

pH	Sample	Integral ∼6.7ppm	Integral ∼7.12ppm	Bound GRGDYP (%)
5.5	1	0.0034	0.0019	0.13
	2	0.0028	0.0014	0.11
6.5	1	0.0054	0.0020	0.19
	2	0.0062	0.0031	0.23

The realtionship between absorbance and percentage coupling of GRGDYP to mannuronan at different pH-values was calculated based on UV/vis spectroscopy. The calculations are shown in table 35.

Table 35: Bound Me-O-Tyr(%) to mannuronan, determined by UV/vis spectroscopy

pH	Parallel	Av. abs λ=280nm	Bound GRGDYP (%)
5.5	1	0.289	0.32
	2	0.289	0.29
6.0	1	0.293	0.27
	2	0.283	0.31

Figure 76 show the absorbance spectra for GRGDYP coupled to mannuronan when the pH is varied.

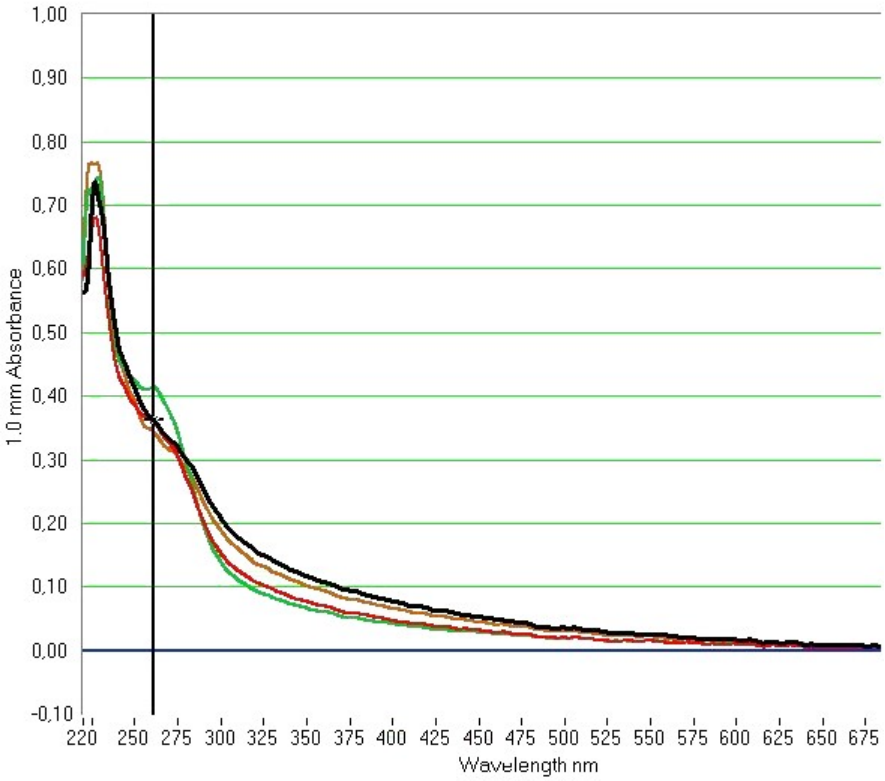

Figure 76: Absorbance spectra of GRGDYP coupled to mannuronan at different pH-values. The samples are identified as *pH(parallel)* and decrease as following: 5.5(1) > 6.0(2) > 5.5(2) > 6.0(1).

Q Varying amount GRGDYP added and pH

The calculated percentage bound GRGDYP was calculated by integration of aromatic GRGDYP protons at ∼6.9 and 7.20 ppm. Table 36 show the integrals and the calculated bound GRGDYP and presence of adducts calculated by ^{1}H NMR.

Table 36: Bound GRGDYP (%) to mannuronan and adducts (%), ^{1}H NMR

			Integral at ppm			Coupling (%)	
pH	GRGDYP(%)	Parallel	6.9	7.2	2.9	GRGDYP	Adduct
4.0	5	1	0.0110	0.0125	0.4402	0.59	7.1
		2	0.0098	0.0109	0.4308	0.52	6.5
	10	1	0.0144	0.0152	0.3367	0.74	5.2
		2	0.0142	0.0160	0.3575	0.76	5.3
	15	1	0.0252	0.0355	0.2769	1.5	4.5
		2	0.0204	0.0237	0.3122	1.1	4.6
	20	1	0.0252	0.0280	0.2829	1.3	4.3
		2	0.0364	0.0543	0.2992	2.3	4.9
6.0	5	1	0.0064	0.0126	0.4870	0.48	7.7
		2	0.0078	0.0229	0.5152	0.77	7.8
	10	1	0.0124	0.0288	0.4443	1.0	6.8
		2	0.0116	0.0270	0.4150	0.97	6.2
	15	1	0.0155	0.0262	0.2811	1.0	4.5
		2	0.0182	0.0336	0.3315	1.3	5.0
	20	1	0.0447	0.0927	0.3682	3.4	5.3
		2	0.0162	0.0276	0.2707	1.1	4.1

Table 37 show the calculated amount of GRGDYP calculated by UV/vis spectroscopy.

Figure 77 show the absorbance spectra for GRGDYP coupled to mannuronan at pH=4.0 and pH=6.0.

Figure 78 show the spectra of aromatic protons of GRGDYP when coupled to mannuronan.

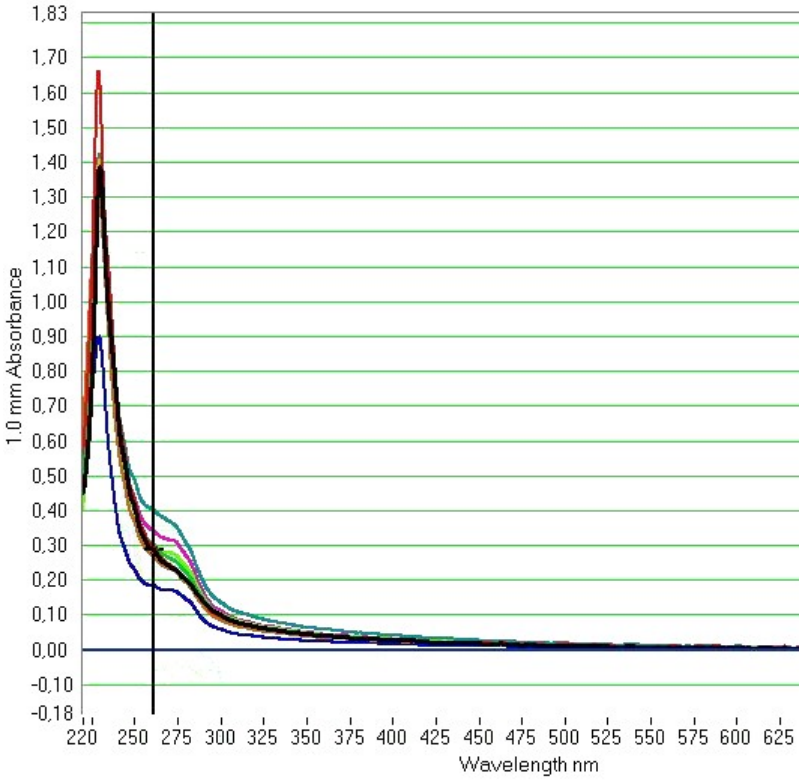

Figure 77: GRGDYP coupled to mannuronan at pH=4.0 and pH=6.0, UV/vis spectroscopy. The samples are identified as *pH(GRGDYP added,parallel)* and decrease as following: 4.0(15,2) > 6.0(15,1) > 4.0(20,2) > 4.0(15,1) =4.0(20,1)=6.0(15,2)=6.0(20,2) > 6.0(20,1) > 6.0(10,2)=6.0(10,2) > 4.0(10,1) > 6.0(5,2) =4.0(10,2) > 4.0(5,1).

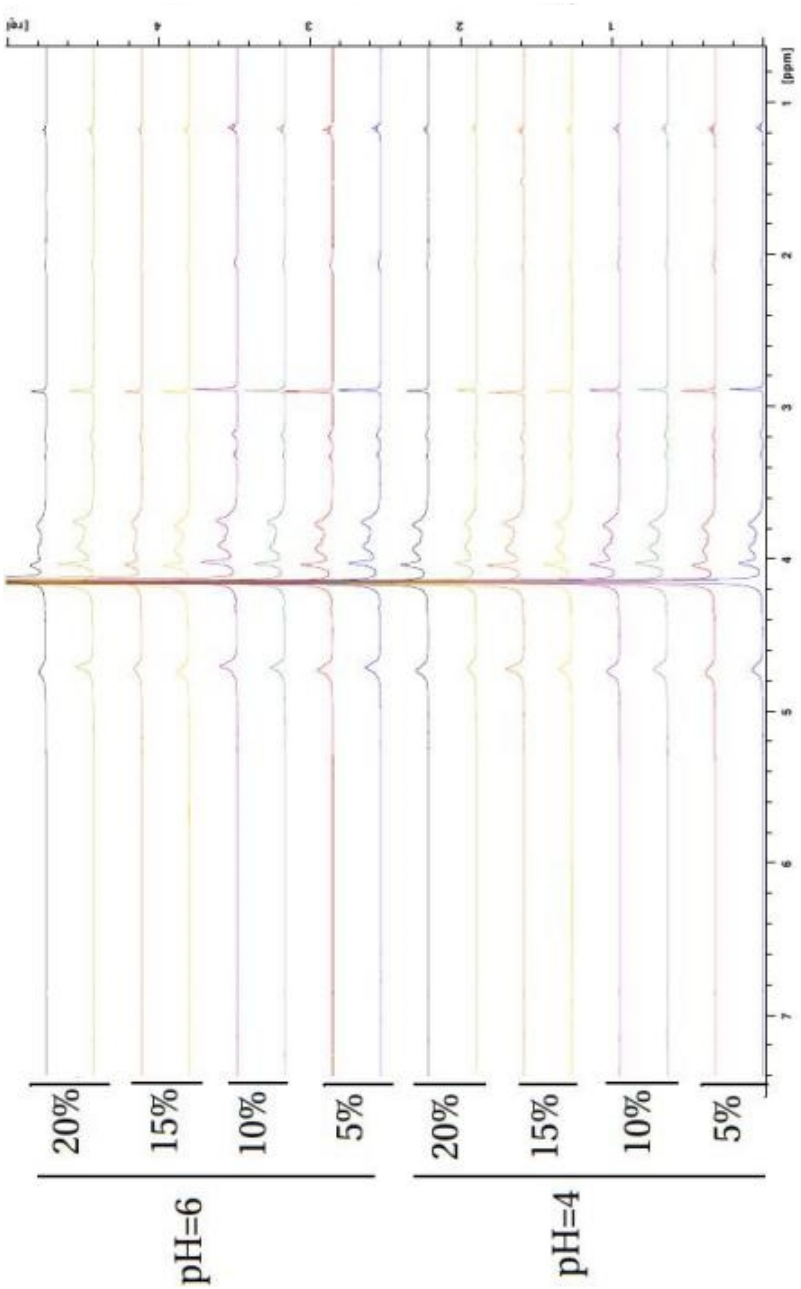

Figure 78: Coupling of GRGDYP to mannuronan when the pH is 4.0 and 6.0.

Table 37: Bound GRGDYP (%) to mannuronan, determined by UV/vis spectroscopy

pH	GRGDYP (%)	Parallel	Av. abs λ=280nm	GRGDYP (%)
4.0	5	1	0.195	0.20
		2	0.196	0.29
	10	1	0.215	0.22
		2	0.190	0.21
	15	1	0.240	0.26
		2	0.300	0.31
	20	1	0.144	0.26
		2	0.268	0.28
6.0	5	1	0.192	0.19
		2	0.191	0.21
	10	1	0.240	0.24
		2	0.241	0.24
	15	1	0.281	0.29
		2	0.245	0.26
	20	1	0.238	0.25
		2	0.262	0.26

R Determining the composition of alginate

Alginates are polydisperse with respect to their molecular weight; meaning that it is an average over the whole distribution of molecular weights. For N_i molecules with the specific weight M_i, the molecular weight average, $\overline{M_w}$, is defined in equation 13 as:

$$\overline{M_w} = \frac{\Sigma N_i M_i^2}{\Sigma N_i M_i} \tag{13}$$

The monomers are not distributed randomly in the polymer chain, therefore its distribution can not be described by Bernoullian statistics.

The monomer sequence and composition in naturally occuring alginates is a result of a complex biochemical pathway. A complete sequencing of alginate is not possible, but a complete characterization of the monomer composition can be determined by high-resonance proton and carbon nuclear magnetic resonance (^{1}H NMR and ^{13}C NMR, respectively)[24]. An important part of the determination of the monomer composition is based on changes in the chemical shifts of the anomeric protons in the chain. A ^{1}H NMR spectra of an alginate sample is depicted in figure 79[24].

Analysis of block chain length using ^{1}H NMR gives the average block chain length over the entire G-block population, but does not give the distribution of the G-blocks within the structure[24].

The polymer composition in alginates is described by its monomers (monads), and measurements of diad, triad and higher order frequencies(F). The four possible diad frequencies; F_{GG}, F_{MM}, F_{MG}, F_{GM} and the eight possible triad frequencies; F_{GGG}, F_{GGM}, F_{GMG}, F_{MGG}, F_{MMG}, F_{MMM}, F_{GMM} and F_{MGM}[2].

The mathematical correlation of the monad and diad frequencies are shown in equation 14 and 15.

$$1 = F_{GG} + F_{MM} + F_{GM} + F_{MG} \tag{14}$$

$$F_M = F_{MM} + F_{MG}, F_G = F_{GG} + F_{MG} \tag{15}$$

Long chains have less contribution from end groups and $\mathrm{F}_{MG} = \mathrm{F}_{GM}$. Mathematical relationships for triad frequencies in long chains are shown in equation 16, 17 and 18.

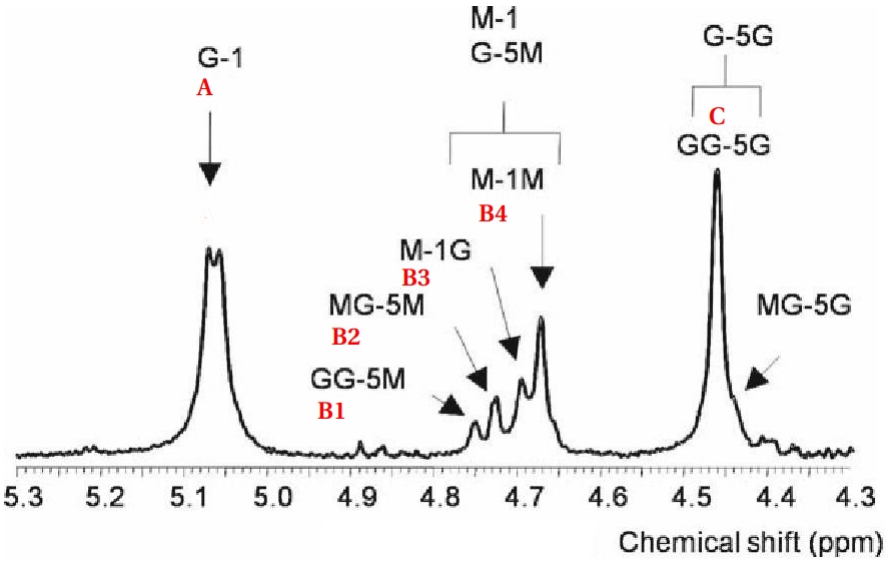

Figure 79: ^{1}H NMR spectra for determination of monomer composition in alginate. Alginate from *Laminaria hyperborea*, F_G ~0.63. The peaks are assigned with letters from A-C in addition to proton number and position. M-1M and M-1G represents the anomeric proton of an M-residue neighbouring another M-, or G-residue, respectively. MG-5M, MG-5G and GG-5M refers to the H-5 proton of a central G-residue in the triad MGM, MGG or GGM, respectively. G1 represents the anomeric protons of G-residues, while GG-5G refers to the anomeric protons of G-residues in G-blocks [24].

$$F_G = F_{GGG} + F_{MGG} + F_{GGM} + F_{MGM} \tag{16}$$

$$F_{MG} = F_{GM} = F_{GGM} + F_{MGM} \tag{17}$$

$$F_{MGG} = F_{GGM} \tag{18}$$

The monads, diads and triads can be calculated from ^{1}H NMR peaks shown in figure 79. The signal assignments that are used to determine the sequential parameters are summarized in table 38.

Table 38: Signal assignments used to determine alginate composition

Peak symbol	Identity	Proton number
A	G	1
B1	GGM	5
B2	MGM	5
B3	MG	1
B4	MM	1
C	GG	5

There are two methods for determining the sequential parameters, named *the quick way* and by *maximum averaging*. The former was used to determine the parameters for the epimerisation test described in subsection 2.8.1 and the latter used to determine the parameters of the large scale production of RGD-coupled alginate (described in subsection 2.8.2).

Both methods are based on the assumption that the chains are longer than 20 units, resulting in F_{GM}=F_{MG} and F_{GGM}=F_{MGG}.

The quick way

The peaks named B1-B4 are summarized into one parameter, B:

$$B = B1 + B2 + B3 + B4 \tag{19}$$

The sequential parameters are calculated as shown below.

$$F_G = \frac{A}{B + C} \tag{20}$$

$$F_M = 1 - F_G \tag{21}$$

$$F_{GG} = \frac{C}{B + C} \tag{22}$$

$$F_{GM} = F_G - F_{GG} \tag{23}$$

$$F_{MM} = F_M - F_{GM} \tag{24}$$

$$F_{GGM} = \frac{B1}{B + C} \tag{25}$$

$$F_{MGM} = F_{GM} - F_{GGM} \tag{26}$$

$$F_{GGG} = F_{GG} - F_{GGM} \tag{27}$$

Maximum averaging

Here, the amount of M, G, MM, MG, MMM, MGM and GGG is calculated prior to calculating the sequential parameters.

$$G = 0.5x((A + C) + 0.5x(B1 + B2 + B3)) \tag{28}$$

$$M = 0.5x(B1 + B2 + B3) + B4 \tag{29}$$

$$GG = 0.5x((A + C) - 0.5x(B1 + B2 + B3)) \tag{30}$$

$$GM = 0.5x(B1 + B2 + B3) \tag{31}$$

$$MM = B4 \tag{32}$$

$$GGM = 0.5x(B1 + B2 + B3)x\frac{B1}{B1 + B2} \tag{33}$$

$$MGM = 0.5x(B1 + B2 + B3)x\frac{B2}{B1 + B2} \tag{34}$$

$$GGG = GG - GGM \tag{35}$$

Examples of how monades, diades and triades frequencies can be calculated is shown below:

$$F_G = \frac{G}{M + G} \tag{36}$$

$$F_{GG} = \frac{GG}{M + G} \tag{37}$$

$$F_{GGG} = \frac{GGG}{M + G} \tag{38}$$

The quick way is more sensitive to bad baselines and thus large errors compared to *maximum averaging*. The latter method offer the possibility to check the value of A,that contain all G1-protons, with C+$0.5x$(B1+B2+B3) which contain all G5-protons. These values should be identical with a limit of $\pm$ 2.5% [74] [75].

A parameter of the average block length can be calculated. For blocks that consist of minimum two contiguous units, the average block-length is calculated as shown in equation 39 [24].

$$\overline{N_{G>1}} = \frac{F_G - F_{MGM}}{F_{MGG}} \tag{39}$$

S Large scale production of RGD-coupled alginate

Two samples of 500mg mannuronan was used as starting point for large scale production of RGD-coupled alginate and alginate without RGD. Both samples were subject to enzymatic epimerisation, with AlgE4 introducing alternating sequences in the first step and AlgE6 introducing G-blocks in the final step. Both products were used as material in encapsulation of olfactory ensheating cells from neonatal rat brain. The encapsulation is performed at the department of Cancer Research and Molecular Medicine by co-student Marthe Fredheim Fjelldal.

An epimerisation test with AlgE6 was performed by incubating the enzyme with polyalternated alginate for 1,2,4 and 6 hours in the enzyme:alginate ratio 1:200. The results for the epimerisation test are shown in table 39.

Table 39: Calculated frequencies from ^{1}H NMR spectroscopy, epimerisation test

Sample	Hours with AlgE6	F_G	F_M	F_{GG}	F_{GM}, F_{MG}	F_{MM}
1	0	0.39	0.61	0.00	0.39	0.22
2	1	0.40	0.60	0.00	0.40	0.20
3	2	0.40	0.60	0.0020	0.40	0.20
4	4	0.42	0.58	0.0090	0.41	0.17
5	6	0.42	0.58	0.026	0.39	0.19

The expected F_G value after AlgE4 epimerisation was 0.40-0.47[55], while epimerisation of AlgE6 was expected to further increase F_G to 0.50-0.60 on a polyalternating backbone[55]. F_G after AlgE4 epimerisation was 0.4, however after six hours incubation time with AlgE6, the F_G was 0.42. The low values after AlgE6 epimerisation were probably due to the low enzyme concentration. Based on these results, it was decided to adjust the AlgE6:alginate ratio to 1:20 and set the incubation time at 2.5 hours. These conditions have been shown to give favorable F_G in a previos student work performed by Kristin Karstensen[54]. Table 40 show the calculations of the G and M fractions of the samples prepared for large scale production, before and after active coal filtration (a.c.f).

Table 40: Bound GRGDYP (%) to mannuronan, ^{1}H NMR

Sample	Enzyme	F_G	F_M	F_{GG}	F_{GM}	F_{MM}	F_{GGM}	F_{MGM}	F_{GGG}	$N_{G>1}$
RGD	AlgE4	0.29	0.71	0.0	0.29	0.42	0.0	0.37	0.0	0
	AlgE4+AlgE6	0.35	0.65	0.070	0.28	0.37	0.020	0.32	0.050	2
	AlgE4+AlgE6 a.c.f	0.34	0.66	0.060	0.29	0.37	0.020	0.29	0.030	3
No RGD	AlgE4	0.43	0.57	0.0	0.39	0.18	0.0	0.41	0.0	0
	AlgE4+AlgE6	0.49	0.51	0.12	0.37	0.14	0.040	0.35	0.12	4
	AlgE4+AlgE6 a.c.f.	0.49	0.51	0.12	0.37	0.14	0.040	0.35	0.12	4

Although the F_{GG} of the peptide coupled sample is larger compared to the test, it is still lower than expected. F_{MGM} for the peptide coupled sample are closer to the non-coupled sample. In all other cases the values are higher for the non-coupled sample.

Figure 80 show the aromatic peaks of GRGDYP taken at 400MHz. This was the sample used to calculate the bound peptide before and after active coal filtration.

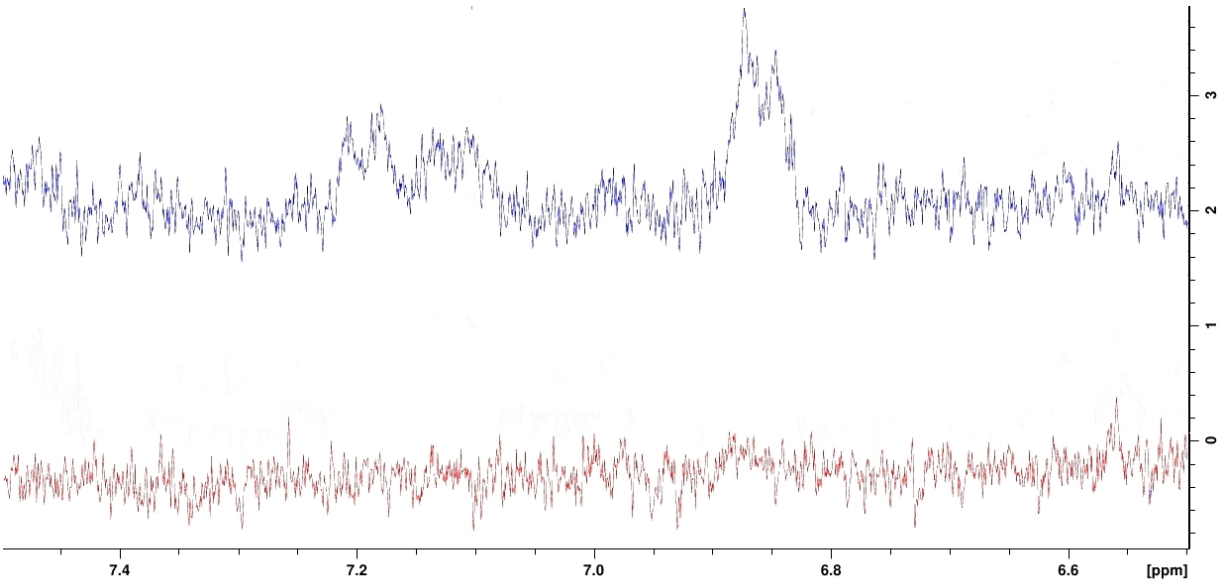

Figure 80: Enhancement of GRGDYP signals, before and after active coal filtration, 400MHz. Blue line show the sample taken before active coal filtration, while the red line represent sample after active coal filtration. The spectra was recorded at 400MHz. These spectras were used to deduce the amount of GRGDYP present.

T Encapsulation of olfactory ensheating cells

Encapsulation of olfactory ensheating cells was performed by master student Marthe Fredheim Fjelldal at the Department of Cancer Research and Molecular Medicine. The results showed below are directly produced from her results.

Figure 81 show the distribution of live (green) and dead cells (red) visualised by 3D Z stack projections by confocal laser scanning microscopy.

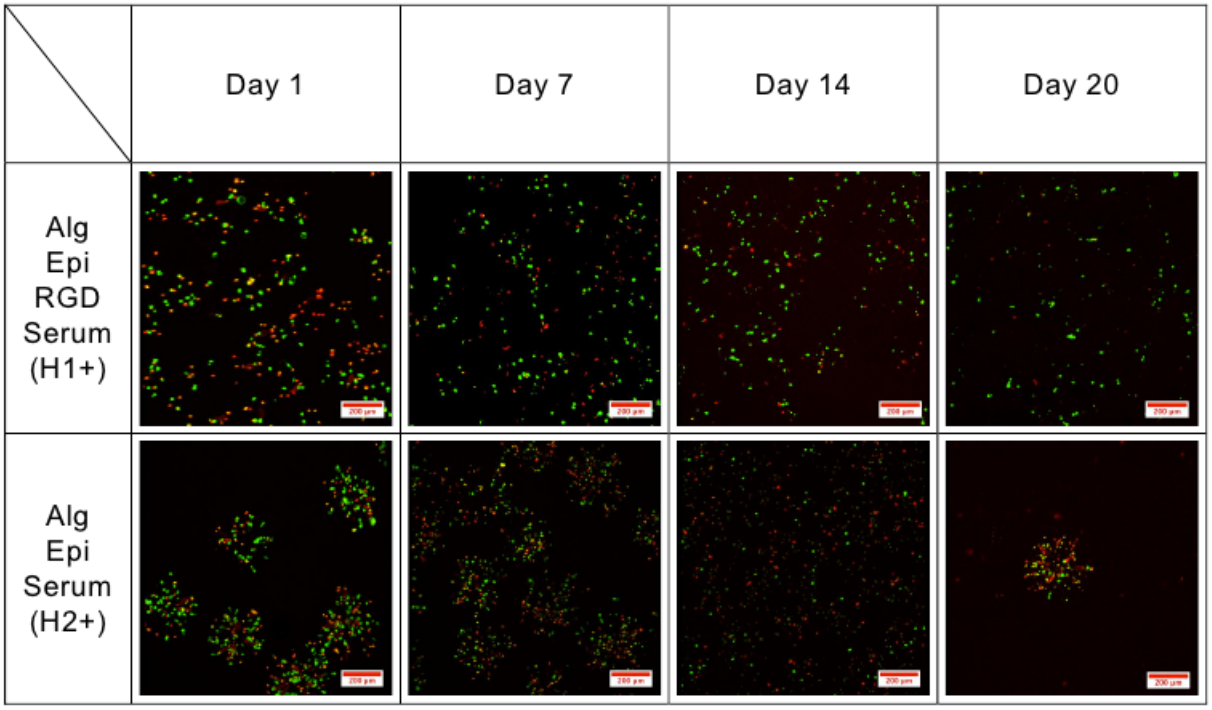

Figure 81: Live/dead assay of encapsulated olfactory ensheating cells, confocal laser scanning microscopy. 3D Z stack projections of alginate capsules with and without RGD containing 1.5 million olfactory ensheating cells per mL. The cells were kept in foetal calf serum. Green fluorescence indicates live cells, while red fluorescence indicates red cells. A 10x objective was used for image aquisition and the size bar is 200μm.

Figure 82 show cross sections through the equator of alginate capsules overlaid with transmitted light from confocal laser scanning microscopy.

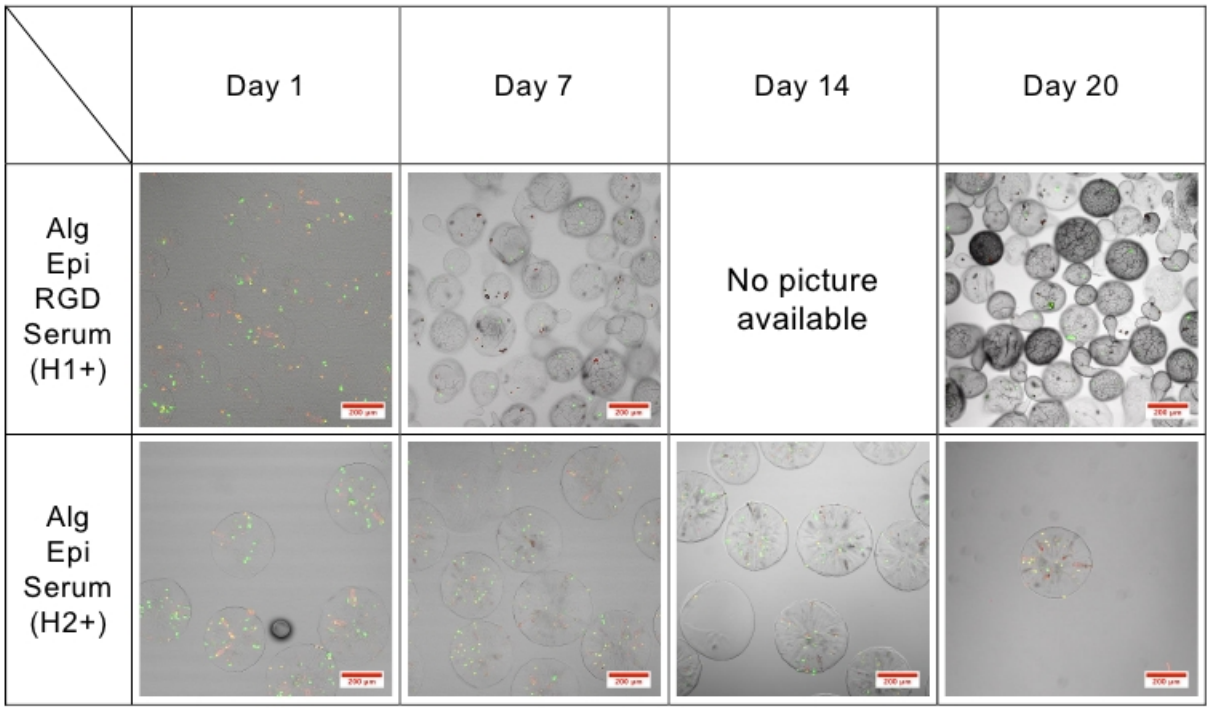

Figure 82: Cross-section of epimerised alginate capsules containing 1.5 million olfactory ensheating cells per mL. The cells were kept in foetal calf serum. Green fluorescence indicates live cells, while red fluorescence indicates red cells. A 10x objective was used for image aquisition and the size bar is 200μm.

U Coupling of chitosan and insulin

Figure 83 show the molecular structure of the AD-dimer that is coupled to mannuronan [76].

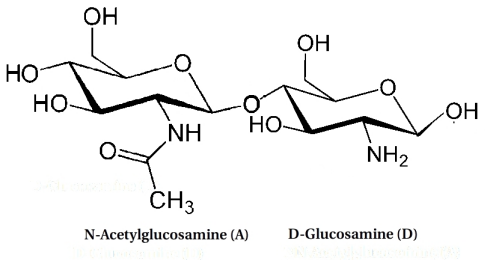

Figure 83: Chitosan dimer consisting of D-glucosamine(D) and N-acetylglucosamine(A) [76].

Insulin from ox and porcine were coupled to mannuronan. Both insuline types have tyrosine residues that will peak around 7.20 ppm. No peaks were recorded, as can be seen in figure 84.

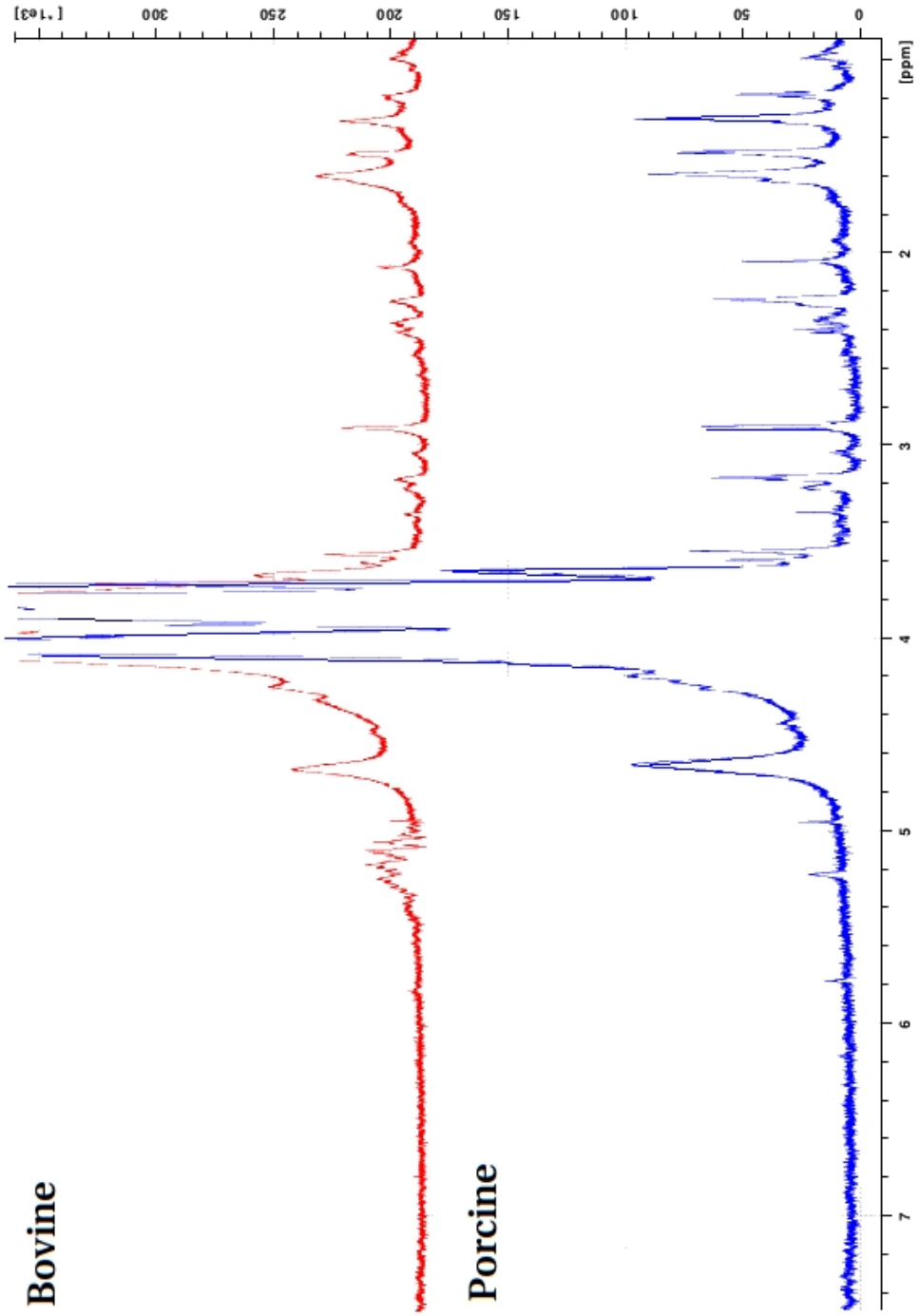

Figure 84: Coupling of insulin to mannuronan. The spectra were obtained at 600MhZ.